

USING DIGITAL RECONSTRUCTIONS, MORPHOMETRY, AND
COMPUTATIONAL MODELS TO GENERATE NOVEL MAPS OF HUMAN BRAIN
VASCULAR ARCHITECTURE

by

Susan Wright
A Dissertation
Submitted to the
Graduate Faculty
of
George Mason University
in Partial Fulfillment of
The Requirements for the Degree
of
Doctor of Philosophy
Neuroscience

Committee:

_____	Dr. Giorgio A. Ascoli, Dissertation Director
_____	Dr. Juan R. Cebal, Committee Member
_____	Dr. Ann B. Butler, Committee Member
_____	Dr. M. Layne Kalbfleisch, Committee Member
_____	Dr. James Olds, Director, Krasnow Institute for Advanced Studies
_____	Dr. Timothy L. Born, Associate Dean for Academic and Student Affairs, College of Science
_____	Dr. Vikas Chandhoke, Dean, College of Science
Date: _____	Spring Semester 2013 George Mason University Fairfax, VA

Using Digital Reconstructions, Morphometry, And Computational Models To Generate
Novel Maps Of Human Brain Vascular Architecture

A Dissertation submitted in partial fulfillment of the requirements for the degree of
Doctor of Philosophy at George Mason University

by

Susan Wright
Bachelor of Science
University of Pittsburgh, 2004

Director: Giorgio A. Ascoli, Professor
Department of Neuroscience

Spring Semester 2013
George Mason University
Fairfax, VA

Copyright: 2013 Susan Wright - All Rights Reserved

DEDICATION

This dissertation is dedicated to my family members, who have been extremely supportive of me and have offered much love, encouragement, and guidance throughout my years in graduate school: My parents, Mary Jo and Harry Wright; my siblings, H. Jeff Wright, Jonathan Wright, Sarah Montag, and Rebecca Search, and their families; my grandmother, Elizabeth Repasky; and my aunt and mentor, Dr. Elizabeth Repasky.

ACKNOWLEDGEMENTS

I am deeply thankful for everyone who has offered support and encouragement during my years in graduate school. There are numerous people who helped make my graduate career an enjoyable experience, and in this limited space, the following people deserve special acknowledgement.

First of all, I would like to thank my advisor, Dr. Giorgio Ascoli, for his expert guidance throughout my studies. Throughout the years, your feedback has helped me to grow as a scientist, and you have provided great inspiration in achieving my future goals. I gratefully attribute my newly acquired knowledge and skills in the field of computational neuroscience to your leadership and dedication. I would also like to thank Dr. Juan Cebral for his expert guidance and mentorship throughout my studies, and for giving me the chance to be a part of the computational fluid dynamics research. I knew nothing about CFD models prior to collaborating on this project, and I gratefully attribute my newly acquired knowledge and skills in this area to your leadership and dedication. Your continuous optimistic outlook was extremely helpful during times of great stress. I would also like to thank the other members of my committee, Dr. Ann Butler and Dr. Layne Kalbfleish, for their expertise in the fields of neuroanatomy and neuroimaging, respectively. Both of you have been excellent role models and great inspirations to me throughout graduate school, and I thank you for your helpful feedback during the development of my thesis. My thanks also go to past and present members of The Computational Neuroanatomy Group, The Center for Neural Informatics, Neural Structures, and Neural Plasticity, as well as The Center for Computational Fluid Dynamics, but especially Fernando Mut, Kerry Brown, Duncan Donohue, Ruggero Scorcioni, Sridevi Polavaram, Maryam Halavi, Stephen Senft, and Maurizio Bergamino for their helpful discussion and feedback during the course of this project. I also thank Dr. James Olds, Dr. Avrama Blackwell, and other members and staff of The Krasnow Institute for Advanced Study for making my graduate school experience enjoyable - working in such a positive environment where everyone has great enthusiasm for science and collaboration has been invaluable. I would also like to thank Dr. German Barrionuevo for encouraging me to apply to the computational neuroscience PhD program at George Mason University, and for his mentorship during my time in his laboratory at the University of Pittsburgh. I thank Peter Kochunov, John Mazziotta, and Arthur Toga for their collaboration on the project and for acquiring the MRA data sets that were used for this study.

I would also like to thank my friends for their support over the years, and for all of the good times that we've shared. I would especially like to thank Ruchi Parekh, Ann Mayles, Ji Sun Lee, Megan Clark, Sara Mengal, and Jonathan Kobaly. You have always been there for me, in good times and bad, and I really appreciate all that you've done to make the last several years of my life an enjoyable experience.

Last but not least, I owe immeasurable thanks and love to my family. My parents, Mary Jo and Harry Wright, have offered constant support over the years, and I realize that without them, I would not have gotten very far. You have been incredibly patient, compassionate, and understanding in times of stress and difficulty, and are always there to celebrate my accomplishments, no matter how small. My siblings, H. Jeff Wright, Jonathan Wright, Sarah Montag, Rebecca Search, and their families, have always inspired me to do the best that I can do, and have been incredibly supportive over the years. Sarah deserves a special thanks for always being willing to teach me Excel shortcuts or to proofread my papers. My grandmother, Elizabeth Repasky, has continuously believed in me, and for this I am eternally grateful. Lastly, my aunt, Dr. Elizabeth Repasky has been a mentor to me since I first became interested in scientific research, as a high school student. I owe her a great deal of thanks for being my constant inspiration and role model, and for always taking the time to provide me with useful advice and encouragement.

TABLE OF CONTENTS

	Page
List of Tables	ix
List of Figures	x
List of Abbreviations	xi
Abstract	xii
Chapter One: Introduction	1
Background and Significance.....	1
Morbidity and Mortality of Cerebrovascular Disease.....	2
The Circle of Willis.....	3
Brain Imaging.....	4
Data Segmentation	7
Digital Reconstructions and Morphological Analysis	10
Computational Fluid Dynamics Models	12
Conclusions from Literature and Dissertation Goals	16
Organization of Dissertation	17
Chapter Two: Digital Reconstruction and Morphometric Analysis of Human Brain Arterial Vasculature From Magnetic Resonance Angiography	19
Abstract	19
Introduction	20
Methods.....	22
MRA Acquisition	22
Digital Reconstructions	23
Morphological Analysis	24
Statistical Analysis	26
Data Archival and Dissemination.....	26
Results	27
Visual Aspect and Inter-Subject Variation of Reconstructed Arterial Vasculature ..	27

Quantitative Anatomy of Human Brain Arteries	33
Size Differences and Proportional Scaling Among Cerebral Arteries	38
Systematic Variation of Selected Morphometric Properties along the Vascular Path	45
Public Online Availability of Reconstructions	47
Discussion	48
Acknowledgements	52
Chapter Three: Subject Specific Models of Blood Flows in Cerebral Arterial Trees From High-Resolution Magnetic Resonance Images	53
Introduction	53
Methods	53
Digital Reconstructions	53
Geometric Models	54
.....	56
Results	58
Conclusions	60
Future Directions	60
Chapter Four: Conclusions and Future Directions.....	61
Conclusions	61
Future Directions	63
Appendix One: Morphometric, Geographic, and Territorial Characterization of Brain Arterial Trees	67
Abstract	67
Introduction	67
Methods	68
Vascular Reconstructions	68
Arterial Tree Characterization	71
Vascular Atlas and Territories	71
Results	74
Branch Geometry	74
Bifurcation Characteristics	76
Tree Shapes.....	78
Territory Characteristics	80

Discussion	86
Conclusions	89
Acknowledgements	90
Appendix Two: BraVa: The Design and Organization of a Neuroscience Digital Archive	91
Introduction	91
Database Design and Organization	91
Navigation of Database	92
References	102

LIST OF TABLES

Table	Page
Table 2.1	36
Table 2.2	41
Table A1.1.....	80
Table A1.2.....	83
Table A1.3.....	86

LIST OF FIGURES

Figure	Page
Figure 2.1	29
Figure 2.2	31
Figure 2.3	32
Figure 2.4	37
Figure 2.5	42
Figure 2.6	44
Figure 2.7	46
Figure 2.8	47
Figure 3.1	56
Figure 3.2	56
Figure 3.3	57
Figure 3.4	58
Figure 3.5	59
Figure A1.1	70
Figure A1.2	73
Figure A1.3	75
Figure A1.4	77
Figure A1.5	79
Figure A1.6	81
Figure A1.7	82
Figure A1.8	85
Figure A2.1	93
Figure A2.2	94
Figure A2.3	95
Figure A2.4	96
Figure A2.5	97
Figure A2.6	98
Figure A2.7	99
Figure A2.8	100
Figure A2.9	101

LIST OF ABBREVIATIONS

Anterior Cerebral Artery	ACA
Anterior Communicating Artery	ACOM
Basilar Artery	BA
Circle of Willis.....	CoW
Computational Fluid Dynamics	CFD
Contrast Enhanced	CE
Graphical User Interface	GUI
Internal Carotid Artery.....	ICA
Left.....	L
Magnetic Resonance Angiography	MRA
Magnetic Resonance Imaging	MRI
Maximum Intensity Projection	MIP
Middle Cerebral Artery	MCA
Posterior Cerebral Artery	PCA
Relational Database Management System.....	RDBMS
Right.....	R
Time of Flight	TOF
Wall Shear Stress	WSS

ABSTRACT

USING DIGITAL RECONSTRUCTIONS, MORPHOMETRY, AND COMPUTATIONAL MODELS TO GENERATE NOVEL MAPS OF HUMAN BRAIN VASCULAR ARCHITECTURE

Susan Wright, Ph.D.

George Mason University, 2013

Dissertation Director: Dr. Giorgio A. Ascoli

Many non-invasive imaging techniques based upon hemodynamic responses of blood vessels have provided data for analysis of brain vasculature. However, these data lack the detail that could be ascertained by exploiting state-of-the-art neuroinformatics tools. A more complete and sufficiently detailed analysis of brain vascular architecture is critical for a wide variety of applications, including the development of models which may help predict or treat cerebrovascular disease.

Taking advantage of image stacks acquired from 3T time-of-flight magnetic resonance angiography and techniques previously used to create 3D neuronal reconstructions, the circle of Willis and the six major arteries that stem from it were reconstructed for sixty-one healthy subjects. The basis of this dissertation research is that recently available neuroinformatics tools can be exploited to create new models of vascular reconstructions that are representative of the general population of healthy subjects. These models can be

used to generate more detailed novel comparative assessments between normal and diseased vasculature found in forms of cerebrovascular disease.

Sixty-one digital reconstructions of healthy human brain vasculature were created and extensive quantitative morphometrical analysis was conducted in order to characterize the anatomy of the human brain vessels, on both global and local levels of size, distances, angles and topology, concentrating in particular on vessel bifurcations. Additional analysis was conducted to provide quantitative description of the arterial branches, bifurcation patterns, shape and geographical distribution of the main cerebral arterial arborizations, as well as estimations of the corresponding vascular territories. Also as part of this analysis, computational models were created to examine fluid dynamics. In order to create these models, the brain was segmented and normal blood flow and wall shear stress values were measured, with the intent to provide a set of baseline values that could then be compared to patient data values. Lastly, the digital reconstructions and their extracted morphological measurements were archived in a database that will be made publicly available.

The information that can be extracted from these detailed reconstructions can be used to examine questions such as how the brain vasculature differs across various populations, such as males and females, different age groups, and healthy individuals versus individuals with cerebrovascular disease. Also, the information that can be extracted from the reconstructions can be used to implement complex computational models of fluid dynamics that may aid in the development of new treatments for individuals afflicted with cerebrovascular disease. Finally, the new information generated here may play a

fundamental role in our ability to recognize vascular defects that could help treat, or even predict, cerebrovascular diseases.

CHAPTER ONE: INTRODUCTION

“How can a three-pound mass of jelly that you can hold in your palm imagine angels, contemplate the meaning of infinity, and even question its own place in the cosmos? Especially awe inspiring is the fact that any single brain, including yours, is made up of atoms that were forged in the hearts of countless, far-flung stars billions of years ago. These particles drifted for eons and light-years until gravity and change brought them together here, now. These atoms now form a conglomerate- your brain- that can not only ponder the very stars that gave it birth but can also think about its own ability to think and wonder about its own ability to wonder. With the arrival of humans, it has been said, the universe has suddenly become conscious of itself. This, truly, is the greatest mystery of all.”

— V.S. Ramachandran, *The Tell-Tale Brain: A Neuroscientist's Quest for What Makes Us Human*

Background and Significance

The study of brain vasculature has attracted intense interest from neuroanatomists for many decades; yet, the precise anatomical relationships which underlie neurovascular structure and function remain unclear. The importance of achieving a more complete understanding of neurovascular structures is highlighted by the fact that aneurysms and other forms of cerebrovascular disease are a major cause of morbidity and death

worldwide. Thus, the central goal of this research has been to apply the techniques that have previously been used for neuronal reconstructions to create digital reconstructions of healthy human brain vasculature, which have then been evaluated in a number of ways. The following section details prior work in this area, and the clinical and biological significance of developing new state-of-the-art vascular mapping of regions of the brain.

Morbidity and Mortality of Cerebrovascular Disease

Cerebrovascular diseases affect a large portion of the human population and are a leading cause of death, devastating morbidity, and long-term disability worldwide. Cerebrovascular diseases can include a variety of vascular-related problems, and two common types of such disease are aneurysms and stroke. Records show that this type of disease is the fourth leading cause of death in the U.S, with an economic cost of \$73.3 billion in 2010 (Towfighi and Savers, 2011). Moreover, survivors usually sustain severe long-term disabilities (Higashida et al., 2003). Individual and group variations in the neurovascular structure-function relationship have not yet been comprehensively investigated. It is not yet known, for example, whether the higher rate of subarachnoid hemorrhages in women are due to hormonal differences and/or wall shear stress variations (Ghods et al., 2012). Another serious problem is determining the role of vascular anomalies and their suspected relationship with migraine and ischemic cerebrovascular disease (Cucchiara and Detre, 2008). Achieving a better understanding of physiological function and pathological dysfunction of the cerebrovascular system requires a detailed and quantitative characterization of its architecture.

In the past decade, studies have correlated population-based information to functional outcome, survival, and recurrence for the different subtypes of strokes (Lemesle et al., 1999, Petty et al., 2000, Chung and Wong, 2004, Alzamora et al., 2008). Aneurysms are also widely studied, especially their detection and treatments (Chang et al., 1998, Lohani, 2004, Jayaraman et al., 2007, Joo et al., 2007, Kelly et al., 2007, Ding et al., 2008, Santos-Franco and Zenteno, 2008). There has also been an increase in studies related to the genetics of cerebrovascular diseases; these studies typically focus largely on only one gene or polymorphism at a time. A recent study examined genetics on a much larger scale (Kostulas et al., 2008) and an editorial has been written regarding the future of atherothrombotic disease genetics highlighting the importance of developing new technological and bioinformatics tools for future research (Brand-Herrmann, 2008).

Unless we know more details about how neurovascular features differ among populations of people, it will not be possible to develop treatments that are effective for large, defined populations. Studies have been done to test how limited the clinical diagnoses are for certain vascular diseases (Allder et al., 1999) and for trial designs and reporting standards (Higashida et al., 2003). The next section describes a particular area of cerebrovasculature with known anomalies in the human population, and explains the importance of increasing knowledge of its morphology.

The Circle of Willis

The circle of Willis (CoW) is a ring of vessels that encircles the optic chiasm and hypothalamus, with the anterior cerebral arteries (ACAs), middle cerebral arteries (MCAs), and posterior cerebral arteries (PCAs) stemming from it. Making up the CoW

are the anterior and posterior communicating arteries and the proximal portions of the ACAs, MCAs and PCAs. Aneurysms commonly form in the bifurcations of the CoW (Keedy, 2006). This ring allows for rapid changes in flow depending on regional metabolic needs. It is well known that the CoW is not complete in all individuals. In fact, approximately 50% of the population has variations of the CoW in which one or more vessels are missing, resulting in an incomplete ring. It follows that many studies have been done on the variations of the CoW, in an effort to answer questions about how these variations may be linked to the different types of cerebrovascular disease (Bingzhen et al., 1998, Krabbe-Hartkamp et al., 1998, Eftekhari et al., 2006, Moritz et al., 2007, Naggara et al., 2008, Papantchev et al., 2007, Cucchiara and Detre, 2008, de Monye et al., 2008, Urbanski et al., 2008). Migraine has been linked to CoW anomalies as well, and it is thought that the identification of anatomical variations of this ring as a risk factor for both migraines and other vascular disorders could be important for clinical associations (Cucchiara and Detre, 2008). It is also known that anatomic variations of the cerebral arteries can occur during development, which has been studied as well (Okahara et al., 2002). However, there is a need for improved imaging techniques in order to increase knowledge about the CoW and cerebral arteries. The next section describes current imaging techniques as well as their advantages and disadvantages.

Brain Imaging

The current diagnostic tools commonly used for many cerebrovascular disorders are magnetic resonance imaging (MRI) and magnetic resonance angiography (MRA). In MRI, strong magnetic fields are used to image biological tissue. MRA is similar, but is

specific to the imaging of blood vessels (Bosmans et al., 1992). There are two main categories of MRA: contrast-enhanced (CE) and non-contrast methods. Within the non-contrast category, the two major methods are phase contrast and time-of-flight (TOF), with TOF being the type of imaging used in this research. TOF, which is more common, is a unique type of angiography where contrast is generated by compressing the signals from spins within the imaging plane, which results in high signals from voxels with inflowing spins, which are the voxels that contain blood vessels (Huettel et al., 2004). This spin saturation is accomplished by an almost constant application of either excitation or gradient pulses to just one imaging plane so that the signal is suppressed (Huettel et al., 2004). As a result, gray or white matter with spins that are within the plane appear to be very dark, as they will produce very little signal (Huettel et al., 2004). On the other hand, blood vessels appear much lighter due to the fact that they contribute normal signal since they receive new spins from outside the plane which have not been affected by the excitation or gradient pulses (Huettel et al., 2004). The amount of blood that enters the slice is proportional to the signal, so repetition times where new columns of blood enter the slice result in maximum signal (Huettel et al., 2004). The amount of flow also differentiates blood vessels in this type of imaging as well, making it flow-dependent (Huettel et al., 2004). Because of this, the slice thickness and repetition times are important factors to consider and must be chosen based on the expected flow (Huettel et al., 2004). One advantage of this type of imaging is that it is able to be reformatted to planes other than the one that it was acquired in (usually axial) (Huettel et al., 2004). There are two techniques used in this type of imaging. The first involves pre-saturation of

the imaging plane by an electromagnetic excitation pulse and gradient saturation pulses, then fresh blood is allowed to enter the plane following a brief waiting period and this signal alone is acquired by a gradient-echo technique (Huettel et al., 2004). Alternatively, a velocity-encoded phase contrast MRA, which takes advantage of gradient fields to differentiate between vasculature and surrounding tissue, produces a velocity-dependent phase difference (Huettel et al., 2004). Numerous imaging studies have been carried out with various types of imaging to assess the cerebral vessels. Such studies include aging vessels (Kusunoki et al., 1999), vascular malformations (Dobson et al., 1997), evaluation of the CoW (Katz et al., 1995, Stock et al., 1996, Bagan et al., 2005), strokes (Bentson, 1997, Schaefer et al., 2002, Minematsu, 2003, Ahmed and Masaryk, 2004, Bagan et al., 2006), and aneurysms, both unruptured (Harrison et al., 1997, Grandin et al., 1998) and those that have bled (Keogh and Vhora, 1998).

There are many advantages to MRA, such as being non-invasive, accurate, cost-effective, fairly simple to perform, and having a flexible display, as well as integration of both vessels and soft tissues (Wilms et al., 2001, Ahmed and Masaryk, 2004, Insko and Carpenter, 2004, Bammer et al., 2005, Vaphiades and Horton, 2005). MRA at 3T leads to especially detailed imaging of the intracranial circulation, because it allows an increased signal-to-noise ratio with better background suppression (Parmar et al., 1005). However, one significant disadvantage of this type of imaging is that for detecting aneurysms, it may *underestimate* the size of intracranial aneurysms or fail to detect aneurysms completely, even if a patient is displaying characteristics of a disorder (Vaphiades and Horton, 2005). Other disadvantages include poor temporal information, a dependence on

blood flow, and reduced visibility of very small or very deep branches in the cortex (Wilms et al., 2001). In TOF MRA, the diameters of blood vessels may appear thinner than in actuality (Vaphiades and Horton, 2005).

Obtaining data sets from imaging techniques is the first step in creating digital reconstructions of the vasculature. It is then necessary to classify the voxels of these images into blood vessels and other tissues, which is referred to as data segmentation, and is discussed in the next section.

Data Segmentation

In order to create digital reconstructions and new computational models, segmentation of the entire data set, just the arteries, or subject-specific defects, such as cerebral aneurysms, must be carried out as one of the first steps. There is a great deal of literature on various segmentation algorithms, as different types of imaging present unique challenges.

Several automated segmentation algorithms have been tested on the various types of data. One such method focuses on extraction of cerebrospinal fluid-tissue boundary from serial structure MRI from imaging studies of aging and dementia (Drapaca et al., 2005). Another automatic segmentation algorithm uses level sets and dense registration (Baillard et al., 2001). One of the problems with automated segmentation is that complicated curvilinear structures exist, and in an attempt to solve this problem, a method was developed to handle curves in 3D (Lorigo et al., 2001). Curve evolution theory has been studied, and one study describes alternative metrics for quantifying distances between distributions and tries to solve the problem of separating the object

from the background in an image (Georgiou et al., 2007). Another automated segmentation method that consisted of two stages resulted in a greater number of detected vessels than ground truth results (Almi'ani and Barkana, 2012).

There have been several attempts to test methods for the segmentation of aneurysm data. One method segmented cerebrovascular structures in addition to aneurysms from 3D Rotational Angiography and Computed Tomography Angiography, which are both challenging due to high levels of noise (Hernandez and Frangi, 2007). An adaptive segmentation algorithm designed for use with TOF MRA uses recursive model fitting in order to classify local subvolumes of data, and was tested on data sets involving various sized artery and aneurysm structures (Wilson and Noble, 1999). Both healthy vascular and diseased vascular data were used for an algorithm that segmented MRA data (Flasque et al., 2001). Another segmentation algorithm was tested on aneurysm patients and was unique because it is based on geodesic active regions (Bogunovic et al., 2011).

Other segmentation techniques have been carried out on vessels of various sizes. An algorithm specific to blood vessels from MRA data was shown to be fairly accurate (Kobashi et al., 2001). For the segmentation of thin blood vessels, an algorithm was designed to accurately model capillary action and derive capillary active contour (Yan and Kassim, 2006). A method that used 3D steerable filters was shown to detect small vessels (Weiping and Huazhong, 2005). Larger cerebral arteries were segmented successfully (Luo et al., 2005). A level set based cerebral vasculature segmentation and diameter quantification algorithm was accurately implemented using CTA data (Manniesing et al., 2006), and another level set based algorithm was used on MRA data

(Hassan and Farag, 2003). Complete vascular trees were segmented with another algorithm, with the authors noting that vessels with a diameter of less than 1mm are difficult to detect (Sabry et al., 2002). The CoW was successfully segmented with multiple segmentation algorithms (Luo et al., 2011, Datta and Chakraborty, 2012).

MRA images have been segmented using various algorithms, including a gradient compensated geodesic active contour based segmentation algorithm (Zonoobi et al., 2009), and tight-frame based (Cai et al., 2013 (accepted for publication)), Affine Cell Decomposition (ACD)-based (McInerney and Terzopoulos, 1997), a thinning step (Qin et al., 2003), and a novel post-processing method to increase the detail of the vasculature that can be visualized was tested (Payne et al., 2005). Another method was shown to be capable of simultaneously carrying out segmentation in MRA and wall signal in MRI (Passat et al., 2007). Several algorithms have been tested for TOF MRA data (Vermandel et al., 2007, El-Baz et al., 2005, Wilson and Noble, 1999). 1.5T (Hao et al., 2008) and 7T MRA data have been used to segment data, and the drawback with 7T was that it wasn't feasible for a large number of data sets due to the number of vessels that are visible at 7T (Liao et al., 2011; Liao et al., 2012).

Phase Contrast MRA data has been used for several segmentation algorithms as well. A method integrating *a priori* knowledge into the segmentation process was carried out (Passat et al., 2006). Statistically based algorithms were also tested (Chung et al., 2004 and Sabry et al., 2002).

Additionally, the charged fluid model simulates charged elements to segment images (Chang and Valentino, 2008). Several deformable contour methods exist for

medical imaging, and research has been done to present the strengths and limitations of such methods (He et al., 2008). For X-ray tomography data, one research group has developed techniques for segmentation and image enhancement of porous materials (Sheppard et al., 2004). Another group focused on the segmentation of cortical and subcortical structures, and the analysis of white matter fiber tracts from DTI, and neuroanatomic analysis from MRI (Duncan et al., 2004). For studies that require realistic models of the head, the segmentation of the skull is an important element, which must be modeled as an independent parameter (Rifai et al., 2000). Segmentation processes can also be used to quantify vascular structures from MRA data (Luo et al., 2011). In order to increase knowledge of vascular anatomy, especially the regions that are prone to disease, the characterization of the geometry of arteries is essential (O’Flynn et al., 2007). The next section will discuss how digital reconstructions of the segmented vasculature can be created and morphometric parameters can then be extracted.

Digital Reconstructions and Morphological Analysis

In neuronal reconstructions, the dendritic tree is represented as a series of cylinders, with information about the diameter, spatial coordinates, and connectivity to other cylinders in the tree represented for each individual compartment (Ascoli et al., 2001, Scorcioni and Ascoli, 2005). Neuron_Morpho, an ImageJ plugin, has been demonstrated to be an effective tool in creating digital reconstructions from neuronal stacks (Brown et al., 2005). Extensive morphology studies from neuronal tree structures have been described in a number of publications (Uylings et al., 1986, Verwer and van Pelt, 1986, Cannon et al., 1998, Ascoli and Krichmar, 2000, Washington et al., 2000,

Ascoli et al., 2001, Scorcioni and Ascoli, 2001, Uylings and van Pelt, 2002, Samsonovich and Ascoli, 2003, Scorcioni et al., 2004, Donohue and Ascoli, 2005, Samsonovich and Ascoli, 2005, Krichmar et al., 2006, Duque et al., 2007). The vasculature of the brain can also be thought of as a tree, with the origin (e.g. soma) being along the basilar artery. Using data stacks from 3T TOF MRA, the Neuron_Morpho ImageJ plugin can be used to create detailed digital reconstructions of the CoW and the 6 major arteries (2 ACAs, 2 MCAs, and 2 PCAs) that stem from it. An extensive study of the morphology of the brain vasculature can then be done, yielding a better understanding of which characteristics are considered normal or healthy, and which are not.

Previous research has included the optimal branching of human arterial bifurcations (Fanucci et al., 1990, Rossitti and Lofgren, 1993, Karch et al., 2000), studies of taper values (MacLean et al., 1992, Roach and MacLean, 1993), and branching characteristics (Fanucci et al., 1988). One of the theories of the growth and adaptation of arterial trees is the principle of minimum work, which is a parametric optimization model, and it has been shown that vascular dimensions of the cerebral arteries follow this principle (Rossitti and Lofgren, 1993). The predominant hypothesis of the design of vascular trees is the minimum dissipation principle known as Murray's Law, which suggests that metabolic consumption in a single vessel segment is proportional to the blood volume, and several studies have been done to test this theory (Sherman, 1981, Painter et al., 2006, Liu and Kassab, 2007). It was shown that all vascular trees which had morphometric data in the literature followed a set of scaling laws (Kassab, 2006). It is known that branching systems that occur in the environment as well as in bodies are

characterized by a fractal nature (Kamiya and Takahashi, 2007, Zamir, 2001).

Morphology studies have been particularly important in studies of aneurysms, in an attempt to figure out why intracranial aneurysms develop (Canham and Finlay, 2004, Ingebrigtsen et al., 2004, Bor et al., 2008). Also, the diameter asymmetry of arterial trees in pigs has been studied (Kaimovitz et al., 2008).

To summarize the above sections, a search of the literature shows that although studies of MRA data have been carried out, these studies have been limited to qualitative or semi-quantitative assessments (El-Barhoun et al., 2009), partial morphometric analyses (Bullitt et al., 2009; Chen et al, 2008), small numbers of subjects (Canham and Finlay, 2004) and proprietary data sets (Nowinski et al., 2009). A more comprehensive structural characterization of cerebral arterial trees can be achieved by reconstructing the vascular arborization into an explicit 3D representation (Passat et al., 2006; Bullitt et al., 2005). These digital reconstructions of vascular trees can also be used to create three-dimensional CFD models of the blood flow in healthy human brain vasculatures, which will provide useful information and insights into the normal cerebral hemodynamics.

Computational Fluid Dynamics Models

In addition to being used for morphometric analysis, vector representations of arterial trees play an important role in subject-specific computational fluid dynamics modeling for investigation of individual risks of vascular malformation (Oshima et al, 2001, Cebal et al., 2003). For these approaches, it is necessary to specify the appropriate boundary conditions and constraints related to arterial branch geometry and bifurcation characteristics (Olufsen et al, 1999; Cebal et al., 2003; Cebal et al., 2000). It is possible

to use surrogate arterial tree models in the absence of representative samples of available complete reconstructions (Olufsen et al., 2000; Karch et al., 1999; Bui et al, 2010; Dozoumetzidis et al., 2003).

Knowledge of how blood flows normally throughout brain vasculature is important so that we may eventually be able to detect or possibly prevent aneurysms or strokes or other cerebrovascular disorders. Therefore, hemodynamics is an area that has been studied extensively, with hopes of finding links between high volume flow to the brain and vascular disorders (Rutgers et al., 2004). Some of the major studies of hemodynamics have included changes in cerebral circulation after a type of treatment of angioplasty known as stent-protected carotid angioplasty, which is one option for treating internal carotid artery (ICA) stenosis (Niesen et al., 2004). Quantitative measurements of blood-flow volume in the carotid and vertebral arteries have been used to estimate the total cerebral blood-flow volume, which is used to help diagnose a number of cerebrovascular diseases and to monitor certain treatments, so it follows that studies have focused on getting an accurate number for this value (Oktar et al., 2006). Related to quantitative measurements of blood-flow volume, studies have also been done to examine whether cerebral ischemia develops during cross-clamping of the carotid artery in carotid endarterectomy patients (Rutgers et al., 2000). The diameters of blood vessels are very important in hemodynamics studies, as even small changes in diameter can have great effects on blood flow (Cassot et al., 1995). Collateral flow patterns have been studied in the CoW and the ophthalmic artery (Rutgers et al., 2000). Rats and pigs have been

studied as well (MacLean et al., 1992, Huo et al., 2007, Chen et al., 2008, Esneault et al., 2008, Kaimovitz et al., 2008, Seo et al., 2008).

Because the CoW plays such an important role in distributing blood flow throughout the brain, many models have focused their attention on this structure. Attempts have been made to determine the effects on hemodynamics when there are variations in this ring of vessels (Hendrikse et al., 2005, Tanaka et al., 2006, Alnaes et al., 2007), and both one-dimensional and three-dimensional models have been created (Moore et al., 2005, Moore et al., 2006, Alastruey et al., 2007). A very simple one-dimensional model of this ring was created to examine hemodynamic autoregulation using a proportional-integral-derivative controller to modify the resistances of efferent arteries (Moorhead et al., 2004, Moorhead et al., 2006). A two-dimensional model similar to the one just described, but also simulating different common variations of the CoW was created to examine autoregulation and cerebral blood flow (Ferrandez et al., 2002). Another two-dimensional model of the CoW was created to examine the steady state of the vessel ring, using porous blocks to simulate peripheral resistance of the cerebrovascular tree (Ferrandez et al., 2000). An extended CoW model that also included the periorbital links and the external carotid arteries was developed in an attempt to explain clinical observations of periorbital arterial flow (Viedma et al., 1997). A model of the CoW that also included jugular venous return was created to test a theory of selective brain cooling in humans (Neimark et al., 2007). In another model that involved the CoW, the two hemispheres of the brain were connected by the ring by various sized anterior

communicating arteries in order to study cerebral and cerebrospinal fluid circulations (Piechnik et al., 2001).

Although not specific to the brain, a one dimensional/Womersley model of pulsatile blood flow to the entire coronary arterial tree was created, and proved to be an efficient way to represent hemodynamics of a complex, large-scale vascular network (Huo and Kassab, 2007). Hemodynamics are thought to be important in many aspects of aneurysms, such as their initiation, growth, and rupture, and a number of computational models have focused on this area (Cebal et al., 2005, Castro et al., 2006, Cebal et al., 2007). It is this last set of hemodynamics models that were built upon in the studies described in this dissertation.

Wall shear stress (WSS) is a very important factor in computational models of hemodynamics and aneurysms. The WSS is the force that is exerted by the wall on the fluid (Katrakis et al., 2007). The dominant theory is that WSS is assumed to be constant along an arterial tree and is the same in a particular artery across species (Reneman and Hoeks, 2008). However, a recent study shows evidence that this theory may not be correct, as it compares data across the literature in both large and small animals (Cheng et al., 2007). Another study investigates allometric scaling of WSS between species, including humans (Greve et al., 2006). Many studies have been done on WSS calculations. In vivo studies of WSS have been examined to see what the effect is on the design of the arterial system (Reneman and Hoeks, 2008) and whether WSS is an important factor in endothelial cell function and structure (Reneman et al., 2006). High-resolution 3D phase contrast mapping for estimation of WSS in vivo was examined and

applied (Wu et al., 2004). Studies have also been done using noninvasive methods of measuring WSS, either by ultrasound (Brands et al., 1995) or by modeling MRI velocity data (Oyre et al., 1998). Another study using phase contrast imaging calculated WSS in the ascending aorta in order to test whether the most straightforward application of WSS calculation can be applied in a clinical setting and yield accurate results (Efsthopoulos et al., 2008). The relationship between vascular WSS and flow-mediated dilation in humans was studied using phase contrast MRA data, and showed that in normal subjects, arterial flow-mediated dilation is linearly proportional to WSS (Silber et al., 2001). The relationship between branching exponent heterogeneity and WSS distribution in vascular trees was studied (Karau et al., 2001) and WSS was also analyzed by experimental and numerical studies of pulsatile flows through stenosis (Deplano and Siouffi, 1999), as well as the effects of WSS on stent implantation (LaDisa Jr. et al., 2006). The previous studies on WSS were helpful in evaluating normal conditions in the models attempted in this dissertation, and would also apply to aneurysm conditions.

Conclusions from Literature and Dissertation Goals

It is clear that although much research has been carried out regarding brain vasculature, what is lacking is a comprehensive structural characterization of these vessels. Extensive morphometric analysis of the brain arteries needs to be carried out on a large number of data sets, and this information needs to be publicly available.

In an attempt to fix this gap in the field, this dissertation reports the first extensive quantitative analysis of the global and local anatomical features of healthy arterial vasculature including size, symmetry, branching characteristics, bifurcation angles and

path meandering. In addition to characterizing normative statistics for this representative population sample, a systematic comparison of arterial geometry between hemispheres, genders, and branch types, among arteries, along the path, and across subject ages is presented. Geographic and territorial characterization of the cerebral arteries is also reported. The results of the analysis presented throughout this dissertation confirm and greatly extend previous knowledge of the human cerebrovascular architecture. Additionally, the entire data set will be publicly distributed online for continuous reanalysis and computational modeling by the research community.

Organization of Dissertation

In addition to this introductory chapter, this dissertation consists of three independent chapters, and two appendices. The first of the independent chapters, Chapter Two, is a manuscript that has been submitted for publication. It outlines the digital reconstruction process of the arterial trees, the extensive morphological analysis, and the data sharing. The second of the independent chapters, Chapter Three, describes work that is ongoing at the time of this write-up. It describes the method used to create subject-specific CFD models from the digital reconstructions presented in the previous chapter. The third independent chapter, Chapter Four, summarizes the results presented throughout this dissertation and discusses questions that remain unanswered, as well as future directions of the research. The two appendices correspond to a collaborative (middle-authored) manuscript that has been prepared for publication but has not yet been submitted, and additional necessary information, respectively. The first appendix provides additional morphometric analysis, as well as geographic and territorial

characterization of the cerebral arteries. The second appendix is a more in-depth explanation of the database, BraVa, which archives the digital reconstructions and their corresponding morphometric analysis results, and will be made available to the public to promote data sharing.

CHAPTER TWO: DIGITAL RECONSTRUCTION AND MORPHOMETRIC ANALYSIS OF HUMAN BRAIN ARTERIAL VASCULATURE FROM MAGNETIC RESONANCE ANGIOGRAPHY

Abstract

Characterization of the complex branching architecture of cerebral arteries across a representative sample of the human population is important for diagnosing, analyzing, and predicting pathological states. Brain arterial vasculature can be visualized by Magnetic Resonance Angiography (MRA). However, most MRA studies are limited to qualitative assessments, partial morphometric analyses, individual (or small numbers of) subjects, proprietary data sets, or combinations of the above limitations. State-of-the-art neuroinformatics tools, developed for neuronal arbor analysis, were used to quantify vascular morphology from 3T time-of-flight MRA high-resolution (620 μm isotropic) images collected in 61 healthy volunteers (36/25 F/M, average age=31.2 \pm 10.7, range=19-64 years). We present in-depth morphometric analyses of the global and local anatomical features of these arbors. The overall structure and size of the vasculature did not significantly differ across genders, ages, or hemispheres. The size of the three major arterial trees stemming from the Circle of Willis (from largest to smallest: the Middle, Anterior, and Posterior Cerebral Arteries; or MCAs, ACAs, and PCAs, respectively) co-varied across individuals: subjects with one artery larger than average tended to have all other arteries also larger than average. There was no net right-left preference across the population in any of the individual arteries, but ACAs were more lateralized than MCAs

within subjects. MCAs, ACAs, and PCAs had similar branch-level properties such as bifurcation angles. Throughout the arterial vasculature, there were considerable differences between branch types: bifurcating branches were significantly shorter and straighter than terminating branches. Furthermore, the length and meandering of bifurcating branches increased with age and with path distance from the Circle of Willis. All reconstructions are freely distributed through a public database to enable additional analyses and modeling (cng.gmu.edu/brava).

Introduction

Better understanding of physiological function and pathological dysfunction of cerebrovascular system requires the quantitative characterization of its architecture. Cerebrovascular disorders affect a large portion of the human population and are a leading cause of death, devastating morbidity, and long-term disabilities worldwide. Individual and group variations in the neurovascular structure-function relationship have not yet been comprehensively investigated. It is not yet known, for example, whether the higher rate of subarachnoid hemorrhages in women is due to hormonal differences and/or wall shear stress variations (Ghods et al., 2012).

Magnetic resonance angiography (MRA) allows non-invasive, three-dimensional visualization of cerebral arteries based on the contrast between rapidly moving arterial blood and stationary tissues that surround the vessel. To date, most MRA studies have been limited to qualitative or semi-quantitative assessments (El-Barhoun et al., 2009), partial morphometric analyses (Bullitt et al., 2009; Chen et al., 2009), small numbers of subjects (Canham and Finlay 2004) and proprietary data sets (Nowinski et al., 2009). A

more comprehensive structural characterization of cerebral arterial tree can be achieved by reconstructing the vascular arborization into an explicit 3D representation (Passat et al., 2006; Bullitt et al., 2005). In addition to enabling extensive morphometric analysis, these reconstructions also provides an essential substrate to implement subject-specific computational fluid dynamics modeling for investigation of individual risks of vascular malformation (Oshima et al., 2001, Cebal et al., 2003). These approaches require specification of appropriate boundary conditions and constraints related to arterial branch geometry and bifurcation characteristics (Olufsen et al., 1999; Cebal et al., 2003; Cebal et al., 2000). In the absence of a representative sample of available complete reconstructions, such numerical simulations so far have mostly relied on surrogate arterial tree models (Olufsen et al., 2000; Karch et al., 1999; Bui et al., 2010; Dokoumetzidis et al., 2003).

We applied a method originally developed for 3D reconstruction and analysis of neuronal trees (Halavi et al., 2012) to digitally reconstruct the cerebral arterial vasculature of 61 healthy human subjects imaged with high-resolution time-of-flight (TOF) MRA. All visible structures were reconstructed, including the basilar and two carotid arteries entering the brain, the circle of Willis (CoW) and the six major arteries stemming from it, namely right and left Middle, Anterior, and Posterior Cerebral Arteries (MCAs, ACAs, and PCAs, respectively). These six arteries in particular could be followed and reconstructed for ~300 mm from the CoW, typically through ~15 bifurcation points along the paths. Such a collection constitutes an unprecedented data set in terms of completeness and sample size.

We report the first extensive quantitative analysis of the global and local anatomical features of arterial vasculature including size, symmetry, branching characteristics, bifurcation angles, and path meandering. We focused on morphological measures most relevant to common pathological conditions and least affected by potential imaging limitations. In addition to characterizing normative statistics for this representative population sample, we systematically compare arterial geometry between hemispheres, genders, and branch types, among arteries, along the path, and across subject ages. Our analysis reproduces and greatly extends previous knowledge of the human cerebrovascular architecture. In addition to the tools to reconstruct, visualize, and analyze the vascular arbors, we are publicly distributing the entire dataset online for continuous re-analysis and computational modeling by the research community.

Methods

MRA Acquisition

Imaging data were collected at the Research Imaging Institute, University of Texas Health Science Center at San Antonio, using Siemens TRIO, 3T scanner and 12-channel head coil. MRA data for 61 healthy, right-handed participants (36/25 F/M, average age=31.2±10.7, range=19-64 years) using a 3D, spoiled, gradient echo time-of-flight (TOF) MRA (Huettel et al., 2004) sequence with the following control parameters: TE/TR/Flip Angle = 4.4 ms / 24.0 ms / 18° and 620 μm isotropic resolution. Two overlapping slabs with thickness of 100 mm and aligned with AC-PC were used to reduce the saturation of TOF effects, while achieving full brain coverage. Head motion was suppressed using expandable foam and mechanical head-holder. The slab thickness and

excitation angles were varied in two healthy volunteers to achieve reliable digital reconstructions. The final parameters used in this study can be downloaded from the reconstruction database. The study design was evaluated and approved by the Institutional Review Board at the University of Texas Health Science Center in San Antonio and all subjects signed an informed consent form.

Digital Reconstructions

MRA image stacks were visualized with ImageJ, a Java imaging program developed and freely distributed by the National Institutes of Health (imagej.nih.gov; Collins TJ, 2007). All reconstructions were carried out by the same person (SNW) using the freeware Neuron_Morpho plugin (personal.soton.ac.uk/dales/morpho; Brown et al., 2005) and were saved as ASCII files in the SWC format (Ascoli et al., 2001). The SWC format fully describes branching structures as a parsimonious series of interconnected tapering cylinders characterized by their x, y, and z positions, radius, the identity of the parent cylinder, and an arbitrary “color” to label structures of interest.

The arterial vasculature was reconstructed as a single arborization in each subject in order to make it amenable to the extensive morphometric characterization available for tree structures. Specifically, we manually reconstructed the trees stemming from the basilar artery (BA) and internal carotid arteries (ICAs), and the first visible point along the BA was chosen as the origin for the vascular tree in every subject. All visible connecting vessels of the CoW were also reconstructed, with the exclusion of the anterior communicating arteries so as to ensure unambiguous maintenance of a binary tree structure of the resulting reconstructions in all subjects, greatly aiding consistent

comparisons within and across the population sample. All six major arteries stemming from the CoW (right and left MCAs, ACAs, and PCAs) were completely reconstructed through each visible ending.

The vascular reconstructions were systematically validated by running a battery of tests to detect defects such as intersecting branches, zero-diameter branches, spatially overlapping branches, disconnected branches, etc. (Halavi et al, 2008) followed by thorough visual inspection to identify and correct these defects. Reconstruction accuracy was also visually verified by overlaying the reconstructed arborization onto the original MRA image stack and 3D volume renderings.

Morphological Analysis

Morphometric parameters were extracted from the digital reconstructions using L-Measure (<http://krasnow1.gmu.edu/cn3>), an open source tool originally developed to quantify axonal and dendritic morphology (Scorcioni et al., 2008). An expansive battery of variables was selected so as to yield a comprehensive statistical characterization of angiographic anatomy at both global and local levels, including measurements of size, distances, angles, and branching structure. In order to explain the definitions of the non-trivial metrics, we adopt the following standard terminological notation (e.g. Brown et al., 2008). Additional details, as well as diagrams accompanying each morphometric definition, are documented online on the L-Measure help page.

We refer to a *branch* as a sequence of reconstruction points starting from a bifurcation (or from the root) and ending at the next bifurcation (*bifurcating branch*) or at a termination (*terminating branch*). The *branch order* is the number of bifurcations

between a given point in the arborization and the root. The branch path length or simply *branch length* is the geodesic distance between the beginning and ending of a branch (i.e., the sum length along the branch). Branch *tortuosity* is the ratio between branch length and the Euclidean (straight) distance between its beginning and ending (Diedrich et al., 2011). The *fractal dimension* is the slope of the linear regression obtained from the log-log scatter plot of path vs. Euclidean length moving from the second to the last reconstruction point along a branch.

The *total length* of an arborization is the sum of all of its branch lengths. Its *maximum path* and *Euclidean distances* are respectively the geodesic and straight distances from the root to the farthest termination points (the farthest geodesic and Euclidean points do not necessarily coincide). The *height* of an arborization is the minimum vertical span of a box encompassing the brain in the horizontal plane that contains 95% of the reconstruction points. *Width* and *depth* are similarly defined for the spans perpendicular to the sagittal and coronal planes, respectively.

Two types of amplitude angles were measured at bifurcations. The *remote bifurcation amplitude* is the angle between the bifurcation point and the last reconstruction points of each of the two branches away from the root. The *local bifurcation amplitude* is the angle between the bifurcation point and the first reconstruction points of each of the two branches away from the root. The (remote) *tilt* is the smaller of the two angles between the bifurcation point, the previous bifurcation towards the root, and each of the last reconstruction points of the two branches away from the root. The *torque* is the angle between the plane of the current bifurcation and the

plane of the previous bifurcation towards the root. The bifurcation *partition* measures the imbalance between the numbers of terminations in the two sub-trees, and is defined as the ratio of the difference between these two numbers over their sum minus two (Van Pelt et al., 1992). This formulation yields a unitary partition for fully asymmetric bifurcations (giving rise to one terminating and one bifurcating branch) and a nil partition for fully symmetric bifurcations (with identical numbers of terminations in the two sub-trees).

Statistical Analysis

Differences between groups of reconstructions were assessed by Student's t test (for normally distributed variables) and Wilcoxon-Mann-Whitney nonparametric test (otherwise). Significance was determined by two-tailed exact p values after Bonferroni correction for multiple testing. Pairwise correlations were determined with Pearson's coefficient, with the p values indicating the probability of independent distributions. The age difference between males (31.48 ± 10.12) and females (30.97 ± 10.23) was not significant ($p > 0.1$). In selected analyses the sample was also divided by median age (28 years) into an older (38.2 ± 9.2 , $N=32$) and a younger (23.4 ± 2.4 , $N=29$) group.

Data Archival and Dissemination

All digital reconstruction files used in this study along with extracted morphological measurements and metadata are available for download at cng.gmu.edu/brava. The relational database was designed with the open source management system MySQL v. 5.0 (<http://www.mysql.com>; Tahaghoghi and Williams, 2006; Zawodny and Balling, 2004). The graphical user interface (GUI) was created with the free scripting language PHP v. 5.2.9 (<http://www.php.net>; Sklar, 2004) and HTML

(Shelly and Woods, 2004) to enable seamless data browsing, searching, organizing, and downloading by metadata or morphometric statistics.

Results

Visual Aspect and Inter-Subject Variation of Reconstructed Arterial Vasculature

Brain arterial arbors were digitally reconstructed from 36 females (31.0 ± 10.2 years old) and 25 males (31.5 ± 10.1 years old), beginning at the first visible point along the basilar artery and including internal carotid arteries, the CoW, and the MCAs, ACAs, and PCAs (Figure 2.1). All three planar views (horizontal, coronal, and sagittal) were used in the course of the reconstruction depending on the orientation of the branch being traced. Although arterial vessels were always reconstructed from individual sections (Figure 2.1A), occasional toggling to maximum intensity projections was useful to assess the full extent of the structure (Figure 2.1B). Throughout the tracing process, the (partial or complete) reconstructed structures were periodically embedded in the data to verify their accuracy and facilitate correction of reconstruction errors using perpendicular views (Figure 2.1C) or pseudo-3D rotational volume rendering. A second investigator (FM) independently inspected all reconstructions for quality.

The reconstruction pipeline successfully yielded complete digital reconstructions (down to the image resolution) for all subjects. The two reconstructions from the same subject imaged twice by independent operators on different scanners confirmed high reproducibility both by visual assessment and morphometric comparison. The six major arteries stemming from the CoW (Figure 2.1D) were present in every subject and the same color scheme (Figure 2.1E) was used consistently across the entire sample. High-

resolution rendering of complete individual reconstructions provided visual information about the detailed vascular patterns within and across hemispheres, subjects, genders, and ages (Figure 2.2). Qualitative comparison among the entire sample revealed noteworthy inter-subject variability of the size and shape of the six major arteries and entire arbors (Figure 2.3), prompting further investigation by morphometric analysis.

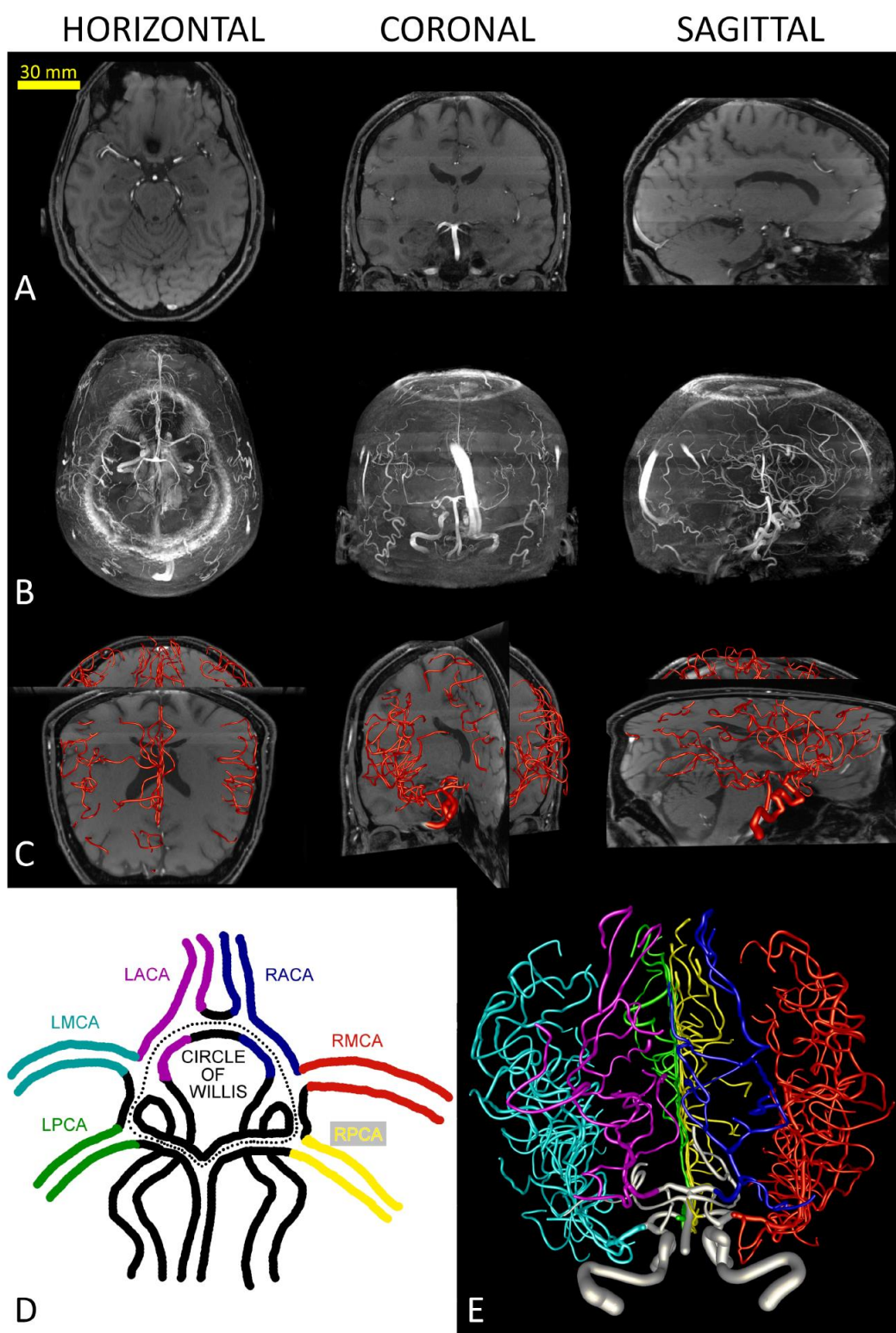


Figure 2.1. Digital reconstructions of human brain vasculature from MRA imaging. **A.** Arterial arbors are semi-manually traced from single planar sections of each image stack in horizontal, coronal or sagittal views. **B.** Maximum intensity projections in the same orientations reveal a fuller extent of the imaged structure. **C.** Embedding of the final reconstructed arborization within the original image stack enables tracing validation by facilitating critical inspection of branch correspondence and identification of incomplete sub-trees. **D.** Color-coded schematic of the Circle of Willis and the six major arteries stemming from it. **E.** Complete reconstruction of the brain vasculature corresponding to panels A-C (from a 59 year-old male) and color-coded by artery according to panel D.

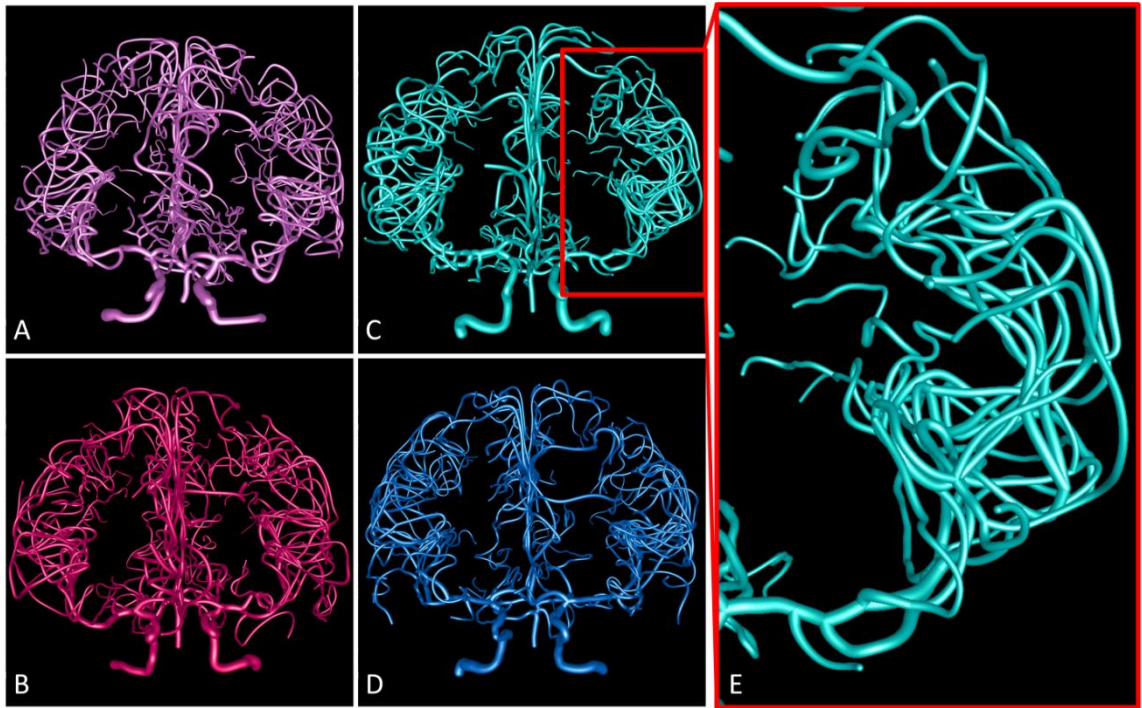


Figure 2.2. Representative arterial reconstructions color-coded by age and gender. **A.** Female, age 19 (light pink). **B.** Female, age 47 (dark pink). **C.** Male, age 21 (light blue). **D.** Male, age 46 (dark blue). **E.** Zoom-in on the left MCA, the largest of the arteries stemming from the Circle of Willis, from panel C.

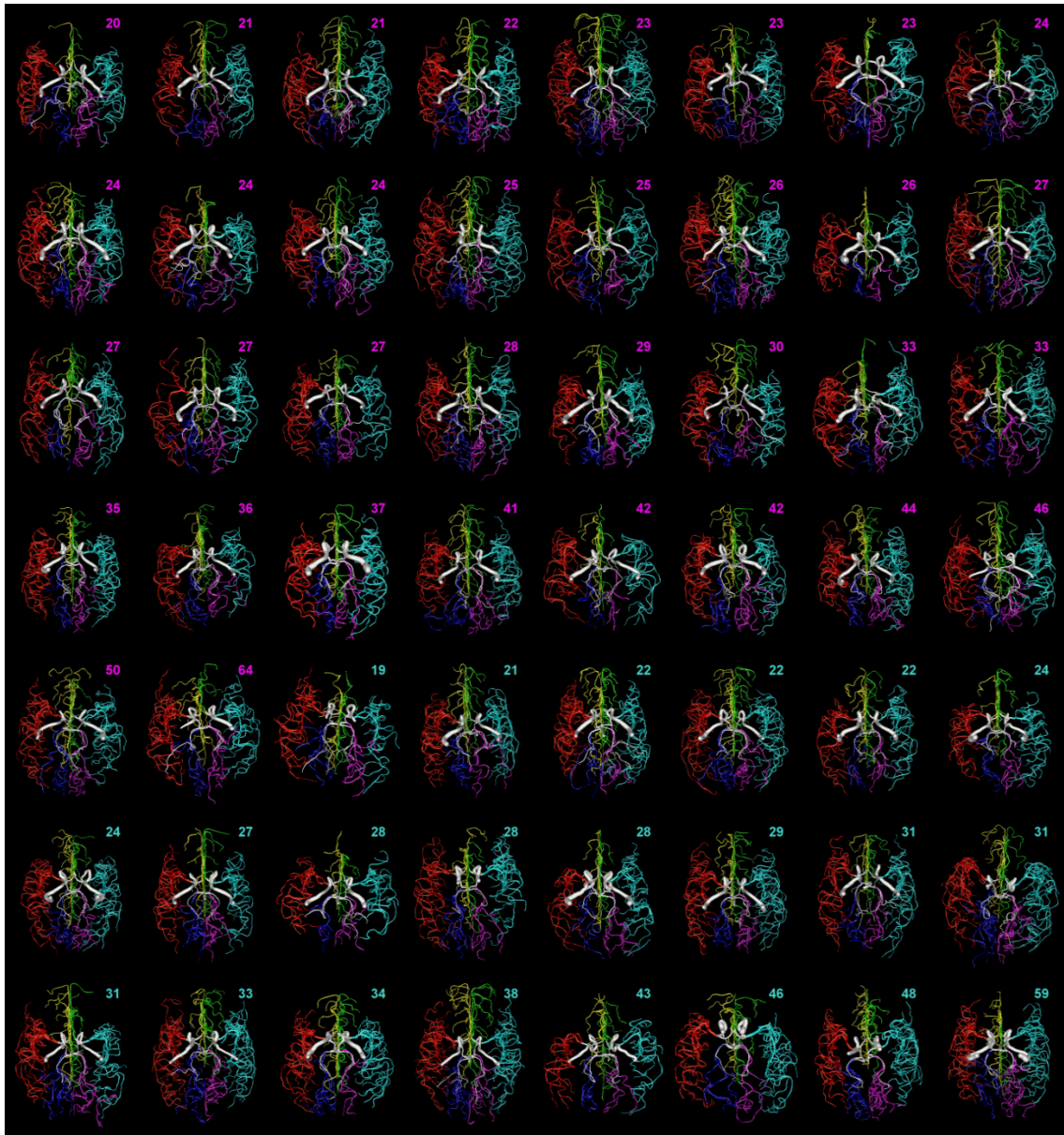


Figure 2.3. Visual variability of arterial structure across the population sample. All complete reconstructions (except those displayed in Figures 2.1 and 2.2) are ordered in this montage by age and gender and color-coded by artery. Ages of females and males are shown in pink and blue, respectively.

Quantitative Anatomy of Human Brain Arteries

As a simple initial normative quantification of arterial morphology and variability within our dataset, we extracted summary statistics for several scalar parameters characterizing the entire vascular structure in terms of overall size, bifurcation angles and symmetry, and branches features (Table 2.1). Because of the sensitivity of the apparent diameter on blood flow in TOF MRA (Lell et al., 2007), we focused our analysis on diameter-independent parameters.

The variability of overall size was similar to that reported for other measures of human body size (e.g. ISO, 2010). For example, the coefficients of variation (CVs) for total length and number of branches were between 0.1 and 0.2, and the corresponding ranges went from 65% to 160% of the respective means. The various metrics of size were highly cross-correlated (e.g. between total length and number of branches: $R=0.83$, $p<0.05$). We also compared each of these metrics between right and left hemispheres, males and females, and as a function of age. None of the differences were statistically significant, with the only exception of height, which was greater in males than in females (85.66 ± 4.14 mm vs. 83.81 ± 2.94 mm, $p=0.0006$), again possibly reflecting the same trend in body size (ISO, 2010). A previously reported measurement of total arterial length from a single (51 year old male) subject, 7519 mm (Nowinski et al., 2011) fell approximately half a standard deviation from our sample mean and within our sample range (Table 2.1) by a comfortable margin.

Bifurcation characteristics are important as the prevalence of aneurysms is higher at or near bifurcations (Lindekleiv et al., 2010). These metrics represent sample means of averages within arbors, and therefore display a substantially lower variability (e.g.

CV<0.05 for mean amplitude and range from 88% to 114% of the mean). Interestingly, the local amplitude angle was nearly one and a half times larger than the remote amplitude angle ($p<10^{-6}$). Bifurcations started at nearly orthogonal angles, but branches tended to grow towards each other before bifurcating again or terminating. The distribution of partition values indicates that arterial bifurcations display an intermediate arbor balance between perfectly symmetric and fully asymmetric trees. As for overall size, there were no statistical differences in measured bifurcation characteristics between hemispheres, genders, and across age, suggesting that these summary scalar metrics alone cannot explain group or bilateral differences of aneurysm prevalence.

Branch features are also relevant to cerebrovascular disease. For example, branch meandering, as measured by tortuosity (Bullitt et al., 2003) is altered in pathologies as different as stroke (Alazzaz et al., 2000), diabetes (Moritani et al., 2001; Liem et al., 1996), anemia (Vicari et al., 2011), and hypertension (Spangler et al., 1994; Diedrich et al., 2011). Earlier morphological investigations on neuronal dendrites described substantially longer terminating branches than bifurcating branches (Claiborne et al., 1990). These studies, however, did not extend to other branch characteristics, such as tortuosity, or multiple neuron types. When separately analyzing bifurcating and terminating branches (Table 2.1), we found surprisingly large and highly significant differences in branch length, tortuosity, and fractal dimension ($p<10^{-4}$ in all three cases). Specifically, terminating branches were on average 73% longer, 28% more tortuous, and 6% more fractal than bifurcating branches.

Although these branch properties, similarly to size and bifurcation features, did not change between hemispheres and genders, we found significant changes with the age of the subjects (Figure 2.4). Tortuosity increased with age in both bifurcating and terminating branches (Figure 2.4A). Fractal dimension increased with age in terminating, but not bifurcating branches (Figure 2.4B). In contrast, branch length increased in bifurcating, but not terminating branches (Figure 2.4C). Further investigation will be necessary to determine the source and functional implication of these distinctions.

We are excluding diameter-based measures in this normative characterization because vascular diameter in TOF MRA depends on blood flow, rendering a purely structural interpretation ambiguous, especially at higher branch order. However, we checked whether diameter differed by gender or changed by age in the first few branch orders, and found no significant differences in either case (data not shown).

Table 2.1 - Whole Arterial Metrics

	Metric	Overall (N=61) $\mu \pm \sigma$ (min-max)
Overall Size	Total # Branches	208.6 \pm 39.6 (138-330)
	Total Length (mm)	7002.8 \pm 945.8 (4752-9171)
	Max Branch Order	15.46 \pm 1.34 (13-19)
	Max Path Distance (mm)	289.0 \pm 23.5 (250-362)
	Max Euclidean Distance (mm)	108.9 \pm 4.8 (98-123)
	Width (mm)	118.3 \pm 5.0 (109-129)
	Height (mm)	84.6 \pm 3.6 (76-93)
	Depth (mm)	130.0 \pm 9.1 (102-146)
Bifurcation	Mean Bifurcation Tilt (°)	45.69 \pm 4.35 (37.13-56.60)
	Mean Bifurcation Torque (°)	54.31 \pm 2.29 (48.61-60.28)
	Mean Bifurcation Amplitude (°)	60.83 \pm 2.97 (53.49-69.21)
	Mean Local Bifurcation Amplitude (°)	89.43 \pm 3.19 (83.21-98.62)
	Mean Partition	0.51 \pm 0.04 (0.41-0.59)
Branch	Mean Bifurcating Tortuosity	1.28 \pm 0.05 (1.17-1.40)
	Mean Terminating Tortuosity	1.64 \pm 0.09 (1.47-1.84)
	Mean Bifurcating Fractal Dimension	1.09 \pm 0.01 (1.06-1.13)
	Mean Terminating Fractal Dimension	1.15 \pm 0.02 (1.11-1.19)
	Mean Bifurcating Branch Length (mm)	25.02 \pm 2.71 (19.35-30.14)
	Mean Terminating Branch Length (mm)	43.25 \pm 5.35 (32.72-60.42)

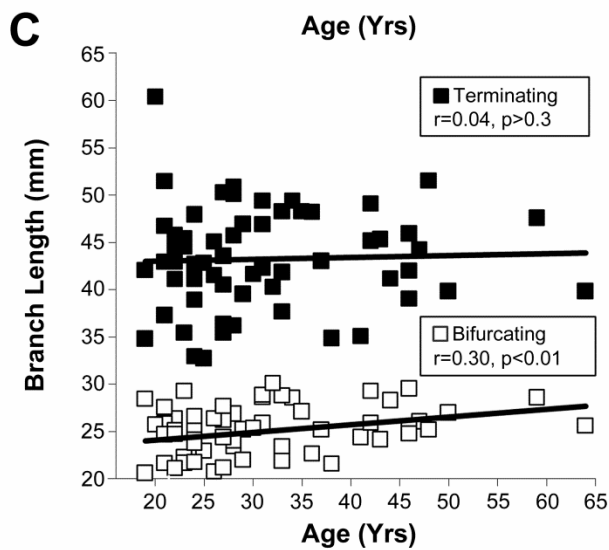
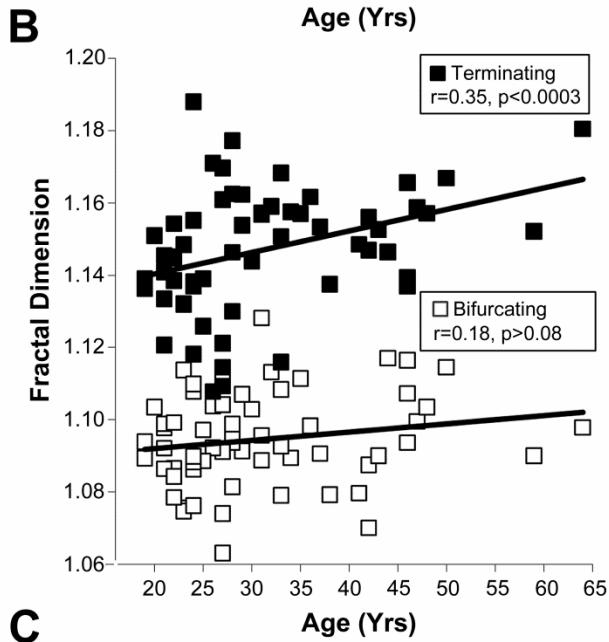
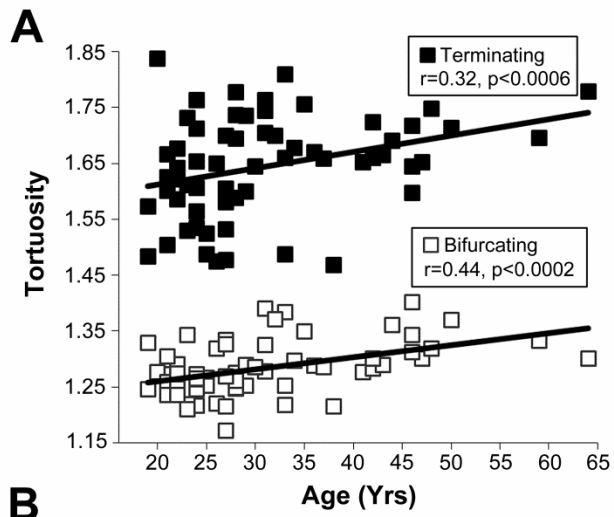


Figure 2.4. Change of bifurcating and terminating branch metrics with age. **A.** Branch tortuosity statistically tends to increase with the age of subjects. **B.** Fractal dimension significantly increases with age in terminating, but not bifurcating, branches. **C.** Branch length significantly increases with age in bifurcating, but not terminating, branches.

Size Differences and Proportional Scaling Among Cerebral Arteries

Next we examined the scalar morphometric characteristics of individual cerebral arteries (Table 2.2). As expected, MCAs were significantly larger than ACAs, and ACAs were significantly larger than PCAs. For example, MCAs had twice as many branches and twice as much total length as ACAs, and ACAs had 50% as many branches and 50% as much total length than PCAs ($p < 10^{-4}$ for each of these comparisons). While these trends tended to be generally true across the sample, the size distribution of ACAs overlapped with both the MCA and PCA size distributions, and there were occasional exceptions of individuals with larger PCAs than MCAs. Moreover, the height, width, and depth of individual arteries did not systematically follow the same trends even at the level of sample means, because of the different orientation of the cerebral arteries relative to the canonical (horizontal, coronal, and sagittal) planes of the brain.

We also extracted all bifurcation and branch scalar morphometrics for the individual cerebral arteries (data not shown), and they were all statistically indistinguishable from the distributions reported in Table 2.1 ($p > 0.1$ in all cases). All the above measurements were also compared between males and females, right and left hemispheres, and across subject age (not shown), and no additional significant differences were found relative to the analysis of whole vasculature. The previously reported length values from an individual subject (Nowinski et al., 2011), while larger than our means (MCA: 2198.7 mm; ACA: 1229.9 mm; PCA: 528.1 mm) fell within statistical expectation and the observed range of our sample.

While summary statistics are useful by providing normative populations baselines and a simple overview of vascular morphology, a more in-depth analysis is necessary to characterize the detailed arterial architecture within and among individual brains. We first focused on individual hemispheric dominance, or laterality (Figure 2.5). There was a strong linear correlation between right and left length across the sample (Figure 2.5A) and within genders, age groups, and artery types ($R > 0.65$, $p < 0.001$ in all cases). Although there was no overall hemispheric dominance across the sample, we investigated individual lateralization by defining *laterality* (\mathcal{L}) as the absolute inter-hemispheric length difference normalized by total length:

$$\mathcal{L} = |R - L| / (R + L),$$

where R and L are the right and left lengths, respectively). The distribution of laterality was statistically equivalent between genders and age groups, and whether calculated from 183 artery pairs (Figure 2.5B) or the complete hemispheric vasculatures

of 61 individuals. Interestingly, however, ACAs were significantly more lateralized than MCAs (Figure 2.5C), but there were no other differences between cerebral arteries.

The within-subject composition of arterial length was further considered to determine whether cerebral arteries might compensate for each other (Figure 2.6). Specifically, we have recently discovered a form of morphological homeostasis in cortical dendrites (Samsonovich and Ascoli, 2006), whereas if a neuron is found to have a dendritic (sub-)tree smaller than expected based on population expectation, it would also tend to possess another (sub-)tree larger than average. It is unknown whether the same phenomenon might apply to brain arterial vasculature. The (bilateral) length of each cerebral artery visually appears to scale proportionally with overall size (Figure 2.6A). Indeed, a significantly positive length cross-correlation was found between each artery and the rest of the vascular arborization (R values for MCA, ACA, and PCA: 0.68, 0.56, and 0.53, respectively, $p < 10^{-4}$ in all cases), as well as between each pair of arteries (not shown). These data do not support the compensatory hypothesis. On the contrary, they suggest proportional scaling of brain arteries: if the vasculature is big, every artery is big, and vice versa.

To further test this possibility, we generated one hundred surrogate datasets by stochastically (but exclusively, i.e. non-repetitively) picking one of the six cerebral arteries from our sample. Then we measured the standard deviation of their total length and compared it to the observed value of the (single) real distribution. Morphological homeostasis and proportional scaling produce opposite predictions that the surrogate variance should be respectively greater and smaller than the real one. The result (Figure

2.6B) provides uncontroversial support for proportional scaling, falsifying the compensation hypothesis. The same analyses (Figures 2.5 and 2.6) repeated with other size metrics (e.g. number of branches) supported the same conclusions.

Table 2.2 - Individual Artery Metrics

Metric	ACA (N=122) $\mu \pm \sigma$ (min-max)	MCA (N=122) $\mu \pm \sigma$ (min-max)	PCA (N=122) $\mu \pm \sigma$ (min-max)
Total Number of Branches	26.0 \pm 8.5 (4-52)	52.7 \pm 11.2 (30-94)	18.9 \pm 5.9 (6-34)
Total Length (mm)	877.4 \pm 201.3 (234-1344)	1878.2 \pm 297.4 (967-2636)	500.8 \pm 124.1 (228-770)
Max Branch Order	6.15 \pm 1.53 (1-10)	8.80 \pm 1.40 (6-13)	5.93 \pm 1.66 (2-10)
Max Path Distance (mm)	187.1 \pm 18.7 (143-268)	224.7 \pm 22.1 (182-298)	150.5 \pm 16.6 (111-194)
Max Euclidean Distance (mm)	96.3 \pm 9.1 (66-113)	98.7 \pm 6.2 (80-112)	90.7 \pm 7.1 (70-102)
Width (mm)	26.0 \pm 5.4 (10-48)	38.5 \pm 3.0 (33-48)	30.5 \pm 6.9 (16-49)
Height (mm)	72.5 \pm 7.5 (50-98)	69.4 \pm 5.6 (52-85)	52.4 \pm 10.2 (21-74)
Depth (mm)	109.1 \pm 14.3 (52-149)	105.6 \pm 10.0 (77-127)	66.3 \pm 6.7 (52-86)

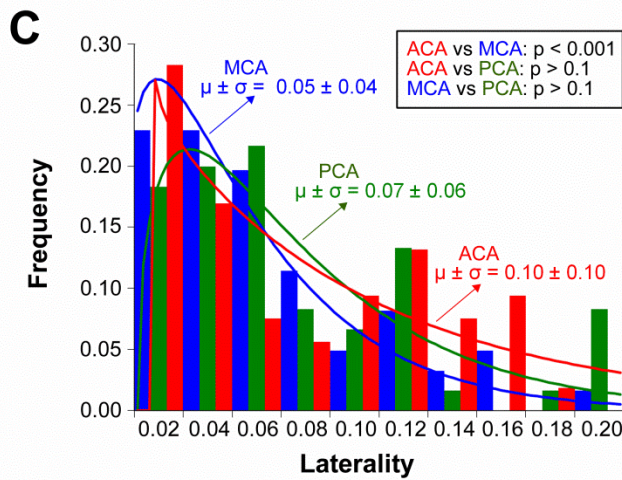
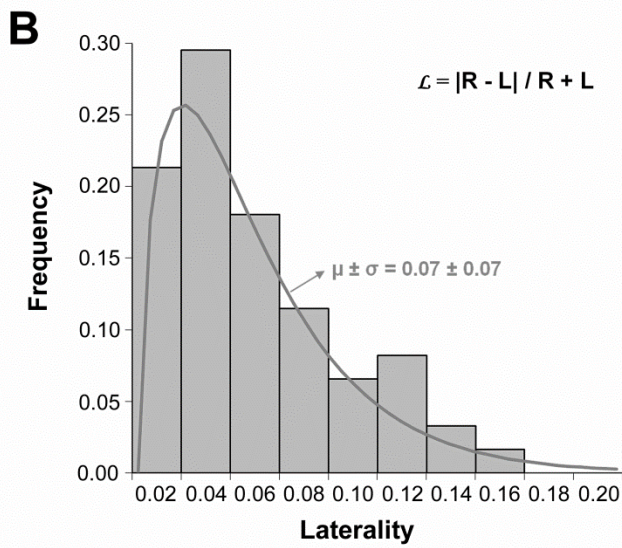
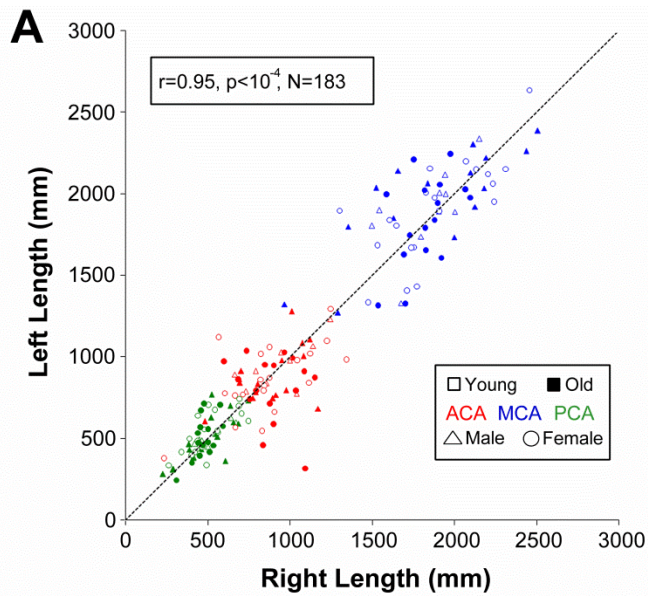


Figure 2.5. Hemispheric laterality of reconstructed vasculature length. A.

The length differences between left and right artery pairs tend to vary in both directions and proportionally across trees. The dashed line indicates where left and right artery pairs would be of identical length. **B.** Laterality is the normalized absolute inter-hemispheres length difference within artery pairs (in the formula, R and L represent right and left lengths, respectively). **C.** ACA is significantly more lateralized than MCA, but there are no other differences between arteries, gender, and age.

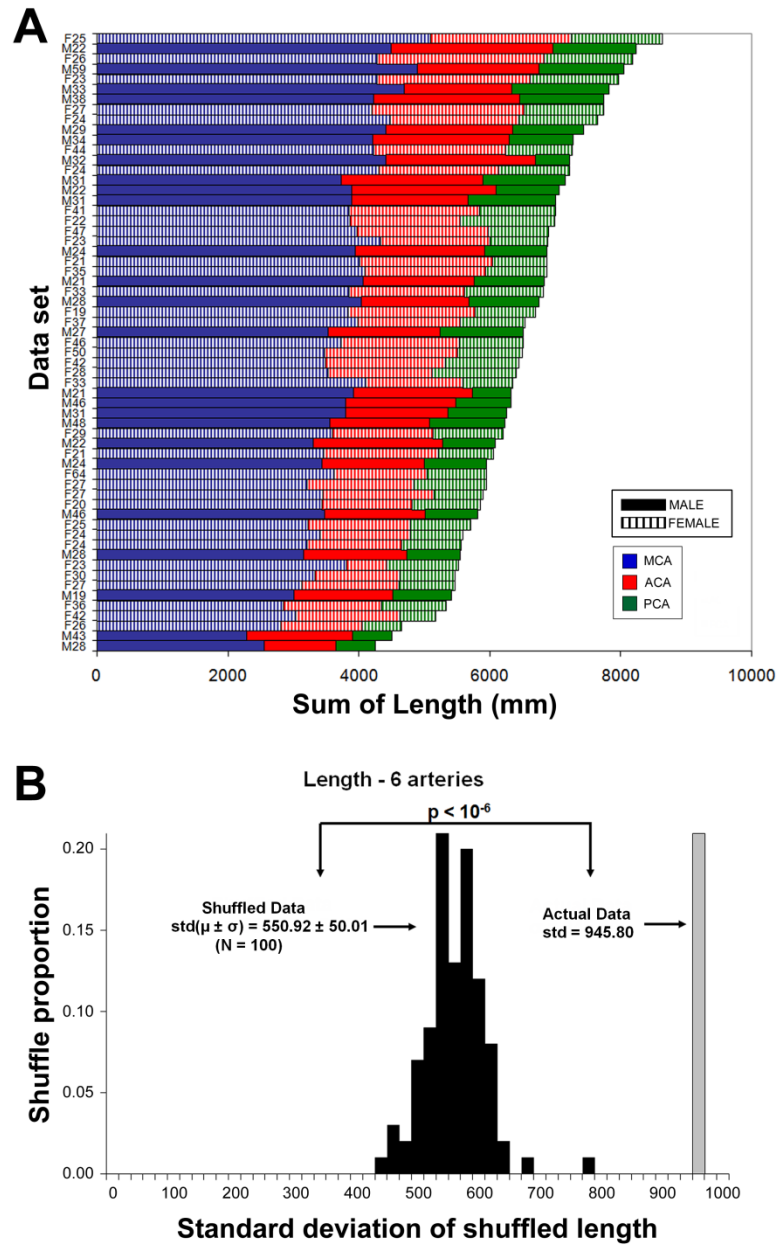


Figure 2.6. Individual artery length co-varies with total vasculature extent. **A.** Combined left/right arterial composition of all individual subjects ranked by total length reveals similar distributions across ages and genders. **B.** The observed population variance of the total arterial length is nearly 8 standard deviations greater than the mean length obtained by stochastically shuffling each of the corresponding 6 arteries within the sample. This indicates that subjects with longer-than-average vasculature also tend to have longer-than-average individual arteries.

Systematic Variation of Selected Morphometric Properties along the Vascular Path

Lastly, we tested whether vascular morphology varied systematically along the arterial path or was uniform from the CoW to the terminations (Figure 2.7). The lengths of the major cerebral arteries were normally distributed across path distance (Figure 2.7A: best fitting means and standard deviations of the sample distributions were 1878.2 ± 297.4 , 877.4 ± 201.3 , and 500.8 ± 124.1 mm for MCAs, ACAs, and PCAs, respectively). Bifurcating and terminating branch distributions had opposite skews (Figure 2.7B): bifurcating branches arborize densely near the CoW and gently drop off; terminating branches increase slowly to peak farther out and decrease suddenly shortly thereafter. The length and tortuosity of bifurcating branches increase linearly along the path from the CoW (Figure 2.7C), whereas terminating branches remain constant throughout the tree. Due to these contrasting behaviors, the values of the two branch types become similar around the distance at which terminating branches are densest (cf. Figure 2.7B).

Branching angles are independent of path distance ($R^2 < 0.04$, $p > 0.3$ in all cases), except near the CoW, where remote amplitude is similar to local amplitude (Figure 7D), decreasing to a constant mean angle after ~ 90 . This may be explained by the shorter branch lengths near the CoW (cf. Figure 2.7C), reducing the opportunity for branches to meander closer toward each other. Indeed, remote amplitude is significantly different between branches shorter and longer than 20 mm length ($66 \pm 4^\circ$, $N=3333$ vs. $54 \pm 32^\circ$, $N = 2965$, respectively, $p < 10^{-4}$). Additionally, remote amplitude is negatively correlated with branch length, but only in shorter (< 20 mm) branches, suggesting a length threshold

to provide branches with enough freedom to reach their optimal angular spread. All individual cerebral arteries had similar trends when analyzed separately (not shown).

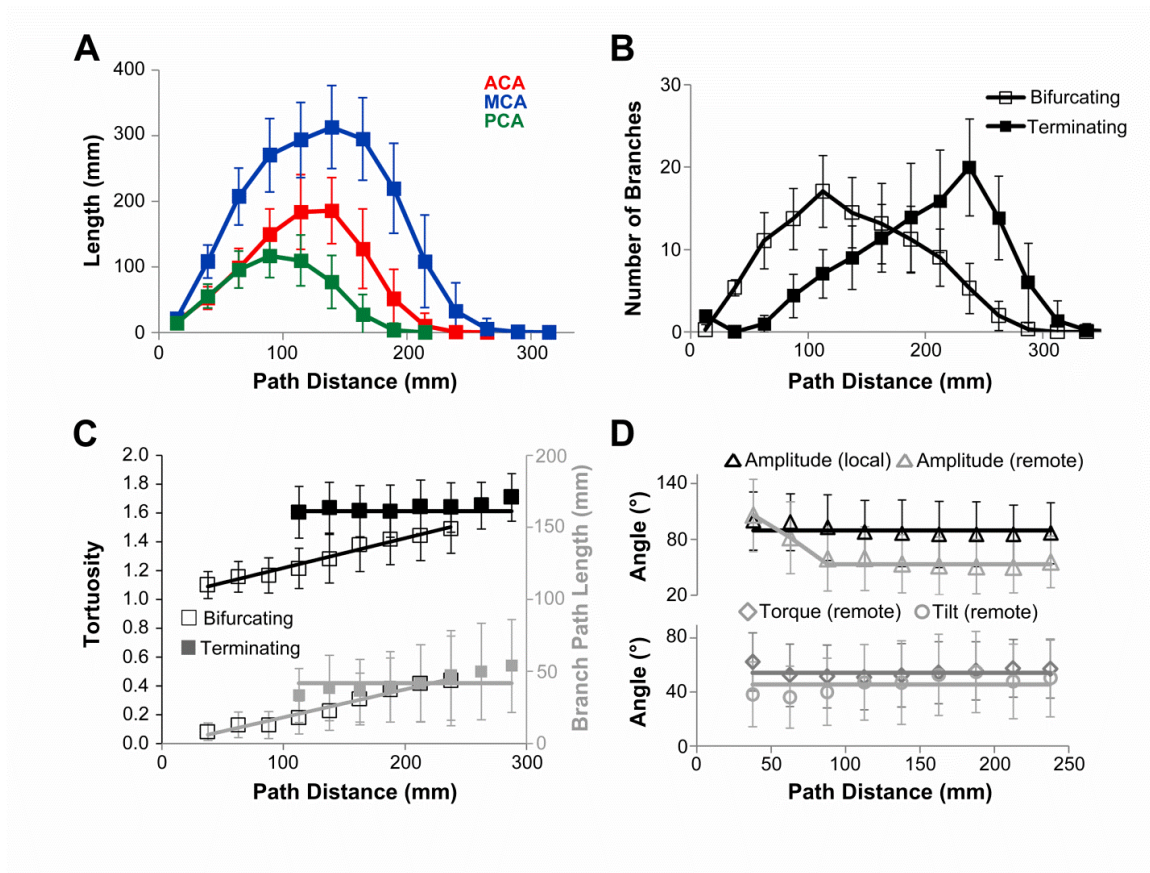


Figure 2.7. Vasculature extent, branching, and selected local metrics vary along the arterial path. **A.** Arterial length is normally distributed across the path distance from the Circle of Willis and scales across MCAs, ACAs, and PCAs. **B.** Bifurcating and terminating branch distributions have opposite skews: the number of bifurcating branches peaks near the circle of Willis and gradually decreases thereafter; the number of terminating branches increases slowly and drops off suddenly at farther path distances. **C.** Branch length and tortuosity increase with path distance for bifurcating, but not terminating branches. **D.** Branching angles are largely constant along the arterial path: local amplitude is always larger than the (“remote”) angle measured at the end of the branch, except near the CoW.

Public Online Availability of Reconstructions

The normative dataset of 61 vascular reconstructions are freely downloadable at cng.gmu.edu/brava (Figure 2.8). Boolean searches allow fast data retrieval filtered by any combination of the described morphometric features as well as subject age and gender. The reconstructions can be viewed as raw coordinate files or pseudo-3D visualized as rotating growth animations with color-coded individual arteries. The data include diameters information, whose analysis may be challenging to interpret. Similar to neuronal reconstructions at NeuroMorpho.Org, users can also render and manipulate the reconstructions within their browser in a built-in virtual reality online display. The morphometric results are also stored in the database and can be queried for complete trees or each of the six major arteries.

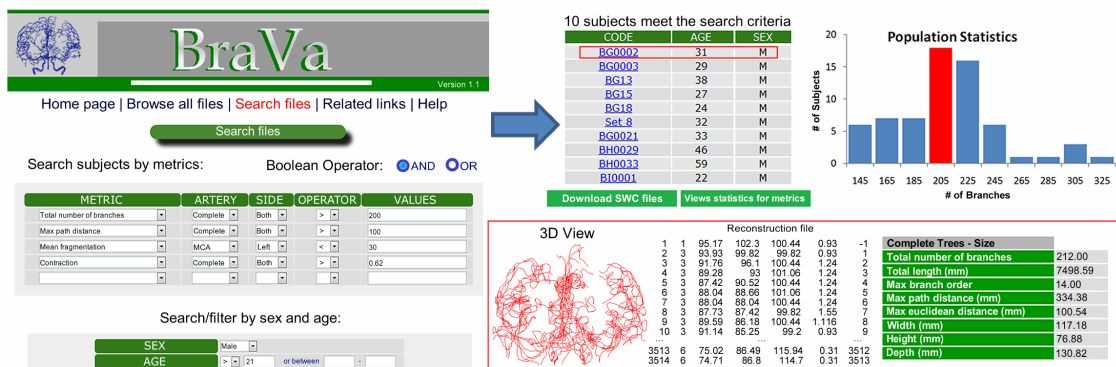


Figure 2.8. Accessibility and function of the BraVa database. The complete digital arterial reconstructions from all 61 MRA-imaged subjects described in this study, as well as the individual arteries, can be searched, downloaded, analyzed, and visualized by morphometric features and metadata.

Discussion

Understanding the structure-function relationship is an important goal in the investigation of all biological systems. Arterial vasculature provides oxygenation and metabolic transport to the territory it invades. Thus, the primary function of vascular arborization is fundamentally linked to its architecture. Moreover, vessel morphology directly affects fluid dynamics, much like the branching structure of dendritic trees affects the passive flow of electric current in neurons (Lindsay et al., 2004).

Computational neuroscience simulations are often based on computer models built on detailed digital reconstructions of neuronal morphology, enabling detailed investigation of the relationship between dendritic structure and activity. Digitally reconstructing neuronal dendrites (from microscopic imaging) also enables extensive statistical analysis and comparison across neuron types, brain regions, species, and experimental conditions. Here we adapted the same approach to a different scale, with the goal of quantitatively characterizing the entire vascular arborization non-invasively imaged by MRA in a sufficiently large sample of human subjects to allow statistical comparison between genders, ages, hemispheres, and main arterial trees. Earlier imaging data based upon hemodynamic response of blood vessels provided useful information on vascular anatomy, including arterial bifurcations (Fanucci et al., 1988, 1990; Rossitti and Lofgren, 1993; Karch et al., 2000) and branch tapering (MacLean et al., 1992, Roach and MacLean, 1993). However, these prior studies were somewhat limited in the number of subject, completeness of the reconstruction, or detail of the quantitative analysis. Our

study confirmed and vastly expanded previous results on the arterial morphology of the human brain.

Precise characterization of vascular anatomy is important for understanding cerebrovascular diseases (O'Flynn et al., 2007) and formation of intracranial aneurysms in particular (Canham and Finlay, 2004; Ingebrigtsen et al., 2004; Bor et al., 2008). For example, aneurysm prevalence varies between genders and hemispheres (Horiuchi et al., 2006), and sharply increases after the age of 50 (Wardlaw and White, 2000). We measured an extensive battery of global and local morphological properties from the entire vascular arbors to individual arterial branches, including but not limited to size, distances, and angles. None of these geometric features explain gender or hemispheric differences in aneurysm prevalence. However, several differences across age emerged when separately examining bifurcating and terminating branches. Nevertheless, of the 61 subjects used in this study only two females and one male were over the age of 50. Therefore, more data will be needed on older individuals to provide accurate insight into morphological characteristics that might support age prevalence of aneurysms. The most dramatic morphological differences were found between bifurcating and terminating branches, and between bifurcating branches farther and closer to the CoW. These findings raise the intriguing possibility of a structural underpinning of the prevalence of aneurysms near bifurcations (Norman et al., 2010) and closer to the CoW (Kayembe et al., 1984), where almost all branches are bifurcating rather than terminating. Interestingly, tortuosity, usually associated with greater hemorrhagic prevalence, *increased* with distance from the CoW and was higher in terminating than bifurcating

branches. As expected, we found significant differences in the sizes of individual arteries (MCA being the largest and PCA the smallest), which were typically, but not always, consistent across subjects. Local branch properties were similar among arteries and no differences were found between genders and hemispheres in individual arterial trees. Thus, the examined morphological parameters cannot explain the prevalence of aneurysms in the right ACA of males (Horiuchi et al., 2006).

Lateralization of brain function is reflected in major behavioral and cognitive traits. Thus, it was somewhat surprising to find no statistically significant differences in any local or global morphological parameter between right and left arterial vasculatures across the population sample. Specifically, inter-hemispheric differences were present to variable degrees in all individuals, but without a net right or left prevalence. Laterality was similar between males and females, across ages, and was greater for ACAs than for MCAs. The variability of whole arterial arbor size was also similar between genders, and was consistent across individual arteries (i.e. larger right MCA was predictive of larger left ACA), indicating that vascular trees do not compete with or compensate for each other. Both local and remote branching angles remained remarkably constant throughout the arterial vasculature. Arterial bifurcations started at near-orthogonal angles and systematically closed in to significantly narrower remote amplitude. These observations are consistent with optimal design principles proposed to explain other aspects of arterial geometry and function, such as the “principle of minimum work” (Rossitti and Lofgren, 1993), Murray’s Law of dissipation (Sherman, 1981; Painter et al., 2006; Liu and Kassab, 2007), and fractal scaling (Kassab, 2006; Zamir, 2001) similar to other biological systems

(Kamiya and Takahashi, 2007). In contrast, the lack of branch-level differences between hemispheres or among MCAs, ACAs, and PCAs suggests an absence of functional differentiation among cortical regions (e.g. visual vs. motor areas).

While 3T TOF MRA remains the preferred routine technique for detailed morphological analysis of brain arteries (Ahmed and Masaryk, 2004; Insko and Carpenter, 2004; Bammer et al., 2005; Parmar et al., 2005), it is important to recognize its limits. These include saturation of the signal in the direction that is parallel to slab orientation and reduced visibility in the branches with slower flow velocity and near the top of the imaging slab (Wilms et al., 2001), which may have affected our analysis. Yet, while the number of missed branches is greatly reduced from 1.5T to 3T, the relative gain is much more modest if not altogether negligible from 3T to 7T (Nowinski et al, 2011). Moreover, in TOF MRA arterial vessels may appear thinner than in actuality (Vaphiades and Horton, 2005), and the apparent vascular caliber varies with blood flow. For these reasons, we have avoided reporting diameter information. All metrics of size, distance, angles, and topology analyzed in this study are independent of diameter and unaffected by related imaging artifacts. It is possible that arterial thickness is essential to explain gender, age, and hemispheric prevalence of aneurysms. Our limited evaluation of arterial diameter in the first few branch orders from the CoW, however, revealed no significant difference by age or gender. The availability of all reconstructions in our database enables future investigation of additional aspects of arterial morphology with due interpretative care. It would be particularly interesting to compare the diameter measures of these reconstructions with physical “ground truth” measures to facilitate better

estimates from non-invasive imaging. Interestingly, diameter determination is a limiting factor in the morphometry of neuronal dendrites as well (Scorcioni et al, 2004), although the source of the problem is obviously different.

Despite these limitations, this study and the accompanying database provide an unprecedented normative collection of quantitative morphometric parameters measured from *in vivo* 3D imaging of the arterial vasculature of the human brain. This data set can be extended in future studies to a broader range of ages, integrated with other imaging modalities, augmented with vein information, and compared with different experimental conditions including pathological states. Moreover, the reconstructions can be used to implement complex computational models of fluid dynamics that may aid understanding of physiological function and cerebrovascular diseases.

Acknowledgements

This work was supported by NIH grants NS39600, EB001955, EB015611 and NS061770 and by the Human Brain Mapping Project, which was jointly funded by NIMH and NIDA (P20 MH/DA52176). We thank Sridevi Polavaram, Duncan Donohue, Ruggero Scorcioni, Stephen Senft, Maryam Halavi, and other members of CN3, for helpful discussion throughout the course of this project.

CHAPTER THREE: SUBJECT SPECIFIC MODELS OF BLOOD FLOWS IN CEREBRAL ARTERIAL TREES FROM HIGH-RESOLUTION MAGNETIC RESONANCE IMAGES

Introduction

Vector representations (digital reconstructions) of vascular trees can be used to create three-dimensional Computational Fluid Dynamics (CFD) models of the blood flow in healthy human brain vasculatures. Hemodynamics variables including velocity, pressure, and wall shear stress (WSS) can be obtained from such models. Computer simulations of blood flow through the circle of Willis and cerebral arteries provide useful information and insights into the normal cerebral hemodynamics, which can be used for quantitative comparison with pathological conditions such as intracranial aneurysms.

Methods

Digital Reconstructions

MRA data stacks were used to create digital reconstructions of human brain vasculature. As described in Chapter Two, these were 3T time-of-flight MRA scans spanning the entire cerebral volume at 0.6mm isotropic resolution. These digital reconstructions consisted of manual reconstructions of the circle of Willis and main cerebral arteries as a series of interconnected tapering cylinders characterized by their coordinates, diameter, and link to the previous node.

Geometric Models

Geometric models ($N = 6$) were then created from these digital reconstructions.

Figure 3.1 outlines the steps used to create these geometric models. The research team at the Center for Computational Fluid Dynamics at George Mason University has developed in-house software that is used in the creation of CFD models, and was used for the creation of these models. The software includes: 1) ZMD for anatomical modeling 2) GEN3D for mesh generation 3) FEFLO for the numerical solution of the blood flow 4) ZFEM for the visualization of the results, and follows the modeling pipeline (Cebal et al., 2005). Figure 3.2 shows examples of the reconstructions used for the geometric models.

In order to create the geometric model, a cubic spline was used to fit the centerline and radius of each arterial branch. A cylindrical surface triangulation was constructed along each branch. Then, all the branches were merged using an adaptive voxelization technique, resulting in watertight surface representation of the brain vasculature. Cuts were made in the models to allow inflow and outflow; all branches were cut perpendicularly to the axis in the last generation of the arterial tree reconstructions. Examples of these steps are shown in Figure 3.3. The models were checked for errors such as zero diameter-branches, intersecting branches, spatially overlapping branches, disconnected branches, etc., (Halavi et al., 2008). The next step was the creation of the volumetric mesh, shown in Figure 3.4. The surface of the models underwent a triangulation (advancing front technique), and this surface was then used to generate a volumetric grid of composed of tetrahedral elements that fill the interior of anatomical model using an advancing front method (Lohner, 2008). The element size, the

fixed number of elements in a cross-section, was specified using vessel skeletons from the reconstructions. Then, CFD models were made and visualized. Unsteady blood flow simulations were carried out on one data set using the computational grid and a flow solver. The 3D compressible Navier- Stokes equations:

$$\nabla \cdot \mathbf{v} = 0$$

$$\rho \left(\frac{\partial \mathbf{v}}{\partial t} + \mathbf{v} \cdot \nabla \mathbf{v} \right) = - \nabla p + \nabla \cdot \boldsymbol{\tau} + \mathbf{f}$$

which are used to mathematically model blood flow (Mazumdar, 1992, Kundu and Cohen, 2004), were numerically solved using an implicit finite element formulation on unstructured grids. In order to solve these equations, boundary conditions must be specified. For these models, pulsatile flow wave forms from reconstructions of phase contrast magnetic resonance images of normal subjects were imposed at inlets (internal carotid arteries and basilar arteries) and zero pressure boundary conditions were imposed at outlets. These boundary conditions assume that distal resistances are equivalent, and are not entirely physiologically correct. A deflated preconditioned conjugate gradients algorithm was used to solve the pressure Poisson equation at each step of the incompressible flow calculation (Aubry et al., 2008). The CFD calculations resulted in values for unsteady pressure, velocity, and WSS fields along the brain arteries. The highest WSS was centered around the CoW, where there is a high incidence of aneurysms. The techniques necessary for calculations of these values were well-suited for elongated domains, and therefore were much faster than previous attempts.

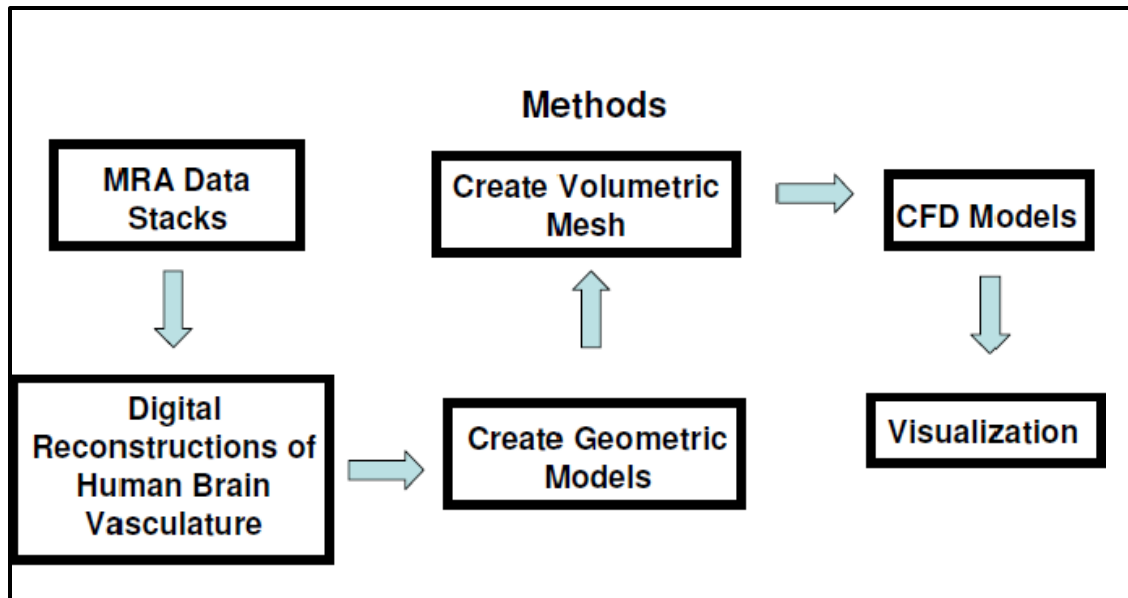


Figure 3.1. Schematic of Methods to create CFD models from MRA data stacks.

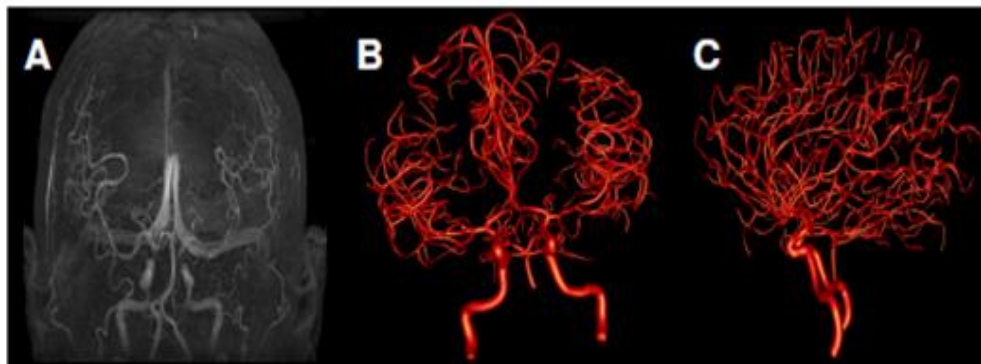


Figure 3.2. **A.** Max-intensity projection of MRA data set in coronal view. **B.** Example of a reconstruction; front view. **C.** Example of a reconstruction; side view.

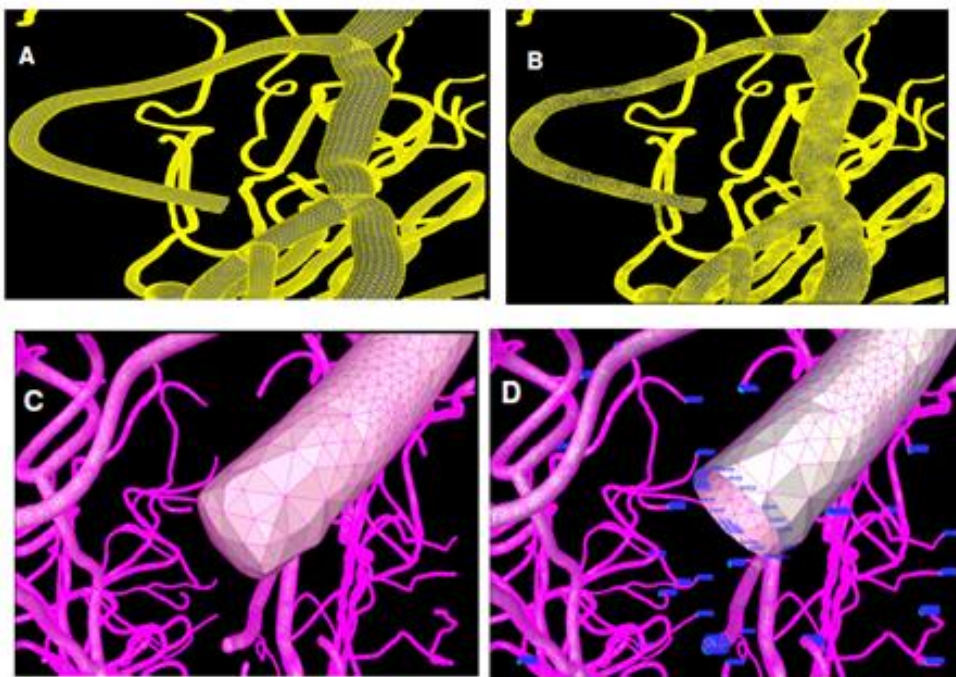


Figure 3.3. **A.** Cylindrical surface triangulation of a cubic spline. **B.** Adaptive voxelation merge. **C.** Uncut termination point. **D.** Cut termination point.



Figure 3.4. Zoom-in of volumetric mesh of the circle of Willis.

Results

CFD simulations were successfully carried out in these complex geometries, shown in Figure 3.5. The deflated conjugate gradient algorithm that was used to solve the pressure Poisson equation at each time-step of the incompressible flow calculation runs approximately 4-5 times faster than conventional conjugate gradient schemes, making these large calculations feasible and practical. This is a feasible method for subject-specific models of blood flow in cerebral arterial trees reconstructed from high-resolution

MRA images. Computer simulations of blood flow through the circle of Willis and cerebral arteries provide useful information and insights into the normal cerebral hemodynamics which is useful for quantitative comparison with pathological conditions such as intracranial aneurysms.

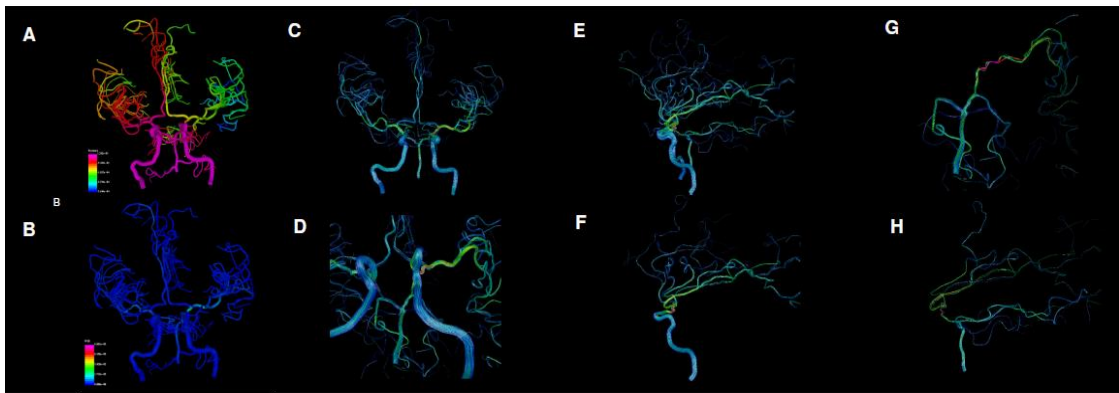


Figure 3.5. A. & B. Surface shading of CFD values, pressure and WSS, respectively. **C. through H.** Stream lines of blood flow at different views; **(C)** Front view, **(D)** Zoom-in of circle of Willis, **(E)** Side view of inflow from both internal carotid arteries, **(F)** Side view of inflow from one internal carotid artery, **(G)** inflow from basilar artery and half of the circle of Willis, **(H)** Inflow from basilar artery to posterior cerebral arteries (cooler colors = lower velocity, warmer colors = higher velocity).

Conclusions

For the CFD models described here, the boundary conditions were idealized. Because of this, these models mostly serve to show that it is possible to make subject-specific models of blood flow in human cerebral arterial trees in this manner. These simulations show that you can use reconstructions to create 3D models of arterial tree networks and using techniques described here, flow simulations can be done in a practical manner which enables future studies in normal subjects. Additionally, these simulations show the feasibility to construct 3D models of hundreds of subjects in an efficient manner. Currently, work is being done to determine the physiological boundary conditions in order to get more realistic flows.

Future Directions

The next step of this project is to study how to best apply the boundary conditions for a vessel network ($N = 1$). This will be carried out by rendering the problem as a minimization problem (e.g. of the total energy required to transport blood to the brain) and estimating the flow distribution to achieve this minimum. Then, simulations ($N = 10$) will be carried out to see how the blood flow distribution looks along the trees. It is estimated that it will take approximately one year to determine the boundary conditions. Future work will focus on improving boundary conditions for WSS, pressure, and flows.

CHAPTER FOUR: CONCLUSIONS AND FUTURE DIRECTIONS

Conclusions

The work described in this dissertation has exploited neuroinformatics tools to create improved digital reconstructions of human brain vasculature and provided an extensive characterization of the morphology of the cerebral arteries, which has the potential to play a fundamental role in the ability to recognize and possibly predict vascular anomalies that lead to pathology/disease. The brain vasculature of 61 healthy volunteers was digitally traced from 3T MRA data, and all cerebral arteries were morphologically quantified with both global and local analyses. The digital reconstructions were used to create subject-specific models of blood flows in the cerebral arterial trees. Estimations of the arterial branch geometry and bifurcation characteristics, as well as information about the regional distribution of these brain arterial trees were also provided, and can be used as a guide and/or as a way to test methods for constructing arterial tree models. Finally, the reconstructions, metadata, and morphometric measurements have been archived in a database that will be made freely available online.

The digital reconstructions created here have verified that it is possible to use the same methods previously used to reconstruct neuronal trees. Taking advantage of the 3T MRA data stacks, the Neuron_Morpho ImageJ plugin was used to create detailed reconstructions of the circle of Willis and the six major arteries that stem from it. The arterial trees are represented as a set of cylinders, with information about the diameter,

spatial coordinates, and connectivity to the other cylinders in the tree represented for each individual compartment. The ACAs, MCAs, and PCAs were reconstructed for approximately 300 mm from the circle of Willis, for approximately 15 bifurcation points along the paths that were traced, resulting in a novel data set regarding the sample size and completeness.

These detailed digital reconstructions of healthy human arterial trees were then used to carry out an extensive morphological study of brain vasculature. Knowledge of the morphology of these arteries leads to increased knowledge of which characteristics are considered normal, and which are not. The major results of the morphometrical analysis were: 1) the size and overall structure varied with artery type but not gender, age, or hemisphere, 2) the size of the three major arterial trees from the circle of Willis covaried across individuals such that subjects with one artery that was larger than average tended to have all other arteries larger than average, 3) a net right-left preference across the population in any of the individual arteries was not present, but within subjects, the ACAs were more lateralized than MCAs, 4) all three types of arteries had similar branch-level properties, 5) throughout the arterial trees, the bifurcating branches were significantly shorter and straighter than terminating branches, and 6) the length and meandering of bifurcating branches increased with age and path distance from the circle of Willis.

These subject-specific digital reconstructions were also used to create 3D CFD models of the blood flow in healthy human brain vasculatures, and hemodynamics variables including velocity, pressure, and wall sheer stress were examined. The main

purpose of these models was to show that it is possible to create subject-specific models of blood flow in human arterial trees in this manner. Also, a new algorithm was used to solve the pressure Poisson equation and was faster than conventional methods, proving that these large calculations were both practical and feasible. Physiological boundary conditions would need to be applied to these models to get more realistic flows as results that could then be used for a quantitative comparison with pathological conditions.

The reconstructions, metadata, and morphometric measurements have been archived in a database that is freely available online. This will allow other researchers to carry out additional studies on the morphology of human brain vasculature, or to do additional analysis of the geographic and territorial characterization of the brain arterial trees. Other researchers may be able to use these reconstructions to create additional subject-specific CFD models.

The morphometric analysis described in this dissertation reproduces and greatly extends previous knowledge of the human cerebrovascular architecture. The variability of overall size was similar to that reported for other measures of human body size (e.g. ISO, 2010). A previously reported measure of total arterial length from a single (51 year old male) subject fell approximately half a standard deviation from our sample mean and within our sample range by a comfortable margin.

Future Directions

Although the research carried out here significantly contributes to the knowledge of cerebrovascular architecture in healthy human adult subjects, there are still several interesting questions that remain. It should be reiterated that the analyses carried out

throughout this dissertation were from healthy subjects where only the gender and age of the subjects was recorded. It would be interesting and helpful if, in the future, arterial reconstructions were done on both healthy and diseased data sets where additional information was also recorded, such as height and weight of the subject, IQ, occupation, and hobbies and interests. Additionally, digital reconstructions of subjects that are younger and older than the subjects used throughout this study, as well as data sets from higher tesla scans or other imaging techniques would also be useful in future studies. The reasoning behind such additional information is outlined below.

Knowledge of the height and weight of the subjects whose brain arteries were reconstructed would allow us to see if the sizes of the vessels in the brain correlate to the sizes of the individuals. Males tend to be taller and weigh more than females. The morphometrical analysis revealed that height was the only metric that was statistically significantly different between males and females (85.66 ± 4.14 mm vs. 83.81 ± 2.94 mm, $p=0.0006$). Additionally, an investigation of the morphological homeostasis of brain arteries found that if the vasculature is big, every artery is big, and if the vasculature is small, every artery is small. It would be interesting to see if these results correspond with the height of the individuals, and also, what role, if any, that weight may have on the size of an individual's arterial dimensions.

Information on the IQ, occupation, hobbies and interests of an individual would be useful for further lateralization analysis. Figure 2.5 shows that an in-depth evaluation of the length and laterality of the digital reconstructions revealed that there are differences across arteries. A strong linear correlation between the right and left lengths

across the sample and within genders, age groups, and artery types was shown. No overall hemispheric dominance was seen across the sample. An investigation of individual lateralization revealed that the laterality was statistically equivalent between age groups and genders, when it was calculated by artery pair or by the complete hemispheric vasculatures of the individuals. The only difference between cerebral arteries was that the ACAs were significantly more lateralized than MCAs. Additional information about the subjects would be useful in determining if the lateralization of individual arteries can predict characteristics that an individual may possess, or provide insight into an individual's behavior, personality, or creative abilities.

The morphological analysis carried out in this dissertation revealed differences in bifurcating and terminating branches. As seen in Table 2.1, large and highly significant differences were seen in branch path length, tortuosity, and fractal dimension, with terminating branches being an average of 73% longer, 28% more tortuous, and 6% more fractal than bifurcating branches. The age of the subjects also had an effect on these metrics, as seen in Figure 2.4, but no differences were observed between genders or hemispheres. For both bifurcating and terminating branches, as age increases, tortuosity also increases. As age increases, fractal dimension increases only with terminating branches, while branch length increases only in bifurcating branches. The reasons for these trends are not clear, and will require further analysis.

None of the results of the morphometrical analysis provided any insights into gender or hemispheric differences in aneurysm prevalence. As most aneurysms occur in individuals over the age of 50, and only two of the 61 subjects included in this study were

over the age of 50, including more data on older subjects in future studies would be useful in providing more information. Including younger subjects as well as patient data would also be useful to answer these questions.

Data from higher tesla scans or other imaging techniques would be useful for increasing the accuracy of the digital reconstructions. Metrics that depended on diameter of the vessels were purposely avoided in the analysis discussed throughout this dissertation, and could be helpful in explaining age, hemispheric, or gender prevalence of aneurysms. Future digital reconstructions of diseased patients would obviously also be quite valuable.

In the immediate future, additional metrics could be analyzed to characterize the arterial trees. L-measure (<http://krasnow1.gmu.edu/cn3>), the tool used for the morphometric analysis, supports several dozen morphometric functions, and only the most relevant metrics for vascular trees were analyzed for this study. The data could also be divided into various age groups and re-analyzed. The geographic and territorial analysis presented here could also be built upon. Additionally, more CFD models could be developed.

The analysis and accompanying database presented in this dissertation provide an extensive collection of normative quantitative morphometric parameters measured from *in vivo* 3D imaging of human vascular arteries. The data and CFD models can be broadened in future studies to help answer the questions that remain, and can potentially aid in understanding and treating cerebrovascular diseases.

APPENDIX ONE: MORPHOMETRIC, GEOGRAPHIC, AND TERRITORIAL CHARACTERIZATION OF BRAIN ARTERIAL TREES

[Fernando Mut, Susan Wright, Giorgio Ascoli, Juan Cebal]

Abstract

Morphometric information of the brain vascularization is valuable for a variety of clinical and scientific applications. In particular, this information is important when creating arterial tree models for imposing boundary conditions in numerical simulations of the brain hemodynamics. The purpose of this work is to provide quantitative descriptions of arterial branches, bifurcation patterns, shape and geographical distribution of the arborization of the main cerebral arteries as well as estimations of the corresponding vascular territories. For this purpose, subject-specific digital reconstructions of the brain vascular network are created from 3T magnetic resonance angiography images of healthy volunteers, and used to derive population averaged morphometric characteristics of the cerebral arterial trees.

Introduction

Detailed knowledge of the brain vascular architecture is important for gaining insight into a variety of vascular pathologies and brain diseases. In particular, knowledge of the distribution of hemodynamic quantities in the cerebral arteries is important to understand the pathophysiology and pathogenesis of cerebrovascular diseases such as intracranial aneurysms (Sforza et al., 2009). The hemodynamics in cerebral arteries has

been studied with patient-specific computational fluid dynamics models (Oshima et al., 2001, Cebal et al., 2003). These numerical simulations require specification of appropriate outflow boundary conditions (Olufsen, 1999, Cebal et al., 2003, Cebal et al., 2000). The flow division among the different arteries is largely determined by the relative impedance of the distal vascular beds. Thus, researchers have estimated these impedances by developing arterial tree models. A variety of methods have been developed to build realistic arterial trees (Olufsen et al., 2000, Karch et al., 1999, Bui et al., 2010, Dokoumetzidis and Macheras, 2003) and scaling laws for vascular trees have been proposed (Kassab, 2006, Zamir, 1999). These approaches require the specification of a number of parameters and constraints related to the arterial branch geometry and bifurcation characteristics. The purpose of this paper is to provide estimations of these parameters as well as information about the regional distribution of the arterial trees of the brain based on *in vivo* human data that can be used to guide and/or test methods for constructing arterial tree models.

Methods

Vascular Reconstructions

A total of 61 digital reconstructions of healthy human arterial networks were created from 3T magnetic resonance angiography (MRA) images. These images were acquired with a field of view that spanned the entire brain at an isotropic voxel resolution of 0.6 mm. The brain arterial network of each subject was manually traced using a software tool originally designed for reconstruction of neuronal trees (www.neuromorpho.org). This tool was implemented as a plug-in extension of the

ImageJ software developed at the National Institute of Health (<http://rsbweb.nih.gov/ij/>).

The centerline and diameter of each arterial branch were reconstructed by interactively selecting voxels on the MRA image rendered as 2D slices in three orthogonal planes.

Arterial branches and bifurcations were digitally represented as a set of interconnected tapering cylinders characterized by the x, y, z coordinates along their centerlines and corresponding radius, and connection to the parent branch or node.

The vascular reconstructions were systematically checked and verified by running a battery of tests in order to detect defects such as intersecting arterial segments, zero diameter branches, overlapping branches, disconnected nodes or branches, etc. The reconstructions were also checked by visual inspection of the vascular model overlaid to the MRA slices and to volume renderings of the 3D MRA images in order to verify the topology and geometry of the vascular models. When detected, the errors were removed by editing the reconstructions and the tests were run again until no new problems were found.

Subsequently, the vascular models were smoothed and re-parametrized by passing cubic splines along the centerline each arterial branch. Finally, the arterial trees corresponding to the six main cerebral arteries emanating from the circle of Willis were identified and labeled: left (L) and right (R) anterior cerebral artery (ACA), middle cerebral artery (MCA) and posterior cerebral artery (PCA).

The reconstruction process is illustrated in Figure A1.1. The top row of this figure shows a coronal slice of the MRA dataset of one of the subjects at the level of the circle of Willis (a), a maximum intensity projection (MIP) of the vasculature (b) and a volume

rendering of the brain arteries (c). The bottom row of this figure shows the reconstructed arterial centerlines colored with the vessel radius (d), the reconstructed arterial model rendered as a 3D surface (e), and the labeling of the main arterial trees (LACA=green, RACA=yellow, LMCA=cyan, RMCA=red, LPCA=magenta, RPCA=blue) of the vascular model (f).

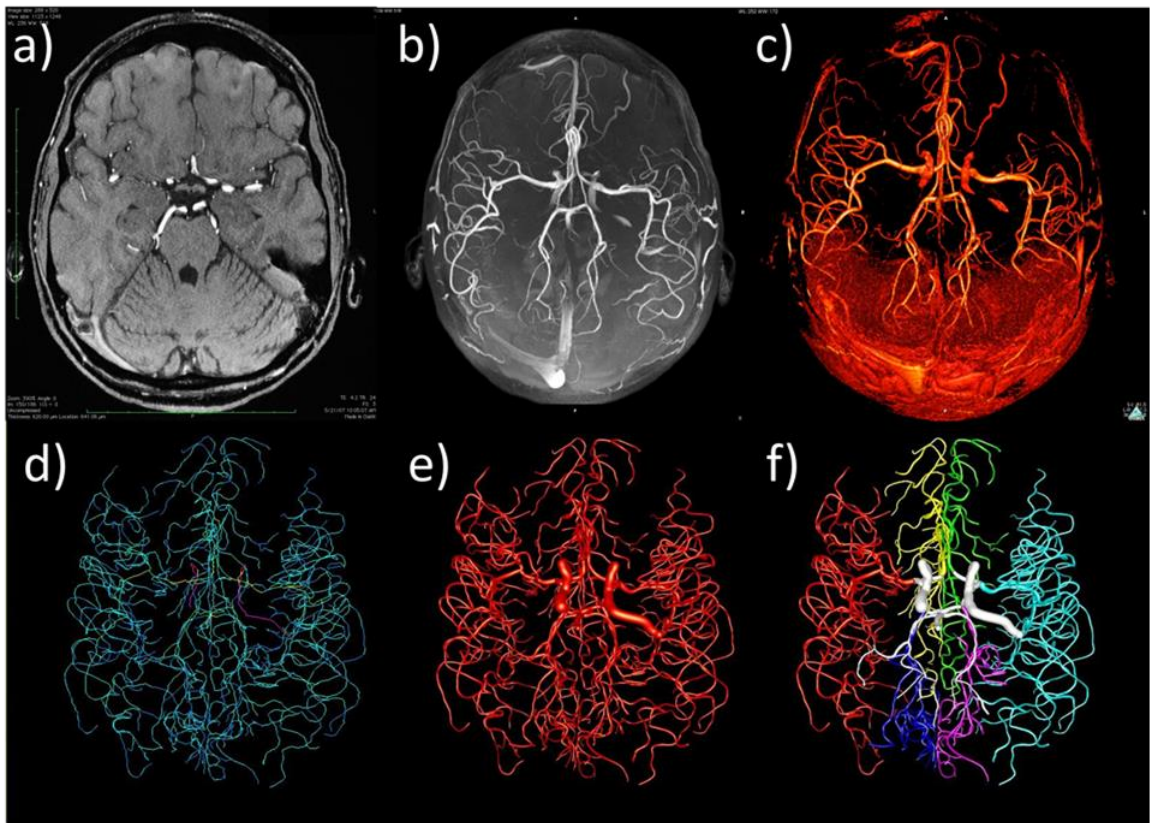


Figure A1.1: Reconstruction of vascular trees from MRA image data: a) slice of MRA at the level of the Circle of Willis, b) maximum intensity projection of MRA image, c) volume rendering of MRA image, d) tracing of arterial network, e) reconstruction of arterial networks, f) labeling of arterial trees.

Arterial Tree Characterization

The nodes of each arterial tree were classified as: a) the root node (node at the origin of the tree with no connection to a parent node), b) terminal nodes (with no children nodes), c) internal nodes (with only one child node and one parent node), and d) bifurcation nodes (with two children nodes and a parent node). Arterial branches were then identified as the set of connected internal nodes between bifurcation or terminal nodes. Arterial branches and bifurcation nodes were assigned a branch order or generation number by recursively traversing the tree starting at the root node and incrementing the generation number at each bifurcation node. The geometry and branching pattern of the tree were then characterized by measuring quantities defined at each branch and at each bifurcation. The geometry of each branch was characterized by its geodesic (S) and Euclidean (L) lengths, the mean radius along the branch (R), the branch tortuosity ($T=S/L$), and its aspect ratio ($A=S/R$). Bifurcations were characterized by measuring parent-children and children-children ratios of branch lengths ($LR=L_0/L_i$ and L_1/L_2), mean radius ($RR=R_0/R_i$ and R_1/R_2), bifurcation law (n such that $R_0^n=R_1^n+R_2^n$), and bifurcation angles between the parent and each of the children branches. Here 0 represents the parent branch, i represents each child branch ordered by size (1 is larger, 2 is smaller).

Vascular Atlas and Territories

In order to build probabilistic vascular and territorial atlases, the 61 vascular reconstructions were aligned to a common reference frame. For this purpose, a landmark point (the tip of the basilar artery) was manually identified in all models and used as the origin of the reference frame. Then, three main directions (left-right, anterior-posterior,

and inferior-superior) were identified using a principal component analysis (PCA). Specifically, the left-right direction was found by performing a PCA analysis that computed the plane that best separates the left and right arterial trees. Then, the anterior-posterior direction was found with a PCA analysis that computed the plane that best separated the anterior cerebral from the posterior cerebral arterial trees. The inferior-superior direction was then defined as perpendicular to the other two directions. Next, all vascular models were translated to the common origin (basilar artery tip) and rigidly rotated to make their principal directions coincide.

The bounding box enclosing all 61 aligned vascular models was computed and used to create a 3D image or voxelization composed of 512^3 isotropic voxels. Subsequently, each arterial tree of each subject was voxelized, i.e. voxels intersecting the vascular model were painted white while empty voxels were left black. A population averaged or generic brain region or mask was then created by rasterizing (i.e. computing the convex hull of) all voxels touched at least once by any branch of any tree of any subject. A probabilistic vascular atlas for each of the six cerebral arterial trees was then created by computing the occupancy probability of each voxel in the rasterized brain region.

Vascular territories, i.e. regions perfused by each arterial tree, of each subject were approximated by assigning each voxel of the population averaged brain to the closest arterial tree using an advancing regions growing technique. Territorial probability maps, i.e. probabilistic territorial atlases, were then computed from the vascular territories of the 61 subjects by counting the number of times a voxel belongs to the

vascular territory of a given tree. Watershed regions between pairs of territories were identified by finding voxels with non-zero probabilities of belonging to the two adjacent territories. Relative volumes of all territories and watershed regions were calculated.

The process is illustrated in Figure A1.2 that shows: the alignment of the vascular models of two subjects (a), the alignment of the arterial trees of all 61 subjects (b), the arterial trees of one subject superposed to the rasterized or population averaged brain region (c), and the vascular territories of the left (transparent red) and right (transparent cyan) middle cerebral arteries of one subjects along with the corresponding arterial trees. In this figure, the vascular territories (d) and the brain volume (c) were rendered by extracting an iso-surface corresponding to 0.5 probability of belonging to each region and plotting these iso-surfaces with transparency.

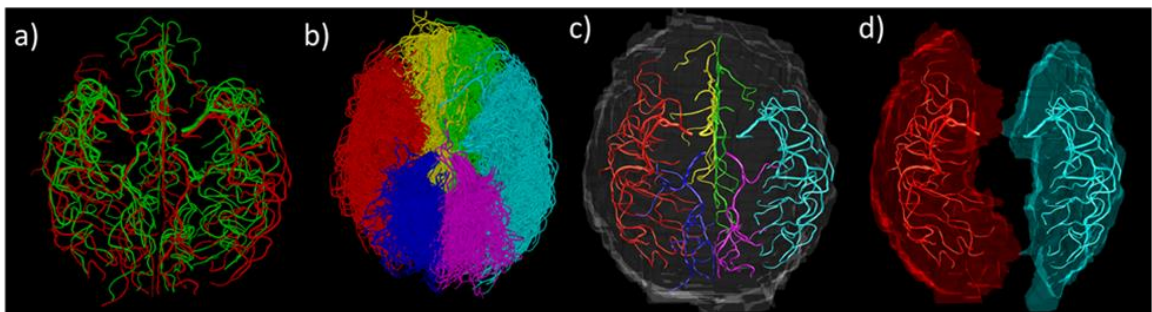


Figure A1.2: Vascular atlas and territories: a) alignment of vascular trees of two subjects, b) alignment of vascular trees of 61 subjects, c) rasterized brain volume and arterial trees of one subject, d) vascular territories corresponding to left and right MCA trees of one patient.

Results

Branch Geometry

Geometric characteristics, including geodesic and Euclidean length, mean radius, aspect ratio, and tortuosity were calculated for each branch of each of the vascular trees and for all subjects. Population averages were computed for each branch order or generation of each of the brain arterial trees. Averages were computed over all subjects and both hemispheres. The results are presented in Figure A1.3. This figure shows how the population average of the branch geodesic length (a), mean radius (b), aspect ratio (c), and tortuosity (d) varies along the generations of each arterial tree. We can see that branch radius decrease with branch order and that lengths and aspect ratio peak between generations 4 and 7 and then continue to decrease as the generation order increases. Branch tortuosity increases up to about generation 8 and then seems to stabilize or slightly decrease in the terminal branches.

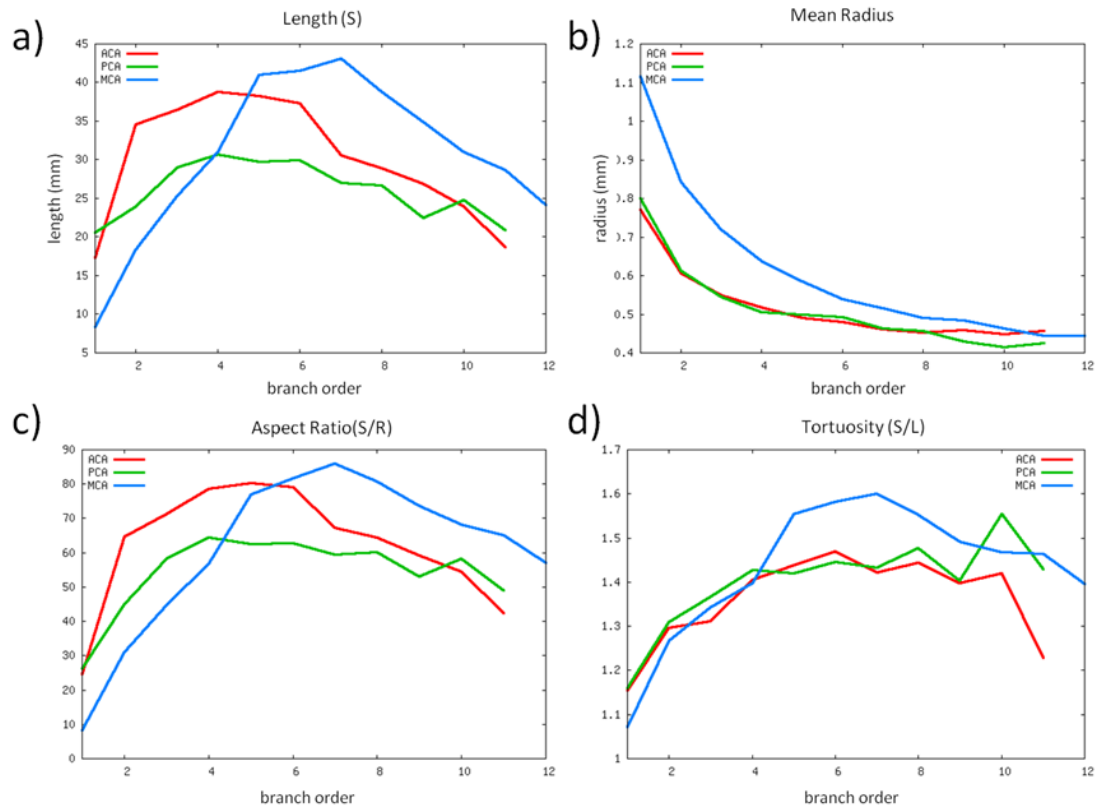


Figure A1.3: Geometric characteristics of arterial tree branches as functions of branch order: a) branch geodesic length along trees, b) branch mean radius along trees, c) branch aspect ratio along trees, d) branch tortuosity along trees.

Bifurcation Characteristics

Similarly, bifurcation characteristics were computed by averaging over subjects (population average) and hemispheres for all bifurcation generations of each arterial tree. The branching pattern characteristics of each arterial tree are presented in Figure A1.4. This figure shows the variation of the population average of the length and radius ratios, the bifurcation power law exponent between parent and children branches, and the parent-child angles along each tree (i.e. as a function of the branch or bifurcation generation). We can see that all these values remain roughly constant after about the third generation, except for the power law exponent of the PCA trees which exhibits a larger variation. These results indicate that the largest child, i.e. with larger mean radius, has roughly a length 130% of the parent branch length (panel a) and a radius about 90% of the radius of the parent branch (panel b). Conversely, the smallest child has a length of about 50% of the parent branch length (panel a) and a radius about 75% of the radius of the parent branch (panel b). Additionally, for each arterial tree the smallest child tends to bifurcate with a larger angle (above 55 degrees) than the largest child (angle below 50 degrees), as can be seen in panel c: red and magenta curves for ACA, green and cyan curves for PCA, and blue and brown curves for MCA. This suggests that the trees do not bifurcate symmetrically. Instead, when each artery reaches a bifurcation point, it curves and gives off a thinner and shorter branch, and continues with roughly the same radius for a longer distance. This branching pattern is schematically illustrated in panel e. Interestingly, the bifurcation power law exponent (panel d) remains roughly constant for all generations with a value around 2.5 (except for larger variations seen in the PCA trees). This value seems to indicate that the branching pattern satisfies a principle of

minimum work. Another interesting observation is that on average the bifurcation characteristics of the cerebral arterial trees seem to remain roughly constant for generations beyond 3, i.e. they exhibit a roughly fractal behavior.

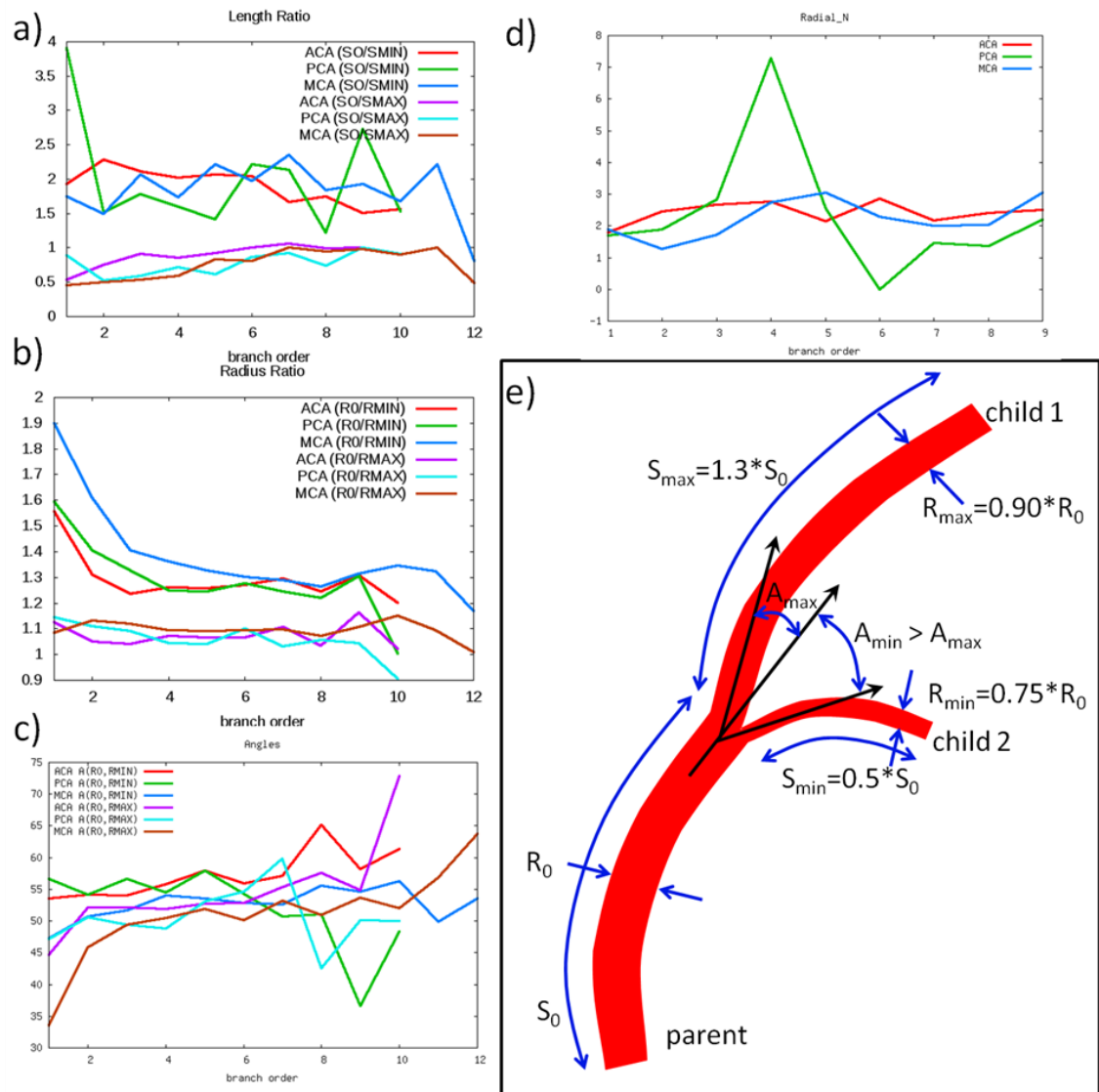


Figure A1.4: Bifurcation characteristics as functions of branch order: a) daughter to parent length ratios, b) daughter to parent radius ratios, c) daughter to parent bifurcation angles, d) bifurcation power law, e) schematics showing the general characteristics of arterial bifurcations.

Tree Shapes

The shapes of the arterial trees of each patient were characterized using a principal component analysis. The shape of each tree was quantified by computing the extension of the tree along three orthogonal principal directions of elongation. The distribution of sizes along the three principal components of each tree is presented in Figure A1.5. Different colors were used for the ACA, MCA and PCA trees. Clustering of the shapes of the ACA, MCA and PCA trees can be clearly observed. This means that the trees of different subjects have similar shapes. The range, mean and standard deviation of the three principal directions of each group of trees computed over the subject population are given in Table A1.1. The trees closest to the mean of each cluster are shown at the right of Figure A1.5. These are representative examples of the shape of the trees in each group. In particular, the ACA trees appear flatter (one dimension smaller than the other two), the MCA trees appear more isotropic (all three dimensions are similar), and the PCA trees appear elongated (one dimension longer than the other two).

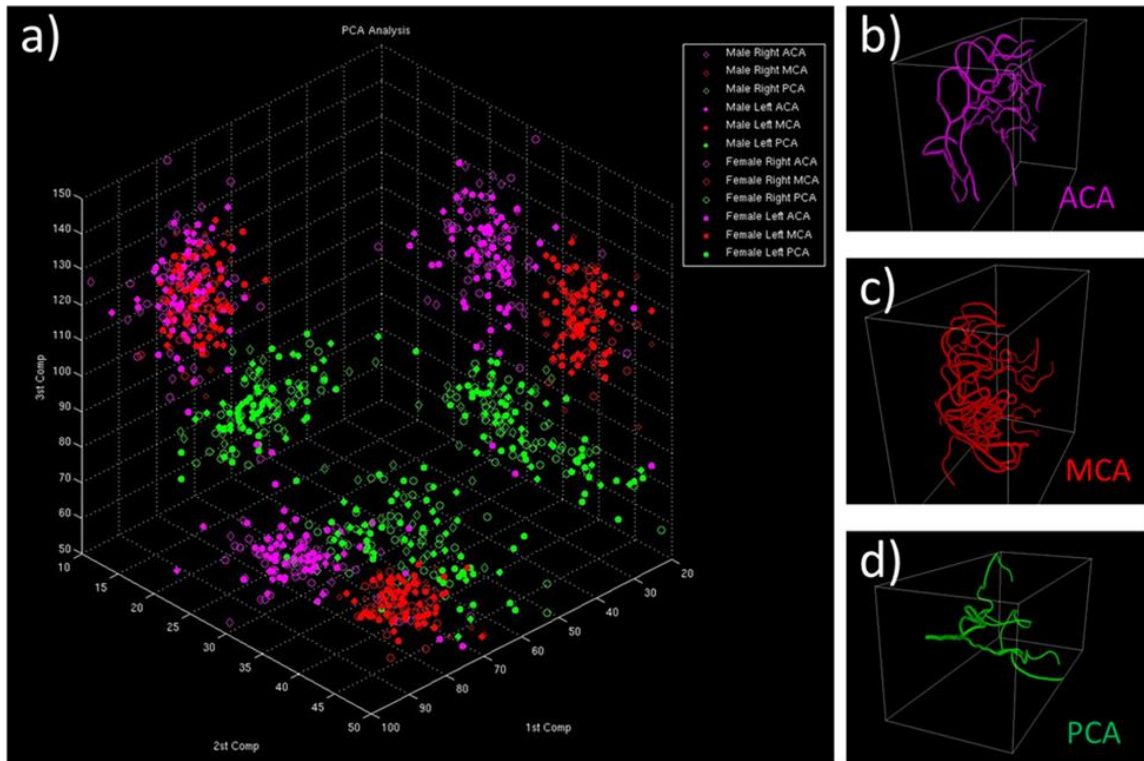


Figure A1.5: Principal component analysis of arterial tree shapes: a) distribution of tree sizes along three principal size directions, b) example of ACA tree closest to the mean, c) example of MCA tree closest to the mean, d) example of PCA tree closest to the mean.

Table A1.1: Distribution of height, depth and width of brain arterial trees.

Arterial tree	Value	Height	Depth	Width
ACA	Mean	72.45	109.07	25.97
	Standard dev	7.44	14.31	5.40
	Min	49.6	51.46	10.23
	Max	97.96	148.8	48.05
MCA	Mean	69.40	105.55	38.48
	Standard dev	5.57	10.01	3.02
	Min	51.46	76.88	32.86
	Max	84.63	127.1	48.05
PCA	Mean	52.43	66.27	30.50
	Standard dev	10.22	6.69	6.86
	Min	21.39	51.46	15.5
	Max	74.09	85.56	49.29

Territory Characteristics

The probabilistic atlases computed from the vascular reconstructions of the 61 subjects are presented in Figure A1.6. In order to visualize the probabilistic vascular atlas of each arterial tree, the probability that a voxel belong to a given arterial tree was encoded with a grey level value and displayed using volume rendering techniques (six leftmost panels). Thus, the grey level values in these images represent the probability of

occupancy of each voxel by a branch of each arterial tree. The territorial probabilities (rightmost panel) were visualized by plotting transparent iso-surfaces corresponding to probability of belonging to each territory > 0.5 .

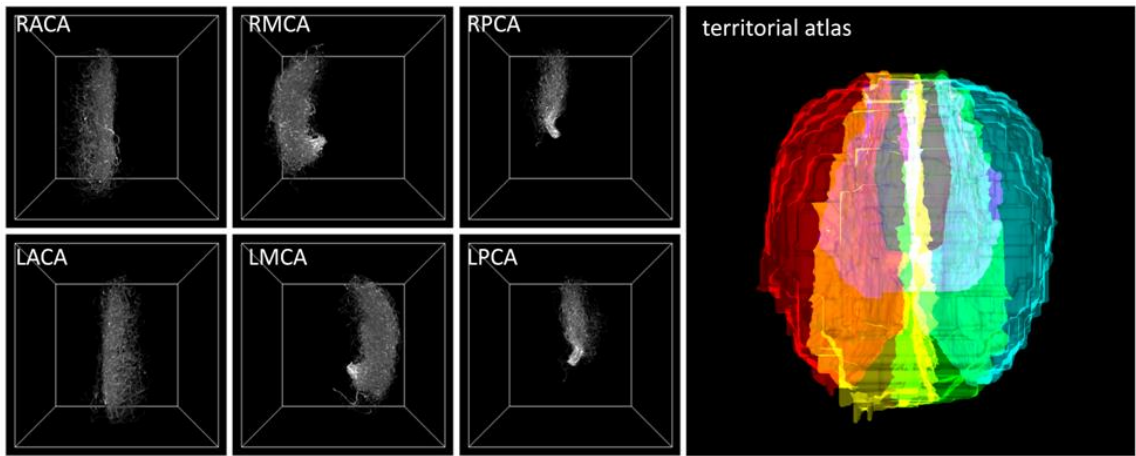


Figure A1.6: Probabilistic vascular atlases (left) and probabilistic territorial atlas (right).

The probabilistic geographic partition of the brain volume into vascular territories corresponding to each cerebral arterial tree is presented in Figure A1.7. This figure shows the territories of the ACAs, MCAs, and PCAs from three orthogonal viewpoints.

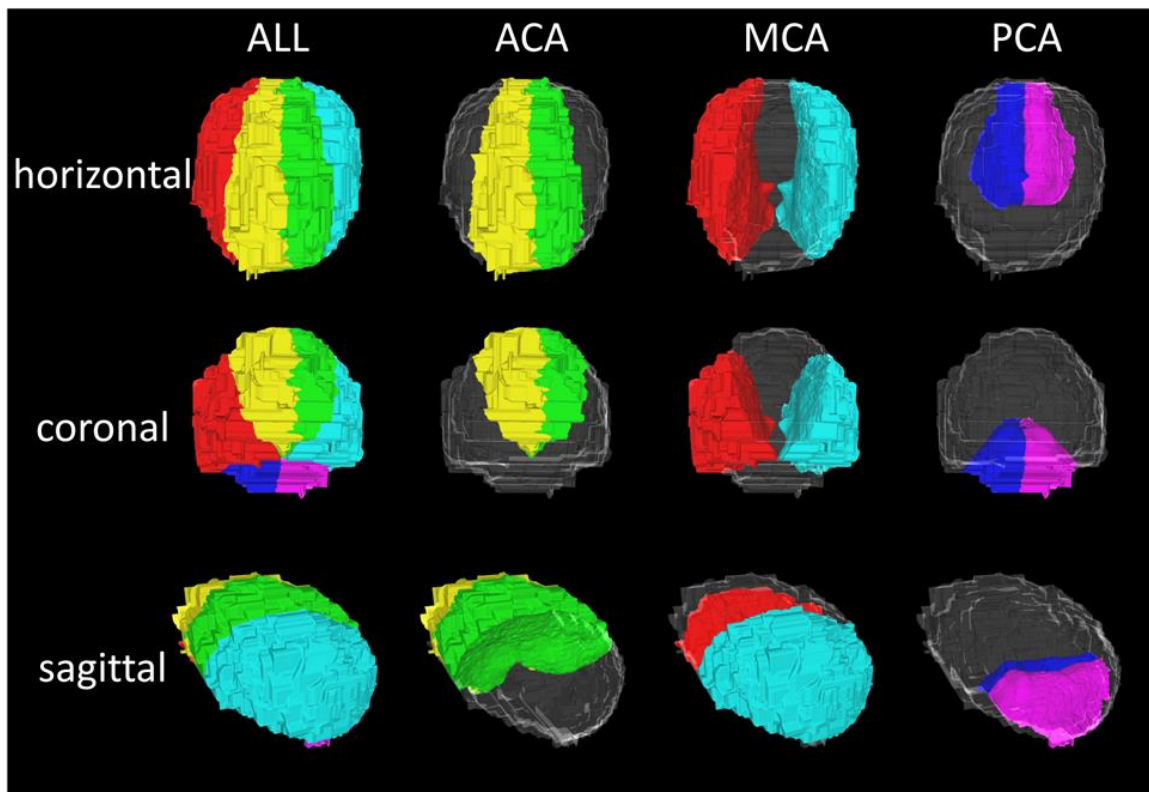


Figure A1.7: Probabilistic territorial atlas from 61 subjects corresponding to each cerebral arterial tree (ACA, MCA and PCA), from three orthogonal viewpoints (horizontal, coronal and sagittal).

Relative volumes of the territories with respect to the PCA territory are presented in Table A1.2 for the left and right hemispheres. The volumes of the vascular territories were estimated by thresholding the probabilistic territorial atlas (denoted Atlas in the table) as well as by averaging the territories of all subjects in the population (denoted population average in the table). Both estimates are in good agreement, they coincide well within one standard deviation. These results indicate that the territories of the middle cerebral arteries are about 2.53 to 2.99 times larger than those of the posterior cerebral arteries. Similarly, the territories of the anterior cerebral arteries are 1.28 to 1.59 times larger than those of the posterior cerebral arteries.

Table A1.2: Relative volumes of vascular territories.

Territory	Side	Relative volume	
		Atlas	Population average
MCA/PCA	Right	2.99	2.8 (± 0.51)
	Left	2.53	2.42 (± 0.42)
ACA/PCA	Right	1.59	1.54 (± 0.42)
	Left	1.28	1.37 (± 0.32)

The geographic locations of the watershed regions are presented in Figure A1.8. This figure shows regions that have probabilities above 0.5 of belonging simultaneously to the territories of the ACA and the MCA (denoted $ACA \cap MCA$), the MCA and PCA (denoted $MCA \cap PCA$), and the PCA and ACA (denoted $PCA \cap ACA$). The relative volumes of the watershed zones with respect to the $PCA \cap ACA$ (smallest watershed region in each hemisphere) are presented in Table A1.3. These results show that the watershed region between the MCA and the ACA are the largest and is about 16 times larger than the PCA and ACA, followed by the MCA and PCA watershed region which is about 12 times larger than the PCA and ACA.

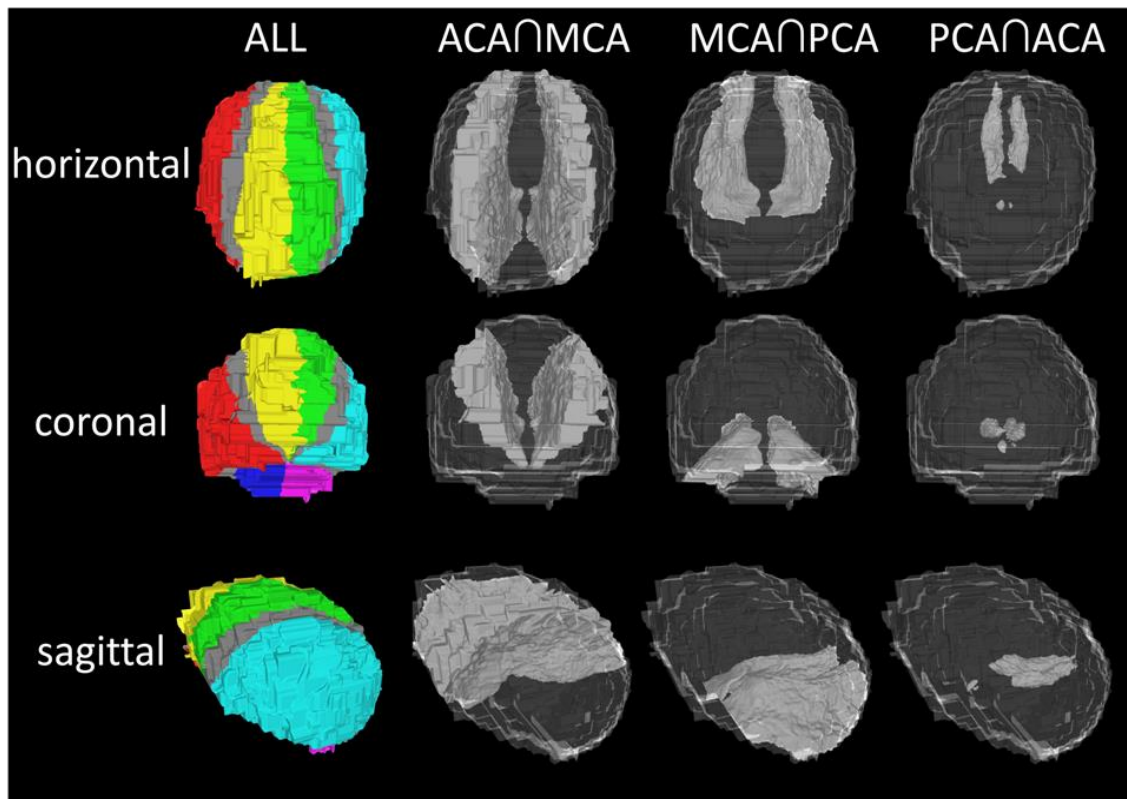


Figure A1.8: Probabilistic atlas based on data from 61 subjects of watershed zones between vascular territories of main cerebral arteries, from three orthogonal viewpoints (horizontal, coronal, and sagittal).

Table A1.3: Relative volumes of watershed regions.

Watershed territory	Side	Relative volume
$(MCA \cap ACA) / (ACA \cap PCA)$	Right	16.57
	Left	16.34
$(MCA \cap PCA) / (ACA \cap PCA)$	Right	11.62
	Left	12.39

Discussion

In vivo morphometric characteristics of the arterial vascularization of the human brain have been extracted from MRA images of healthy subjects. These characteristics include geometric properties of the arterial branches of the main cerebral arteries as well as their bifurcation or branching pattern and their geographical and territorial distributions. Generic values of a variety of geometric and bifurcation parameters were given as population averages at each generation along the arterial trees of the anterior cerebral artery, middle cerebral artery and the posterior cerebral artery. The results indicate that the geometric properties of arterial branches follow similar variations along the generations of the different cerebral artery trees (see Figure A1.3) Likewise, these trees seem to follow similar asymmetric bifurcation patterns in which the main arterial trunk gives off smaller branches as it extends on the brain surface (as illustrated in Figure A1.4 – panel e). The bifurcation characteristics were found to be roughly constant after about the third generation for all trees, suggesting a “fractal” branching pattern (i.e. invariant along arterial generations). However, the vascular trees of the ACA, MCA and

PCA have in general different shapes (Figure A1.5) and cover territories of different extensions (Figure A1.7).

Additionally, the artery radius seems to follow a power law at arterial bifurcations (Figure A1.4 – panel d). Conservation of mass at a bifurcation implies $Q_0 = Q_1 + Q_2$, where Q_0 , Q_1 and Q_2 represent the volumetric blood flow in the parent and children branches, respectively. The principle of minimum work applied to a straight circular cylinder under steady flow conditions implies $Q = A \times r^3$ (Murray's law), where A is a constant, and r the radius of the artery. This law was obtained by minimizing the energy required to move a volume of blood through a straight artery with a steady flow (i.e. Poiseuille's flow) (Murray, 1926). An optimal value of 3 has been proposed for laminar flow and 2.33 for turbulent flow (Olufsen, 1999). Values ranging from 2 to 3 have been suggested for pulsatile flows (Painter et al., 2006). Similarly, an extension of Murray's law for non-Newtonian flows suggests a value between 2.42 and 3. In this work, a power law of the form $r_0^n = r_1^n + r_2^n$ was proposed and the value of n was fitted at each bifurcation and population averaged for each generation along the different arterial trees. It was observed that n fluctuated between 2 and 3 for all generations greater than 3 of all trees (except for the PCA trees that exhibited larger variations). Thus, the arterial trees of the brain seem to obey a principle of minimum work, i.e. they are close to the optimal design for transporting blood with the minimum possible energy. However, it is not exactly clear which form of the principle of minimum work is the most appropriate to describe the branching pattern observed in the data presented in this paper. Additionally, our results indicate that bifurcation angles cluster around a value of 50-55 degrees. These

values are consistent with optimal values estimated to minimize work in vascular trees (Huo et al., 2012).

The information and quantitative values provided in this paper are important for a variety of applications. In particular, they are useful for specifying morphometric parameters required by different techniques used for generating computer models of brain arterial trees. For instance, arterial tree models have been generated using fractal structured trees (Olufsen, 1999, Olufsen et al., 2000), or using constrained constructive optimization techniques (Karch et al, 1999, Bui et al., 2010, Schreiner et al., 2000). These models require for example specification of the bifurcation law exponent, length to radius ratios, etc. These models have been constructed, for example, with the objective of estimating impedances of the distal vascular beds and imposing outflow boundary conditions in computational fluid dynamics models of the brain circulation. The data presented in this paper is not only useful to prescribe the values of required parameters but also to impose constraints to the geometric, bifurcation and geographic characteristics produced by these algorithms, as well as evaluating the anatomical and physiologic realism of the generated trees.

The current study has several limitations that could affect the values of morphometric characteristics calculated and should be taken into consideration when interpreting the results presented in this paper. The limited resolution of the MRA images used to build the digital reconstructions of the brain vascular network can affect the estimations of geometric and bifurcation characteristics of the arterial trees, especially in the smallest arteries. This can be observed as larger variability of the morphometric

parameters with increasing branch generation, especially beyond generation 10. The reconstruction method approximates vessel cross sections as circular. This assumption can have an important effect if the reconstructions are used for instance to calculate hemodynamic parameters along the trees. The digital reconstructions were created from 3T time-of-flight MRA images. These images suffer from artifacts related to signal loss in regions of low flow or disturbed flow patterns, which can affect the estimations of the diameter of the arteries in these regions. The vascular territories were estimated by partitioning a generic brain volume instead of each subject's brain volume, and they were identified by computing the distance to the closest blood vessel instead of estimating flow distributions. These assumptions can affect the estimations of the relative volumes of the vascular territories of each cerebral artery. It is worth noting that some parameters are likely less affected by these sources of errors. For example, estimations of the length of arterial branches, or bifurcation angles, are likely less affected by limited resolution or flow related imaging artifacts than estimations of the arterial diameters. Despite these limitations and potential sources of inaccuracy, this study provides quantitative values of a number of important morphometric parameters based on measurements performed on 3D images acquired *in vivo* in human subjects.

Conclusions

Geometric characteristics, bifurcation patterns, and shape and geographical distributions of brain arterial structures were quantified from MRA data of normal subjects. Population averaged quantities are independent of the brain hemisphere, subject's gender or age, and therefore can be considered a normative set of generic values

valid for all subjects in these groups. The parameters that characterize the brain vascularization are useful to guide and/or constraint methods for building realistic arterial tree models and to evaluate whether such models are capable of reproducing the morphometric characteristics extracted from *in vivo* human data presented here. Additionally, these vascular and territorial characteristics can be useful for comparing normal to pathological conditions, and help understand the effects of different diseases and their treatments.

Acknowledgements

This work was supported by NIH grant R21NS061770-02 in collaboration with the UCLA National Center for Computational Biology (Drs. Arthur Toga, John Mazziota, and Ivo Dinov).

APPENDIX TWO: BRAVA: THE DESIGN AND ORGANIZATION OF A NEUROSCIENCE DIGITAL ARCHIVE

Introduction

Structured databases have proven useful in biomedical research, and are starting to gain popularity in the field of neuroscience. The creation of BraVa aims to promote and enable sharing of the digital reconstructions of the human brain vasculature described in this dissertation. The MRA acquisition for the data sets used to create these digital reconstructions was expensive and time-consuming. The manual digital reconstruction process was also very time-consuming, although the software tools used to create these reconstructions were free. The sixty one digital reconstructions of the human brain arterial trees used throughout the research in this dissertation have been archived in BraVa so that other researches may benefit from the work that has already been done. The intent is that by making these digital reconstructions publicly available, other investigators may use these reconstructions as a baseline for healthy human brain vasculature and can analyze these reconstructions further. These digital reconstructions may also be used for future CFD models, which may help to improve diagnostics and treatments for cerebrovascular diseases.

Database Design and Organization

All sixty-one of the reconstruction files used throughout the research described in these studies were archived in the database BraVa and are available for download at

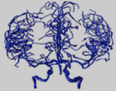
cng.gmu.edu/brava. In addition to the digital reconstructions of healthy human brain arterial trees, BraVa also contains the extracted morphological measurements that were outlined in Chapter Two. This primary design of this database was carried out using MySQL v. 5.0 (Tahaghoghi and Williams, 2006, Zawodny and Balling, 2004). The graphical user interface (GUI) was created using PHP v. 5.2.9 (Sklar, 2004) and HTML (Shelly and Woods, 2004) programming languages. MySQL is a popular open source relational database management system (RDBMS) and can be downloaded from <http://www.mysql.com>. PHP is a general-purpose scripting language specifically designed for use on the web that has extensive capabilities to interact with many different RDBMSs and is freely available at <http://www.php.net/index.php>. The GUI, implemented using PHP and HTML, simplifies the user interaction with the database by making it accessible via generally available web browsers. BraVa was designed to allow the user to browse all subjects by their statistics and retrieve information with a search engine.

Navigation of Database

The following screenshots and descriptions (Figures A2.1, A2.2, A2.3, A2.4, A2.5, A2.6, A2.7, A2.8, and A2.9) give an overview of the content found in the database as well as how to navigate the database.



Figure A2.1. Screen shot of the main page of BraVa. This is the starting point for navigating through the database. The options ‘Browse All Files,’ ‘Search Files,’ ‘Related Links,’ and ‘Help’ are on the left.



BraVa

Tuesday, January 15 2013
 Version 1.1

[Home page](#)
[Browse all files](#)
[Search files](#)
[Related Links](#)
[Help](#)

61 subjects are present in the database

[Download swc files](#)
[View statistics for metrics](#)

☒ Complete
 ☐ ACA
 ☐ MCA
 ☐ PCA

CODE	AGE	SEX
BG001	24	F
BG0002	31	M
BG0003	29	M
BG04	21	M
BG05	35	F
BG06	20	F
BG07	41	F
BG08	27	F
BG09	23	F
BG10	21	F
BG11	44	F
BG12	36	F
BG13	38	M
BH0015	25	F
BH0016	28	M
BH0017	24	F
BH0018	21	F
BH0019	27	F
BH0020	21	M
BH0021	33	F
BH0022	47	F
BH0023	19	F
BH0024	22	M
BH0025	24	M
BH0026	37	F
BH0027	46	F
BH0029	46	M
BH0030	33	F
BH0031	24	F
BH0032	48	M
BH0033	59	M
BH0034	27	F
BH0035	24	F
BH0036	29	F
BH0037	50	F
BH0038	22	F
BH0039	42	F
BH0040	30	F
BI0001	22	M
BH0002	25	F

Figure A2.2. Screen shot of the ‘Browse All Files’ page of BraVa. All 61 files are archived here, with the option to download the swc files, and view statistics for the metrics, either by complete tree or selected artery.



BraVa

Tuesday, January 15 2013 Version 1.1

[Home page](#)
[Browse all files](#)
[Search files](#)
[Related Links](#)
[Help](#)

Search files

You can search the subjects by using the metrics:

METRIC	ARTERY	SIDE	OPERATOR	VALUES
Total number of branches	-	-	=	
-	-	-	=	
-	-	-	=	
-	-	-	=	
-	-	-	=	

And the boolean operator: ☒ AND ☐ OR

AND

You can also search the subjects by only sex and age or filter the Metrics search by:

SEX	Both	
AGE	=	or between -

SEARCH

Figure A2.3. ‘Search Files’ page. The user can search the files by metric, artery, hemisphere, or a combination of those metrics, and can also filter by sex and age.

You can also search the subjects by only sex and age or filter the Metrics search by:

SEX

AGE -

SEARCH



BraVa

Tuesday, January 15 2013 Version 1.1

Home page

Browse all files

Search files

Related Links

Help

11 subjects that meet the search criteria appear in the database:
 SEX: Male
 AGE between 25 and 35 years

Download swc files

☒ Complete
 ☐ ACA
 ☐ MCA
 ☐ PCA

CODE	AGE	SEX
BG0002	31	M
BG0003	29	M
BG15	27	M
BG17	31	M
Set 8	32	M
BG0019	34	M
BG0020	31	M
BG0021	33	M
BH0008	28	M
BH0013	28	M
BH0016	28	M

Figure A2.4. Example of a user searching for Male data between the ages of 25 – 35. 11 subjects that match this criteria exist within the database.



Figure A2.5. The ‘Related Links’ page.

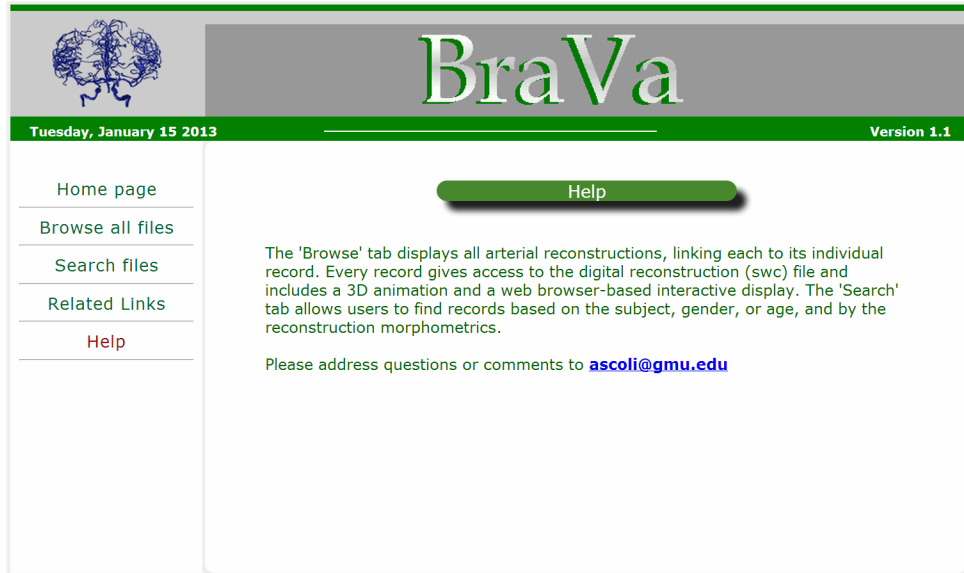
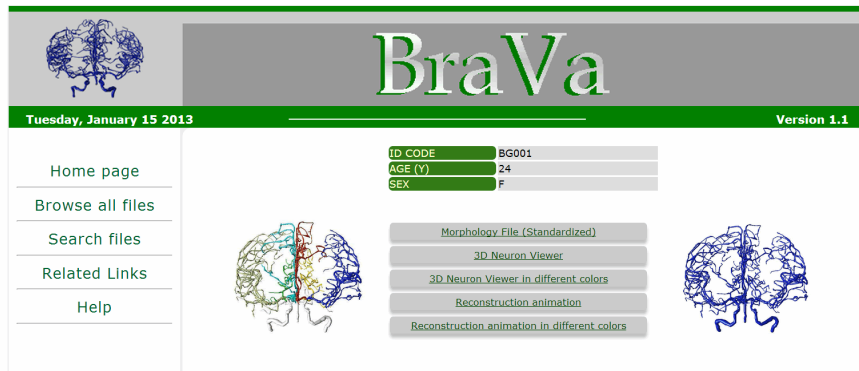


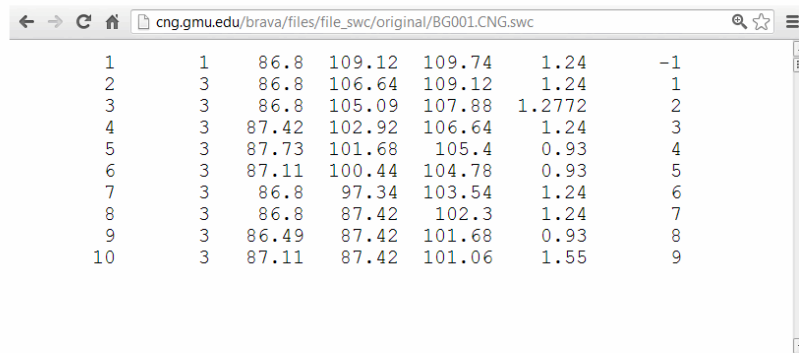
Figure A2.6. The ‘Help’ page.



COMPLETE TREES			ANTERIOR CEREBRAL ARTERY (ACA)		
Complete Trees - Size			ACA - Size		
Total number of branches	198.00		Total number of branches	24.00	17.00
Total length (mm)	6058.64		Total length (mm)	762.28	668.85
Max branch order	15.00		Max branch order	5.00	5.00
Max path distance (mm)	272.59		Max path distance (mm)	170.20	162.44
Max euclidean distance (mm)	107.04		Max euclidean distance (mm)	90.63	76.44
Width (mm)	124.62		Width (mm)	25.42	29.76
Height (mm)	85.25		Height (mm)	75.64	76.88
Depth (mm)	124.00		Depth (mm)	102.92	81.84
Complete Trees - Branch			ACA - Branch		
Mean local bifurcation amplitude (°)	86.98		Mean local bifurcation amplitude (°)	88.18	80.07
Mean bifurcation amplitude (°)	65.56		Mean bifurcation amplitude (°)	63.82	73.58
Contraction	0.73		Contraction	0.72	0.67
Partition asymmetry	0.48		Partition asymmetry	0.43	0.63
Fractal dimension	1.11		Fractal dimension	1.13	1.14
Branch path length (mm)	30.75		Branch path length (mm)	33.14	41.80
Mean bifurcation tilt (°)	107.00		Mean bifurcation tilt (°)	117.23	102.61
Mean bifurcation torque (°)	91.87		Mean bifurcation torque (°)	63.23	101.21
Mean fragmentation	14.30		Mean fragmentation	16.00	17.86

MIDDLE CEREBRAL ARTERY (MCA)			POSTERIOR CEREBRAL ARTERY (PCA)		
MCA - Size			PCA - Size		
Total number of branches	40.00	56.00	Total number of branches	22.00	24.00
Total length (mm)	1433.76	1775.72	Total length (mm)	454.36	458.43
Max branch order	9.00	8.00	Max branch order	6.00	7.00
Max path distance (mm)	203.90	213.21	Max path distance (mm)	142.49	125.34
Max euclidean distance (mm)	88.45	90.68	Max euclidean distance (mm)	84.25	80.32
Width (mm)	41.54	45.88	Width (mm)	28.83	34.72
Height (mm)	69.75	77.50	Height (mm)	60.14	48.36
Depth (mm)	92.38	112.22	Depth (mm)	58.28	62.00
MCA - Branch			PCA - Branch		
Mean local bifurcation amplitude (°)	81.60	88.79	Mean local bifurcation amplitude (°)	65.77	102.84
Mean bifurcation amplitude (°)	50.36	51.82	Mean bifurcation amplitude (°)	55.02	74.44
Contraction	0.72	0.73	Contraction	0.72	0.75
Partition asymmetry	0.40	0.50	Partition asymmetry	0.36	0.52
Fractal dimension	1.11	1.12	Fractal dimension	1.12	1.09
Branch path length (mm)	36.76	32.29	Branch path length (mm)	21.64	19.93
Mean bifurcation tilt (°)	107.47	100.22	Mean bifurcation tilt (°)	121.83	108.54
Mean bifurcation torque (°)	83.98	94.96	Mean bifurcation torque (°)	97.39	74.99
Mean fragmentation	16.39	14.61	Mean fragmentation	10.75	10.14

Figure A2.7. Overview of metrics for an individual subject. The ID Code, Age, & Sex for the subject, 2 views of the reconstructed data, and options for more views of the reconstructed data. The metrics for the complete tree, as well as the individual arteries are also shown.



1	1	86.8	109.12	109.74	1.24	-1
2	3	86.8	106.64	109.12	1.24	1
3	3	86.8	105.09	107.88	1.2772	2
4	3	87.42	102.92	106.64	1.24	3
5	3	87.73	101.68	105.4	0.93	4
6	3	87.11	100.44	104.78	0.93	5
7	3	86.8	97.34	103.54	1.24	6
8	3	86.8	87.42	102.3	1.24	7
9	3	86.49	87.42	101.68	0.93	8
10	3	87.11	87.42	101.06	1.55	9

Figure A2.8. The archived data can be viewed as an SWC file.

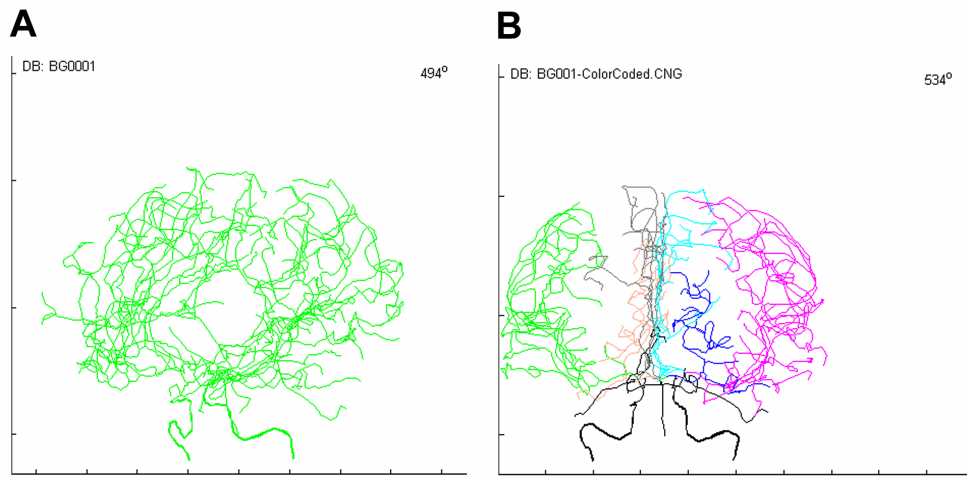


Figure A2.9. Examples of the various options for viewing the archived data. A. Animated rotation of data. **B.** Color-coded animated rotation of data.

REFERENCES

- Ahmed M, Masaryk TJ. Imaging of acute stroke: state of the art. *Seminars in Vascular Surgery*. 2004 17(2); 181-205.
- Alastruey J, Parker KH, Peiro J, Byrd SM, Sherwin SJ. Modeling the circle of Willis to assess the effects of anatomical variations and occlusions on cerebral flows. *Journal of Biomechanics*. 2007 (40); 1794-1805.
- Alazzaz A, Thornton J, Aletich VA, Debrun GM, Ausman JI, Charbel F. Intracranial percutaneous transluminal angioplasty for arteriosclerotic stenosis. *Archives of Neurology*. 2000 57(11); 1625-30.
- Almi'ani MM and Barkana BD. Automatic segmentation algorithm for brain MRA images. *The Eighth Annual IEEE Conference on Long Island Systems, Applications and Technology (IEEE LISAT 2012)*, May 2012, (Accepted).
- Alnaes MS, Isaksen J, Mardal KA. Computation of hemodynamics in the Circle of Willis. *Stroke*. 2007 (38); 2500-05.
- Ascoli GA and Krichmar JL. L-neuron: A modeling tool for the efficient generation and parsimonious description of dendritic morphology. *Neurocomputing*. 2000 (32-33); 1003-11.
- Ascoli GA, Krichmar JL, Nasuto SJ, Senft SL. Generation, description and storage of dendritic morphology data. *Philosophical Transactions of the Royal Society B: Biological Sciences*. 2001 356(1412); 1131-45.
- Ascoli GA, Krichmar JL, Scorcioni R, Nasuto SJ, Senft SL. Computer generation and quantitative morphometric analysis of virtual neurons. *Anatomy and Embryology*. 2001 (204); 283-301.
- Allder SJ, Moody AR, Martel AL, Morgan PS, Delay GS, Gladman JR, Fentem P, Lennox GG. Limitations of clinical diagnosis in acute stroke. *The Lancet*. 1999 (254); 1523.

- Alzamora MT, Sorribes M, Heras A, Vicheto M, Fores R, Sanchez-Oranguren J, Vila N, Sancho A, Pera G. Ischemic stroke incidence in Santa Coloma de Gramenet (ISISCOG), Spain: A community-based study. *BMC Neurology*. 2008 (8:5).
- Aubry R, Mut F, Lohner R, Cebal JR. Deflated preconditioned conjugate gradient solvers for the Pressure-Poisson equation. *Journal of Computational Physics*. 2008 227 (24); 10196-208.
- Bagan P, Azorin J, Salama J, Dumas JL. The value of phase-contrast magnetic resonance angiography of the circle of Willis in predicting cerebral ischemia-hypoxia (shunt need) during carotid endarterectomy. *Surgical and Radiologic Anatomy*. 2005 (27); 544-47.
- Bagan P, Vidal R, Martinod E, Destable MD, Tremblay B, Dumas JL, Azorin JF. Cerebral Ischemia during Carotid Artery Cross-Clamping: Predictive Value of Phase-Contrast Magnetic Resonance Imaging. *Annals of Vascular Surgery*. 2006 (20:6); 747-52.
- Baillard C, Hellier P, Barillot C. Segmentation of brain 3D images using level sets and dense registration. *Medical Image Analysis*. 2001 (5); 185-94.
- Bammer R, Skare S, Newbould R, Liu C, Thijs V, Ropele S, Clayton DB, Krueger G, Moseley ME, Glover GH. Foundations of advanced magnetic resonance imaging. *NeuroRx: The Journal of the American Society for Experimental NeuroTherapeutics*. 2005 2(2); 167-96.
- Bentson JR. Present Status of the Imaging of Acute Strokes. *Journals of Stroke and Cerebrovascular Diseases*. 1997 (6:4); 200-03.
- Bingzhen C, Yasaka M, Kimura K, Nagatsuka K, Minematsu K, Yamaguchi T. Side-to-side differences of the common carotid artery diameter in presence of asymmetry of the circle of Willis or different vasculopathies. *European Journal of Ultrasound*. 1998(8); 221-23.
- Bogunovic H, Pozo JM, Villa-Uriol MC, Majoie CBLM, van den Berg R, Gratama van Andel HAF, Macho JM, Blasco J, San Roman L, Frangi AF. Automated segmentation of cerebral vasculature with aneurysms in 3DRA and TOF-MRA using geodesic active regions: an evaluation study. *Journal of Medical Physics*. 2011 38(1); 210-22.
- Bor AS, Velthuis BK, Majoie CB, Rinkel GJ. Configuration of intracranial arteries and development of aneurysms: a follow-up study. *Neurology*. 2008 70(9); 700-5.

- Bosmans H, Marchal G, Van Hecke P, Vanhoenacker P. MRA review. *Journal of Clinical Imaging Science*. 1992 16(3): 152-67
- Brand-Herrmann SM. Where Do We Go for Atherothrombotic Disease Genetics (Editorial). *Stroke*. 2008 (39); 1070-75.
- Brands PJ, Hoeks APG, Hofstra L, Reneman RS. A Noninvasive Method to Estimate Wall Shear Rate Using Ultrasound. *Ultrasound in Medicine & Biology*. 1995 (21:2); 171-85.
- Brown KM, Donohue DE, D'Alessandro G, Ascoli GA. A cross-platform freeware tool for digital reconstruction of neuronal arborizations from image stacks. *Neuroinformatics*. 2005 3; 343-59.
- Brown KM, Gillette TA, Ascoli GA. Quantifying neuronal size: summing up trees and splitting the branch difference. *Seminars in Cell & Developmental Biology*. 2008 19(6); 485-93.
- Bui AV, Manasseh R, Liffman K, Sutalo ID. Development of optimized vascular fractal tree models using level set distance function. *Medical Engineering & Physics*. 2010 32(7); 790-4.
- Bullitt E, Guido G, Pizer SM, Lin W, Aylward SR. Measuring tortuosity of the intracerebral vasculature from MRA images. *IEEE Transactions on Medical Imaging*. 2003 22(9); 1163-71.
- Bullitt E, Muller KE, Jung I, Lin W, Aylward S. Analyzing attributes of vessel populations. *Medical Image Analysis*. 2005 9(1); 39-49.
- Bullitt E, Rahman FN, Smith JK, Kim E, Zeng D, Katz LM, Marks BL. The effect of exercise on the cerebral vasculature of healthy aged subjects as visualized by MR angiography. *American Journal of Neuroradiology*. 2009 30(10); 1857-63.
- Cai X, Chan RH, Morigi S, Sgallari F. Vessel Segmentation in Medical Imaging Using a Tight-Frame Based Algorithm, accepted for publication by *SIAM Journal on Imaging Science*, 2013.
- Canham PB, Finlay HM. Morphometry of medial gaps of human brain artery branches. *Stroke*. 2004 35; 1153-57.
- Cannon RC, Turner DA, Pyapali GK, Wheal HV. An on-line archive of reconstructed hippocampal neurons. *Journal of Neuroscience Methods*. 1998 (84); 49-54.

- Cassot F, Vergeur V, Bossuet P, Hillen B, Zagzoule M, Marc-Vergnes JP. Effects of Anterior Communicating Artery Diameter on Cerebral Hemodynamics in Internal Carotid Artery Disease. *Circulation*. 1995 (92); 3122-31.
- Castro MA, Putnam CM, Cebal JR. Patient-Specific Computational Modeling of Cerebral Aneurysms With Multiple Avenues of Flow From 3D Rotational Angiography Images. *Academic Radiology*. 2006 (13); 811-21.
- Cebal, JR, Löhner R, Burgess JE. Computer simulation of cerebral artery clipping: relevance to aneurysm neuro-surgery planning. In *ECCOMAS*. 2000. Barcelona, Spain.
- Cebal, JR, Castro MA, Soto O, Löhner R, Alperin N. Blood flow models of the circle of Willis from magnetic resonance data. *Journal of Engineering Mathematics*. 2003 47(3-4); 369-86.
- Cebal JR, Castro MA, Appanaboyina S, Putnam CM, Millan D, Frangi AF. Efficient pipeline for image-based patient-specific analysis of cerebral aneurysm hemodynamics: technique and sensitivity. *IEEE Transactions on Medical Imaging*. 2005 (24); 457-467.
- Cebal JR, Castro MA, Burgess JE, Pergolizzi RS, Sheridan MJ, Putnam CM. Characterization of Cerebral Aneurysms for Assessing Risk of Rupture By Using Patient-Specific Computational Hemodynamics Models. *American Journal of Neuroradiology*. 2005 (26); 2550-59.
- Cebal JR, Pergolizzi RS, Putnam CM. Computational Fluid Dynamics Modeling of Intracranial Aneurysms: Qualitative Comparison with Cerebral Angiography. *Academic Radiology*. 2007 (14); 804-13.
- Chang CC, Noji M, Kuwana N. J. Clin. Dissecting aneurysm of the middle cerebral artery associated with subarachnoid haemorrhage. *Neuroscience*. 1998(5:3); 361-63.
- Chang HH and Valentino DJ. An electrostatic deformable model for medical image segmentation. *Computerized Medical Imaging and Graphics*. 2008 (32); 22-35.
- Chen G, Frokiaer J, Pedersen M, Nielsen S, Si Z, Pang Q, Stodkilde-Jorgensen H. Reduction of ischemic stroke in rat brain by alpha melanocyte stimulating hormone. *Neuropeptides*. 2008 (42:3); 331-38.
- Chen YC, Li MH, Qiao RH. Analysis of correlation between the number of lenticulostriate arteries and hypertension based on high-resolution MR

- angiography findings. *American Journal of Neuroradiology*. 2011 32(10); 1899-903.
- Chen G, Frokiaer J, Pedersen M, Nielsen S, Si Z, Pang Q, Stodkilde-Jorgensen H. Reduction of ischemic stroke in rat brain by alpha melanocyte stimulating hormone. *Neuropeptides*. 2008 (42:3); 331-38.
- Cheng C, Helderma F, Tempel D, Segers D, Hierck B, Poelmann R, van Tol A, Duncker DJ, Robbers-Visser D, Ursem NTC, van Haperen R, Wentzel JJ, Gijzen F, van der Steen AFW, de Crom R, Krams R. Large variations in absolute wall shear stress levels within one species and between species. *Atherosclerosis*. 2007 (195); 225-35.
- Chung AC, Noble JA, Summers P. Vascular segmentation of phase contrast magnetic resonance angiograms based on statistical modeling and local phase coherence. *IEEE Transactions on Medical Imaging*. 2004 (23:12); 1490-507.
- Chung B and Wong V. Pediatric Stroke Among Hong Kong Chinese Subjects. *Pediatrics*. 2004 (114); e206-12.
- Claiborne BJ, Amaral DG, Cowan WM. Quantitative, three-dimensional analysis of granule cell dendrites in the rat dentate gyrus. *Journal of Comparative Neurology*. 1990 302(2); 206-19.
- Collins TJ. ImageJ for microscopy. *Biotechniques*. 2007 43(1 Suppl); 25-30.
- Cucchiara B and Detre J. Migraine and circle of Willis anomalies. *Medical Hypotheses*. 2008(70); 860-65.
- Datta S and Chakraborty M. Extraction of circle of willis from 2D magnetic resonance angiograms. *ACEEE International Journal on Information Technology*. 2012 2(1): 52-55.
- de Monye C, Dippel DWJ, Siepmann TAM, Dijkshoorn ML, Tanghe HLJ, van der Lugt A. Is a fetal origin of the posterior cerebral artery a risk factor for TIA or ischemic stroke?: A study with 16-multidetector-row CT angiography. *Journal of Neurology*. 2008 (255); 239-45.
- Deplano V and Siouffi M. Experimental and numerical study of pulsatile flows through stenosis: Wall shear stress analysis. *Journal of Biomechanics*. 1999 (32); 1081-90.
- Diedrich KT, Roberts JA, Schmidt RH, Kang CK, Cho ZH, Parker DL. Validation of an arterial tortuosity measure with application to hypertension collection of clinical hypertensive patients. *BMC Bioinformatics*. 2011 18(12 Suppl); S15.

- Ding H, You C, Yin H. Nontraumatic and noninfectious pseudoaneurysms on the circle of Willis: 2 case reports and review of the literature. *Surgical Neurology*. 2008 (69); 414-17.
- Dobson MJ, Hartley RWJ, Ashleigh R, Watson Y, Hawnaur JM. MR Angiography and MR Imaging of Symptomatic Vascular Malformations. *Clinical Radiology*. 1997 (52); 595-602.
- Dokoumetzidis, A. and P. Macheras, A model for transport and dispersion in the circulatory system based on the vascular fractal tree. *Annals of Biomedical Engineering*, 2003. 31(3): p. 284-93.
- Donohue DE and Ascoli GA. Local Diameter Fully Constrains Dendritic Size in Basal but not Apical Trees of CA1 Pyramidal Neurons. *Journal of Computational Neuroscience*. 2005 (19); 223-38.
- Drapaca CS, Cardenas V, Studholme C. Segmentation of tissue boundary evolution from brain MR image sequences using multi-phase level sets. *Computer Vision and Image Understanding*. 2005 (100); 312-29.
- Duncan JS, Papademetris X, Yang J, Jackowski M, Zeng X, Staib LH. Geometric strategies for neuroanatomic analysis from MRI. *Neuroimage*. 2004 (23); S34-45.
- Duque A, Tepper JM, Detari L, Ascoli GA, Zaborszky L. Morphological characterization of electrophysiologically and immunohistochemically identified basal forebrain cholinergic and neuropeptide Y-containing neurons. *Brain Structure and Function*. 2007 (212); 55-73.
- Efstathiopoulos EP, Patatoukas G, Pantos I, Benekos O, Katritsis D, Kelekis NL. Wall shear stress calculation in ascending aorta using phase contrast magnetic resonance imaging. Investigating effective ways to calculate it in clinical practice. *Physica Medica: European Journal of Medical Physics*. 2008; 1-7.
- Eftekhari B, Dadmehr M, Ansari S, Ghodsi M, Nazparvar B, Ketabchi E. Are the distributions of variations of circle of Willis different in different populations? – Results of an anatomical study and review of literature. *BMC Neurology*. 2006 (6:22).
- El-Barhoun EN, Gledhill SR, Pitman AG. Circle of Willis artery diameters on MR angiography: an Australian reference database. *Journal of Medical Imaging and Radiation Oncology*. 2009 53(3); 248-60.

- El-Baz A, Farag AA, Gimel'farb G, Hushek SG. Automatic cerebrovascular segmentation by accurate probabilistic modeling of TOF-MRA images. *Medical Image Computing and Computer Assisted Intervention Conference* 2005 (8:1); 34-42.
- Esneault E, Castagne V, Moser P, Bonny C, Bernaudin M. D-JNKi, A Peptide Inhibitor of c-Jun N-Terminal Kinase, Promotes Functional Recovery After Transient Focal Cerebral Ischemia in Rats. *Neuroscience*. 2008 (152); 308-320.
- Fanucci E, Oriacchio A, Pocek M. The vascular geometry of human arterial bifurcations. *Investigative Radiology*. 1988 1; 713-8.
- Fanucci E, Oriacchio A, Pocek M, Magrini A, Salomoni E. Optimal branching of human arterial bifurcations. *Investigative Radiology*. 1990 25(1); 62-6.
- Ferrandez A, David T, Bamford J, Scott J, Guthrie A. Computational models of blood flow in the circle of Willis. *Computer Methods in Biomechanics and Biomedical Engineering*. 2000 (4:1); 1-26.
- Ferrandez A, David T, Brow MD. Numerical models of auto-regulation and blood flow in the cerebral circulation. *Computer Methods in Biomechanics and Biomedical Engineering*. 2002 (5:1); 7-19.
- Flasque N, Desvignes M, Constans JM, Revenu M. Acquisition, segmentation and tracking of the cerebral vascular tree on 3D magnetic resonance angiography images. *Medical Image Analysis*. 2001 (5): 173-83.
- Georgiou T, Michailovich O, Rathi Y, Malcolm J, Tannenbaum A. Distribution metrics and image segmentation. *Linear Algebra and its Applications*. 2007 (425); 663-72.
- Ghods AJ, Lopes D, Chen M. Gender differences in cerebral aneurysm location. *Frontiers in Neurology*. 2012 3:78.
- Grandin CB, Mathurin P, Duprez T, Stroobandt G, Hammer F, Goffette P, Cosnard G. Diagnosis of Intracranial Aneurysms: Accuracy of MR Angiography at 0.5 T. *American Journal of Neuroradiology*. 1998 (19); 245-52.
- Greve JM, Les AS, Tang BT, Blomme MTD, Wilson NM, Dalman RL, Pelc NJ, Taylor CA. Allometric scaling of wall shear stress from mice to humans: quantification using cine phase-contrast MRI and computational fluid dynamics. *American Journal of Physiology - Heart and Circulatory Physiology*. 2006 (291); H1700-08.

- Halavi M, Hamilton KA, Parekh R, Ascoli GA. Digital reconstructions of neuronal morphology: three decades of research trends. *Frontiers in Neuroscience*. 2012 6:49.
- Halavi M, Polavaram S, Donohue DE, Hamilton G, Hoyt J, Smith KP, Ascoli GA. NeuroMorpho.Org implementation of digital neuroscience: dense coverage and integration with the NIF. *Neuroinformatics*. 2008. 6(3); 241-52.
- Hao JT, Li ML, Tang FL. Adaptive segmentation of cerebrovascular tree in time-of-flight magnetic resonance angiography. *Medical & Biological Engineering & Computing*. 2008 (46):75-83.
- Harrison MJ, Johnson BA, Gardner GM, Welling BG. Preliminary Results on the Management of Unruptured Intracranial Aneurysms with Magnetic Resonance Angiography and Computer Tomographic Angiography. *Neurosurgery*. 1997 (40:5); 947-57.
- Hassan H and Farag AA. MRA data segmentation using level sets. *IEEE International Conference on Image Processing, ICIP-03, Barcelona, Spain, September 14-17, 2003*, pp. II 173-176.
- He L, Peng Z, Everding B, Wang X, Han CY, Weiss KL, Wee WG. A comparative study of deformable contour methods on medical image segmentation. *Image and Vision Computing*. 2008 (26); 141-63.
- Hendrikse J, van Raamt AF, van der Graaf Y, Mali WPTM, van der Grond J. Distribution of Cerebral Blood Flow in the Circle of Willis. *Radiology*. 2005 (235:1) 184-89.
- Hernandez M and Frangi AF. Non-parametric geodesic active regions: Method and evaluation for cerebral aneurysm segmentation in 3DRA and CTA. *Medical Image Analysis*. 2007 (11); 224-41.
- Higashida RT and Furlan AJ. Trial Design and Reporting Standards for Intra-Arterial Cerebral Thrombolysis for Acute Ischemic Stroke. *Stroke*. 2003 (34:8); e109-37.
- Horiuchi T, Tanaka Y, Hongo K. Sex-related differences in patients treated surgically for aneurysmal subarachnoid hemorrhage. *Neurologia medico-chirurgica (Tokyo)*. 2006 46; 328-332.
- Huettel SA, Song AW, McCarthy G. *Functional Magnetic Resonance Imaging*. Sunderland, Massachusetts, Sinauer Associates, Inc. 2004.
- Hugdahl K. Symmetry and asymmetry in the human brain. *European Review*. 2005 13(2);119-33.

- Huo Y and Kassab GS. A hybrid one-dimensional/Womersley model of pulsatile blood flow in the entire coronary arterial tree. *American Journal of Physiology - Heart and Circulatory Physiology*. 2007 (292); H2623-33.
- Huo Y, Wischgoll T, Kassab GS. Flow patterns in three-dimensional porcine epicardial coronary arterial tree. *American Journal of Physiology - Heart and Circulatory Physiology*. 2007 (293); H2959-70.
- Huo Y, et al., Which diameter and angle rule provides optimal flow patterns in a coronary bifurcation? *Journal of Biomechanics*, 2012. 45(7): p. 1273-9.
- Ingebrigtsen T, Morgan MK, Faulder K, Ingebrigtsen L, Sparr T, Schrimmer H. Bifurcation geometry and the presence of cerebral artery aneurysms. *Journal of Neurosurgery*. 2004 101; 108-13.
- Insko EK, Carpenter JP. Magnetic resonance angiography. *Seminars in Vascular Surgery*. 2004 17(2); 83-101.
- ISO (International Organization for Standardization): Basic human body measurements for technological design - Part 2: statistical summaries of body measurements from individual ISO populations. TR 7250-2:2010
- Jayaraman MV, Do HM, Versnick EJ, Steinberg GK, Marks MP. Morphologic Assessment of Middle Cerebral Artery Aneurysms for Endovascular Treatment. *Journal of Stroke and Cerebrovascular Diseases*. 2007 (16:2); 52-56.
- Joo SP, Kim TS, Choi JW, Lee JK, Kim YS, Moon KS, Kim JH, Kim SH. Characteristics and management of ruptured distal middle cerebral artery aneurysms. *Acta Neurochirurgica*. 2007 (149); 661-67.
- Kaimovitz B, Huo Y, Lanir Y, Kassab GS. Diameter asymmetry of porcine coronary arterial trees: structural and functional implications. *American Journal of Physiology - Heart and Circulatory Physiology*. 2008 (294); H714-23.
- Kamiya A, Takahashi T. Quantitative assessments of morphological and functional properties of biological trees based on their fractal nature. *Journal of Applied Physiology*. 2007 102; 2315-23.
- Karau KL, Krenz GS, Dawson CA. Branching exponent heterogeneity and wall shear stress distribution in vascular trees. *American Journal of Physiology – Heart and Circulatory Physiology*. 2001 (280:3); H1256-63.

- Karch, R, Neumann F, Neumann M, Schreiner W. A three-dimensional model for arterial tree representation, generated by constrained constructive optimization. *Computers in Biology and Medicine*. 1999 29(1); 19-38.
- Karch R, Neumann F, Neumann M, Schreiner W. Staged growth of optimized arterial model trees. *Annals of Biomedical Engineering*. 2000 28; 495-511.
- Kassab GS. Scaling laws of vascular trees: of form and function. *American Journal of Physiology – Heart and Circulatory Physiology*. 2006 290; H894-903.
- Katrtsis D, Kaiktsis L, Chaniotis A, Pantos J, Efstathopoulos EP, Marmarelis V. Wall Shear Stress: Theoretical Considerations and Methods of Measurement. *Progress in Cardiovascular Diseases*. 2007 (49:5); 307-29.
- Katz DA, Marks MP, Napel SA, Bracci PM, Roberts SL. Circle of Willis: Evaluation with Spiral CT Angiography, MR Angiography, and Conventional Angiography. *Radiology*. 1995 (195:2); 445-49.
- Kayembe KN, Sasahara M, Hazama F. Cerebral aneurysms and variations in the circle of Willis. *Stroke*. 1984 15; 846-50.
- Keedy A. An overview of intracranial aneurysms. *Mcgill Journal of Medicine*. 2006 9(2): 141-46.
- Kelly ME, Turner R, Gonugunta V, Woo HH, Rasmussen PA, Masaryk TJ, Fiorella D. Stent Reconstruction of Wide-Necked Aneurysms Across the Circle of Willis. *Operative Neurosurgery*. 2007 (61); 249-54.
- Keogh AJ, Vhora S. The Usefulness of Magnetic Resonance Angiography in Surgery for Intracranial Aneurysms That Have Bled. *Surgical Neurology*. 1998 (50); 122-9.
- Kobashi S, Kamiura N, Hata Y, Miyawaki F. Volume-quantization-based neural network approach to 3D MR angiography image segmentation. *Image and Vision Computing*. 2001 (19); 185-93.
- Kostulas K, Brophy VH, Moraitis K, Manolescu A, Kostulas V, Gretarsdottir S, Cheng S, Hilbert J. Genetic profile of ischemic cerebrovascular disease and carotid stenosis. *Acta Neurologica Scandinavica*. 2008; 1-7.
- Krabbe-Hartkamp MJ, van der Grond J, de Leeuw FE, de Groot JC, Algra A, Hillen B, Breteler MMB, Mali WPTM. Circle of Willis: Morphologic Variation on Three-Dimensional Time-of-Flight MR Angiograms. *Radiology*. 1998 (207); 103-11.

- Krichmar JL, Velasquez D, Ascoli GA. Effects of β -Catenin on Dendritic Morphology and Simulated Firing Patterns in Cultured Hippocampal Neurons. *The Biological Bulletin*. 2006 (211); 31-43.
- Kundu PK and Cohen IM. *Fluid Mechanics*. Amsterdam, The Netherlands: Elsevier, 2004.
- Kusunoki K, Oka Y, Saito M, Sadamoto K, Sakaki S, Miki H, Nagasawa K. Changes in visibility of intracranial arteries on MRA with normal ageing. *Neuroradiology*. 1999 (41); 813-19.
- LaDisa Jr. JF, Olson LE, Douglas HA, Warltier DC, Kersten JR, Pagel PS. Alterations in regional vascular geometry produced by theoretical stent implantation influence distributions of wall shear stress: analysis of a curved coronary artery using 3D computational fluid dynamics modeling. *Biomedical Engineering Online*. 2006 (5:40).
- Lell M, Fellner C, Baum U, Hothorn T, Steiner R, Lang W, Bautz W, Fellner FA. Evaluation of carotid artery stenosis with multisection CT and MR imaging: influence of imaging modality and postprocessing. *American Journal of Neuroradiology*. 2007 28(1); 104-10.
- Lemesle M, Milan C, Faivre J, Moreau T, Giroud M, Dumas R. Incidence Trends of Ischemic Stroke and Transient Ischemic Attacks in a Well-Defined French Population From 1985 Through 1994. *Stroke*. 1999 (30:2); 371-77.
- Liao W, Rohn K, Kang CK, CHO ZH, Worz S. A generative approach for automatic 3D segmentation of cerebral vasculature from 7 tesla MRA images. *Biomedical Imaging: From Nano to Macro*, 2011 IEEE International Symposium, March 30-April 2, 2011: 2041-44.
- Liao W, Rohr K, Kang CK, Cho ZH, Worz S. Automatic human brain vessel segmentation from 3D 7 tesla MRA images using fast marching with anisotropic directional prior. *Biomedical Imaging*, 2012 9th IEEE International Symposium, May 2-5, 2012:1140-43.
- Liem MD, Gzesh DJ, Flanders AE. MRI and angiographic diagnosis of lupus cerebral vasculitis. *Diagnostic Neuroradiology*. 1996 38; 134-36.
- Lindekleiv HM, Valen-Sendstad K, Morgan MK, Mardal KA, Faulder K, Magnus JH, Waterloo K, Romner B, Ingebrigtsen T. Sex differences in intracranial arterial bifurcations. *Gender Medicine*. 2010 7(2); 149-55.

- Lindsay KA, Rosenberg JR, Tucker G. From Maxwell's equations to the cable equation and beyond. *Progress in Biophysics and Molecular Biology*. 2004. 85(1); 71-116.
- Liu Y, Kassab GS. Vascular metabolic dissipation in Murray's law. *American Journal of Physiology – Heart and Circulatory Physiology*. 2007 292; H1336-39.
- Lohani B. Fusiform middle cerebral artery aneurysm. *Journal of Neuroscience*. 2004 (1); 50-52.
- Lohner R. *Applied CFD Techniques: An Introduction based on Finite Element Methods*, 2nd ed. Wiley, 2008.
- Lorigo LM, Faugeras OD, Grimson WEL, Keriven R, Kikinis R, Nabavi A, Westin CF. CURVES: Curve evolution for vessel segmentation. *Medical Image Analysis*. 2001 (5); 195-206.
- Luo S, Jin JJ, Li J. A knowledge-based approach for segmenting cerebral vasculature in neuroimages. 2011 Third International Conference on Measuring Technology and Mechatronics Automation. January 6-7, 2011 (1): 74-77.
- Luo S, Lee S, Ma X, Aziz A, Nowinski WL. Automatic extraction of cerebral arteries from magnetic resonance angiography data: Algorithm and validation. *International Congress Series*. 2005 (1281); 375-80.
- MacLean NF, Kratky RG, Macfarlane TWR, Roach MR. Taper: an important feature of y-bifurcations in porcine renal arteries and human cerebral arteries. *Journal of Biomechanics*. 1992 25(9); 1047-52.
- Manniesing R, Velthuis BK, van Leeuwen MS, van der Schaaf IC, van Laar PJ, Niessen WJ. Level set based cerebral vasculature segmentation and diameter quantification in CT angiography. *Medical Image Analysis*. 2006 (10); 200-14.
- Mazumdar J. *Biofluid Mechanics*. Singapore: World Scientific, 1992.
- McInerney T and Terzopoulos D. Medical image segmentation using topologically adaptable surfaces. *Proceedings. CVR Medicine*. 1997.
- Minematsu K. MR imaging in acute stroke. *International Congress Series*. 2003 (1252); 309-14.
- Moore SM, Moorhead KT, Chase JG, David T, Fink J. One-dimensional and three-dimensional models of cerebrovascular flow. *Journal of Biomechanical Engineering*. 2005 (127:3); 440-9.

- Moore S, David T, Chase JG, Arnold J, Fink J. 3D models of blood flow in the cerebral vasculature. *Journal of Biomechanics*. 2006 (39); 1454-63.
- Moorhead KT, Doran CV, Chase JG, David T. Lumped parameter and feedback control models of the auto-regulatory response in the Circle of Willis. *Computational Methods in Biomechanics and Biomedical Engineering*. 2004 (7:3); 121-30.
- Moorhead KT, Chase JG, David T, Arnold J. Metabolic model of autoregulation in the Circle of Willis. *Journal of Biomechanical Engineering*. 2006 (128:3); 462-6.
- Moritani T, Shrier DA, Numaguchi Y, Takahasi C, Yano T, Nakai K, Zhong J, Wang HZ, Shibata DK, Naselli SM. Diffusion-weighted echo-planar MR imaging of CNS involvement in systemic lupus erythematosus. *Academic Radiology*. 2001 8(8); 741-53.
- Moritz A, Koci G, Steinlechner B, Holzenbein T, Nasel C, Grubhofer G, Dworschak M. Contralateral stroke during carotid endarterectomy due to abnormalities in the circle of Willis. *Wien Klin Wochenschr*. 2007 (119/21-22); 669-73.
- Murray CD. The Physiological Principle of Minimum Work. *Proceedings of the National Academy of Sciences of the United States of America*, 1926. 12(3): p. 207-214.
- Naggara O, Touze E, Seiller N, Gobin-Metteil MP, Mas JL, Meder JF, Oppenheim C. Asymmetry of intracranial internal carotid artery on 3D TOF MR angiography: a sign of unilateral extracranial stenosis. *European Journal of Radiology*. 2008 (18:5); 1038-42.
- Niemark MA, Konstas AA, Laine AF, Pile-Spellman J. Integration of jugular venous return and circle of Willis in a theoretical model of selective brain cooling. *Journal of Applied Physiology*. 2007 (103); 1837-47.
- Niesen WD, Rosenkranz M, Eckert B, Meissner M, Weiller C, Sliwka U. Hemodynamic Changes of the Cerebral Circulation after Stent-Protected Carotid Angioplasty. *American Journal of Neuroradiology*. 2004 (25); 1162-67.
- Norman PE, Powell JT. Basic Science for Clinicians. Site Specificity of Aneurysmal Disease. *Circulation*. 2010 121; 560-68.
- Nowinski WL, Chua BC, Marchenko Y, Puspitsari F, Volkau I, Knopp MV. Three-dimensional reference and stereotactic atlas of human cerebrovasculature from 7 Tesla. *Neuroimage*. 2011 55(3); 986-98.
- Nowinski WL, Puspitsaari F, Volkau I, Marchenko Y, Knopp MV. Comparison of magnetic resonance angiography scans on 1.5, 3, and 7 Tesla units: a quantitative

- study of 3-dimensional cerebrovasculature. *Journal of Neuroimaging*. 2011 Mar 29. doi: 10.1111/j.1552-6569.2011.00597.x. [Epub ahead of print]
- Nowinski WL, Thirunavuukarasuu A, Volkau I, Marchenko Y, Aminah B, Puspitasari F, Runge VM. A three-dimensional interactive atlas of cerebral arterial variants. *Neuroinformatics*. 2009 7(4); 255-64.
- Nowinski WL, Volkau I, Marchenko Y, Thirunavuukarasuu A, Ng TT, Runge VM. A 3D model of human cerebrovasculature derived from 3T magnetic resonance angiography. *Neuroinformatics*. 2009 7(1); 23-36.
- O'Flynn PM, O'Sullivan G, Pandit AS. Methods for three-dimensional geometric characterization of the arterial vasculature. *Annals of Biomedical Engineering*. 2007 35(8); 1368-81.
- Okahara M, Kiyosue H, Mori H, Tanoue S, Sainou M, Nagatomi H. Anatomic variations of the cerebral arteries and their embryology: a pictorial review. *European Journal of Radiology*. 2002 (12); 2548-61.
- Oktar SO, Yucel C, Karaosmanoglu D, Akkan K, Ozdemir H, Tokgoz N, Tali T. Blood-Flow Volume Quantification in Internal Carotid and Vertebral Arteries: Comparison of 3 Different Ultrasound Techniques with Phase-Contrast MR Imaging. *American Journal of Neuroradiology*. 2006 (27); 363-69.
- Olufsen MS. Structured tree outflow condition for blood flow in larger systemic arteries. *American Journal of Physiology – Heart and Circulatory Physiology*, 1999 276; 257-68.
- Olufsen MS, Peskin CS, Kim WY, Pedersen EM, Nadim I, Larsen J. Numerical simulation and experimental validation of blood flow in arteries with structured-tree outflow conditions. *Annals of Biomedical Engineering*. 2000 28(11); 1281-99.
- Oshima M, Ryo T, Toshio K, Nobuyuki T, Kiyoshi T. Finite element simulation of blood flow in the cerebral artery. *Computer Methods in Applied Mechanics and Engineering*. 2001 191(6-7); 661-71.
- Oyre S, Ringgaard S, Kozerke S, Paaske WP, Erlandsen M, Boesiger P, Pederson EM. Accurate Noninvasive Quantitation of Blood Flow, Cross-Sectional Lumen Vessel Area and Wall Shear Stress by Three-Dimensional Paraboloid Modeling of Magnetic Resonance Imaging Velocity Data. *Journal of the American College of Cardiology*. 1998 (32:1); 128-34.

- Painter PR, Eden P, Bengtsson HU. Pulsatile blood flow, shear force, energy dissipation and Murray's Law. *Theoretical Biology and Medical Modeling*. 2006 3:31.
- Papantchev V, Hristov S, Todorova D, Naydenov E, Paloff A, Nikolov D, Tschirkov A, Ovtscharoff W. Some variations of the circle of Willis, important for cerebral protection in aortic surgery – a study in Eastern Europeans. *European Journal of Cardio-thoracic Surgery*. 2007(31); 982-89.
- Parmar H, Sitoh YY, Hui F. Normal variants of the intracranial circulation demonstrated by MR angiography at 3T. *European Journal of Radiology*. 2005 56; 220-8.
- Passat N, Ronse C, Baruthio J, Armspach JP, Foucher J. Watershed and multimodel data for brain vessel segmentation: Application to the superior sagittal sinus. *Image and Vision Computing*. 2007 (25); 512-21.
- Passat N, Ronse C, Baruthio J, Armspach JP, Maillot C. Magnetic resonance angiography: from anatomical knowledge modeling to vessel segmentation. *Medical Image Analysis*. 2006 10(2); 259-74.
- Payne AH, Vemuri P, Parker DL, Roemer RB. A complete vascular description of a human brain using TOF-MRA for application in thermal modeling. *Proceedings of the International Society of Magnetic Resonance Medicine*. 13 (2005).
- Petty GW, Brown RD, Whisnant JP, Sicks JD, O'Fallon WM, Wiebers DO. Ischemic Stroke Subtypes: A Population-Based Study of Functional Outcome, Survival, and Recurrence. *Stroke*. 2000 (31:5); 1062-68.
- Piechnik SK, Czosnyka M, Harris NG, Minhas PS, Pickard JD. A Model of the Cerebral and Cerebrospinal Fluid Circulations to Examine Asymmetry in Cerebrovascular Reactivity. *Journal of Cerebral Blood Flow and Metabolism*. 2001 (21); 182-92.
- Qin Z, Mou X, Zhang R. A 3D modeling scheme for cerebral vasculature from MRA datasets. *IEEE Computer Society Conference*. 2003. p. 346-.
- Ramachandran VS. *The Tell-Tale Brain: A Neuroscientist's Quest for What Makes Us Human*. W.W. Norton & Company; Reprint Edition, 2012.
- Reneman RS, Arts T, Hoeks APG. Wall Shear Stress – an Important Determinant of Endothelial Cell Function and Structure – in the Arterial System in vivo. *Journal of Vascular Research*. 2006 (43:3); 251-69.
- Reneman RS and Hoeks APG. Wall shear stress as measured in vivo: consequences for the design of the arterial system. *Medical & Biological Engineering & Computing*. 2008 (46:5); 499-507.

- Rifai H, Bloch I, Hutchinson S, Wiart J, Garner L. Segmentation of the skull in MRI volumes using deformable model and taking the partial volume effect into account. *Medical Image Analysis*. 2000 (4); 219-33.
- Roach MR, MacLean NF. The importance of taper proximal and distal to Y-bifurcations in arteries. *Frontiers of Medical & Biological Engineering*. 1993 5(2); 127-33.
- Rossitti S, Lofgren J. Vascular dimensions of the cerebral arteries follow the principle of minimum work. *Stroke*. 1993 24(3); 371-7.
- Rossitti S, Lofgren J. Optimality principles and flow orderliness at the branching points of cerebral arteries. *Stroke*. 1993 24(7); 1029-32.
- Rutgers DR, Klijn CJM, Kappelle LJ, van Huffelen AC, van der Grond J. A Longitudinal Study of Collateral Flow Patterns in the Circle of Willis and the Ophthalmic Artery in Patients With a Symptomatic Internal Carotid Artery Occlusion. *Stroke*. 2000 (31:8); 1913-20.
- Rutgers DR, Klijn CJM, Kappelle LJ, van der Grond J. Recurrent Stroke in Patients With Symptomatic Carotid Artery Occlusion Is Associated With High-Volume Flow to the Brain and Increased Collateral Circulation. *Stroke*. 2004 (35); 1345-49.
- Sabry M, Sites CB, Farag AA, Hushek S, Moriarty T. A fast automatic method for 3D volume segmentation of the human cerebrovascular. *Computer Assisted Radiology and Surgery*. 2002; 382-87.
- Samsonovich AV and Ascoli GA. Statistical Morphological Analysis of Hippocampal Principal Neurons Indicates Cell-Specific Repulsion of Dendrites From Their Own Cell. *Journal of Neuroscience Research*. 2003 (71); 173-87.
- Samsonovich AV and Ascoli GA. Algorithmic description of hippocampal granule cell dendritic morphology. *Neurocomputing*. 2005 (65-66); 253-60.
- Samsonovich A, Ascoli G. Morphological homeostasis in cortical dendrites. *Proceedings of the National Academy of Sciences. USA*. 2006 103; 1569-74.
- Santos-Franco JA, Zenteno M. Dissecting aneurysms of the vertebrobasilar system: a comprehensive review on natural history and treatment options. *Neurosurgical Review*. 2008 (31:2); 131-40.
- Schaefer PW, Romero JM, Grant PE, Wu O, Sorensen AG, Koroshetz W, Gonzales RG. Diffusion Magnetic Resonance Imaging of Acute Ischemic Stroke. *Seminars in Roentgenology*. 2002 (37:3); 219-29.

- Schreiner, W., et al., Constrained constructive optimization of arterial tree models, in *Scaling in biology*. 2000, Oxford University Press: Oxford, UK. p. 145-165.
- Scorcioni R and Ascoli GA. Algorithmic Extraction of Morphological Statistics from Electronic Archives of Neuroanatomy. *Lecture Notes in Computer Science*. 2001 (2084); 30-37.
- Scorcioni R and Ascoli GA. Algorithmic reconstruction of complete axonal arborizations in rat hippocampal neurons. *Neurocomputing*. 2005 (65-66); 15-22.
- Scorcioni R, Lazarewicz M, Ascoli G. Quantitative morphometry of hippocampal pyramidal cells: differences between anatomical classes and reconstructing laboratories. *Journal of Comparative Neurology*. 2004 273; 177-93.
- Scorcioni R, Polavaram S, Ascoli GA. L-Measure: a web-accessible tool for the analysis, comparison and search of digital reconstructions of neuronal morphologies. *Nature Protocols*. 2008 3(5); 866-76.
- Seo Y, Hashimoto T, Nuki Y, Hasegawa BH. In vivo microCT imaging of rodent cerebral vasculature. *Physics in Medicine and Biology*. 2008 (53); N99-107.
- Sforza, D., C.M. Putman, and J.R. Cebral, Hemodynamics of Cerebral Aneurysms. *Annual Review of Fluid Mechanics*, 2009. 41: p. 91-107.
- Shelly GB, Woods DM. (2004). *HTML: Complete Concepts and Techniques*. Course Technology, 5th Ed., Shelly Cashman Series.
- Sheppard AP, Sok RM, Averdunk H. Techniques for image enhancement and segmentation of tomographic images and porous materials. *Physica A: Statistical Mechanics and its Applications*. 2004 (339); 145-51.
- Sherman TF. On connecting large vessels to small: the meaning of Murray's Law. *The Journal of General Physiology*. 1981 78; 431-53.
- Silber HA, Bluemke DA, Ouyang P, Du YP, Post WS, Lima JAC. The Relationship Between Vascular Wall Shear Stress and Flow-Mediated Dilation: Endothelial Function Assessed by Phase-Contrast Magnetic Resonance Angiography. *Journal of the American College of Cardiology*. 2001 (38:7); 1859-65.
- Sklar D. (2004). *Learning PHP 5*, 1st Ed. O'Reilly Media.

- Spangler KM, Challa VR, Moody DM, Bell MA. Arteriolar tortuosity of the white matter in aging and hypertension. A microradiographic study. *Journal of Neuropathology and Experimental Neurology*. 1994 53(1); 22-6.
- Stock KW, Wetzel S, Kirsch E, Bongartz G, Steinbrich W, Radue EW. Anatomic Evaluation of the Circle of Willis: MR Angiography versus Intraarterial Digital Subtraction Angiography. *American Journal of Neuroradiology*. 1996 (17); 1495-99.
- Tahaghoghi MM, Williams H. (2006). *Learning MySQL*, 1st Ed. O'Reilly Media.
- Tanaka H, Fujita N, Enoki T, Matsumoto K, Watanabe Y, Murase K, Nakamura H. Relationship between Variations in the Circle of Willis and Flow Rates in Internal Carotid and Basilar Arteries Determined by Means of Magnetic Resonance Imaging with Semiautomated Lumen Segmentation: Reference Data from 125 Healthy Volunteers. *American Journal of Neuroradiology*. 2006 (27); 1770-75.
- Towfighi A and Saver JL. Stroke declines from third to fourth leading cause of death in the United States: historical perspective and challenges ahead. *Stroke*. 2011 42(8); 2351-5.
- Urbanski PP, Lenos A, Blume JC, Ziegler V, Griewing B, Schmitt R, Diegeler A, Dinkel M. Does anatomical completeness of the circle of Willis correlate with sufficient cross-perfusion during unilateral cerebral perfusion? *European Journal of Cardiothoracic Surgery*. 2008(33); 402-08.
- Uylings HBM, Marcos AR, van Pelt J. The metric analysis of three-dimensional dendritic patterns: a methodological review. *Journal of Neuroscience Methods*. 1986 (18); 127-51.
- Uylings HBM and van Pelt J. Measures for quantifying dendritic arborizations. *Computation in Neural Systems*. 2002 (13); 397-414.
- Van Pelt J, Uylings HB, Verwer RW, Pentney RJ, Woldenberg MJ. Tree asymmetry—a sensitive and practical measure for binary topological trees. *Bulletin of Mathematical Biology*. 1992 54(5); 759-84.
- Vaphiades MS, Horton JA. MRA or CTA, that's the question. *Survey of Ophthalmology*. 2005 50(4); 406-10.
- Vermandel M, Betrouni N, Viard R, Dewalle AS, Blond S, Rousseau J. Combining MIP images and fuzzy set principles for vessels segmentation: application to TOF MRA and CE-MRA. *Conference Proceedings IEEE Engineering in Medicine & Biology Society*. 2007 (2007); 6256-9.

- Verwer RWH and van Pelt J. Descriptive and comparative analysis of geometrical properties of neuronal tree structures. *Journal of Neuroscience Methods*. 1986 (18); 179-206.
- Vicari P, Silva GS, Nogutti MA, Neto FM, dos Santos NJ, Massaro AR, Figueiredo MS. Absence of association between TNF- α polymorphism and cerebral large-vessel abnormalities in adults with sickle cell anemia. *Acta Haematologica*. 2011 125(3); 141-4.
- Viedma A, Jimenez-Ortiz C, Marco V. Extended Willis Circle Model To Explain Clinical Observations In Periorbital Arterial Flow. *Journal of Biomechanics*. 1997 (3:3); 265-72.
- Wardlaw JM, White PM. The detection and management of unruptured intracranial aneurysms. *Brain*. 2000 123(2); 205-21.
- Washington SD, Ascoli GA, Krichmar JL. A statistical analysis of dendritic morphology's effect on neuron electrophysiology of CA3 pyramidal cells. *Neurocomputing*. 2000 (32-33); 261-69.
- Weiping Z and Huazhong S. Detection of cerebral vessels in MRA using 3D steerable filters. *Proceedings of the 2005 IEEE Engineering in Medicine and Biology 27th Annual Conference*. Shanghai, China, September 1-4, 2005.
- Wilms G, Bosmans H, Demaerel PH, Marchal G. Magnetic resonance angiography of the intracranial vessels. *European Journal of Radiology*. 2001 38; 10-18.
- Wilson DL and Noble JA. An Adaptive Segmentation Algorithm for Time-of-Flight MRA Data. *IEEE Transactions on Medical Imaging*. 1999 (18:10); 938-45.
- Wu SP, Ringgaard S, Pederson EM. Three-dimensional phase contrast velocity mapping acquisition improves wall shear stress estimation in vivo. *Magnetic Resonance Imaging*. 2004 (22); 345-51.
- Yan P and Kassim AA. Segmentation of volumetric MRA images by using capillary active contour. *Medical Image Analysis*. 2006 (10); 317-29.
- Zamir M. Fractal dimensions and multifractality in vascular branching. *Journal of Theoretical Biology*. 2001 212; 183-90.
- Zamir M. On the fractal properties of arterial trees. *Journal of Theoretical Biology*, 1999. 197: p. 517-526.

Zawodny JD and Balling DJ. (2004). High Performance MySQL Optimization, Backups, Replication, Load Balancing & More, 1st Ed. O'Reilly Media.

Zonoobi D, Kassim AA, Shen W. Vasculature segmentation in MRA images using gradient compensated geodesic active contours. Journal of Signal Processing Systems. 2009 (54): 171-81.

BIOGRAPHY

Susan Wright graduated from Norwin High School, in North Huntingdon, PA, in 2000. She received her Bachelor of Science from The University of Pittsburgh in 2004, with a double major in neuroscience and computer science and a minor in mathematics. While at The University of Pittsburgh, she completed an undergraduate thesis: Designing a Back-propagation Neural Network to Detect Changes in ERP Data.